Finite Element Model of Two-Dimensional Gas Flow and Transport of Radon in Cracked Soil

by

Diana J. Holford

Submitted in Partial Fulfillment
of the Requirements for the degree of
Master of Science in Hydrology

New Mexico Institute of Mining and Technology

Socorro, New Mexico

May, 1986

ABSTRACT

Measurements of radon fluxes from the soil at a field site showed greater changes in flux density than could be explained by model including the effects of atmospheric pressure changes on a one-dimensional, homogeneous and isotropic soil model which included advection, diffusion, radioactive decay, and production of radon. One possible explanation is that cracks in the soil could be enhancing the flux of radon. Modeling the gas flow and transport of radon gas in cracked soil involves more complex governing equations and boundary conditions than modeling solute transport in fractured rock. Therefore, although many analytical solutions and numerical models created to simulate groundwater flow and solute transport in fractured rock, they were not appropriate for this study.

Therefore, it was necessary to create a two-dimensional numerical model to simulate the effect of changes in surface pressure on a homogeneous, isotropic soil with parallel, partially penetrating cracks. This work presents the theory and development of the finite element equations used in the FORTRAN computer code, CRACK. The governing flow equation assumes transient, compressible, ideal gas flow. The governing transport equation includes advection, diffusion, radioactive decay, and a source of radon in the soil.

A sensitivity analysis investigates the response of

the model to changes in crack width, depth, and spacing, soil porosity, permeability, and diffusion coefficient, and constant and sinusoidal surface pressure changes. A comparison between the results of the sensitivity analysis and flux measurements from the field yields some unexpected conclusions. Even a soil model with very deep cracks cannot account for all of the changes in flux observed in the field. High frequency changes in surface pressure, attributed to wind, can cause an increase in mean flux of radon from cracked soil, and also large deviations in flux. Changes in atmospheric pressure, coupled with changes in wind speed acting on soil with deep cracks or holes left by plant roots is the most likely explanation for the changes in radon flux densities observed in the field.

ACKNOWLEDGEMENTS

This work is lovingly dedicated to my beautiful mother, Eunice Smith, who has always believed in me.

Much appreciation is due to:

Stephen Schery, whose research led to, and funded this work. Also, for believing I'd actually get the program to work.

My thesis advisor, Fred Phillips, for endless patience and good advice.

John Wilson and David Peterson, who shared their expertise in numerical modeling with me.

Stephen Conrad, for a plethora of excellent editorial comments, and for helping me stay on top of things.

To my many friends here at Tech: Laura Myers, Chris Mikell, Valda Terauds, Stephen Heermann, Ward Herst, Tom Duval, Barb Kickham, Deb McElroy, Janine Jennings, Chuck Spaulding, Mike Tansey, and Aster, to name a few, who kept me from blowing up the DEC-20.

This work was funded in part by the Department of Energy, Office of Health and Environmental Radiation, Grant Number DE-FG04-86ER60432, the Tech Computer Center, and my mom and dad.

TABLE OF CONTENTS

TABLE OF FIGURES

LIST OF TABLES

1. INTRODUCTION

Radon-222 gas is produced as a daughter product of radium-226 which is found in soils that have weathered from rocks containing uranium-238 (figure 1-1). Exposure to radon gas has been linked to lung cancer and may be toxic if allowed to accumulate in a closed space, such as a uranium mine or a well-insulated house. Factors which may increase the flux of radon out of the soil are of great concern; cracks in soil are one of those factors.

1.1 PREVIOUS WORK

Clements (1974) measured radon fluxes from soil at a site near the New Mexico Institute of Mining and Technology campus in Socorro, New Mexico. Data collected over 12-hour intervals were simulated satisfactorily by a one-dimensional, homogeneous and isotropic porous media model which included a constant gas velocity, diffusion of radon in the soil, radioactive decay, and production of radon (see section 3.1 for governing equation).

Schery et. al. (1984) also measured radon fluxes from soil at another site near the New Mexico Institute of Mining and Technology campus. Their data, collected over 2-hour intervals, showed greater changes in radon flux density than in the subsurface concentration gradient. Fick's Law (see equation 2.2.1.1) predicts that diffusive flux density should be proportional to the concentration

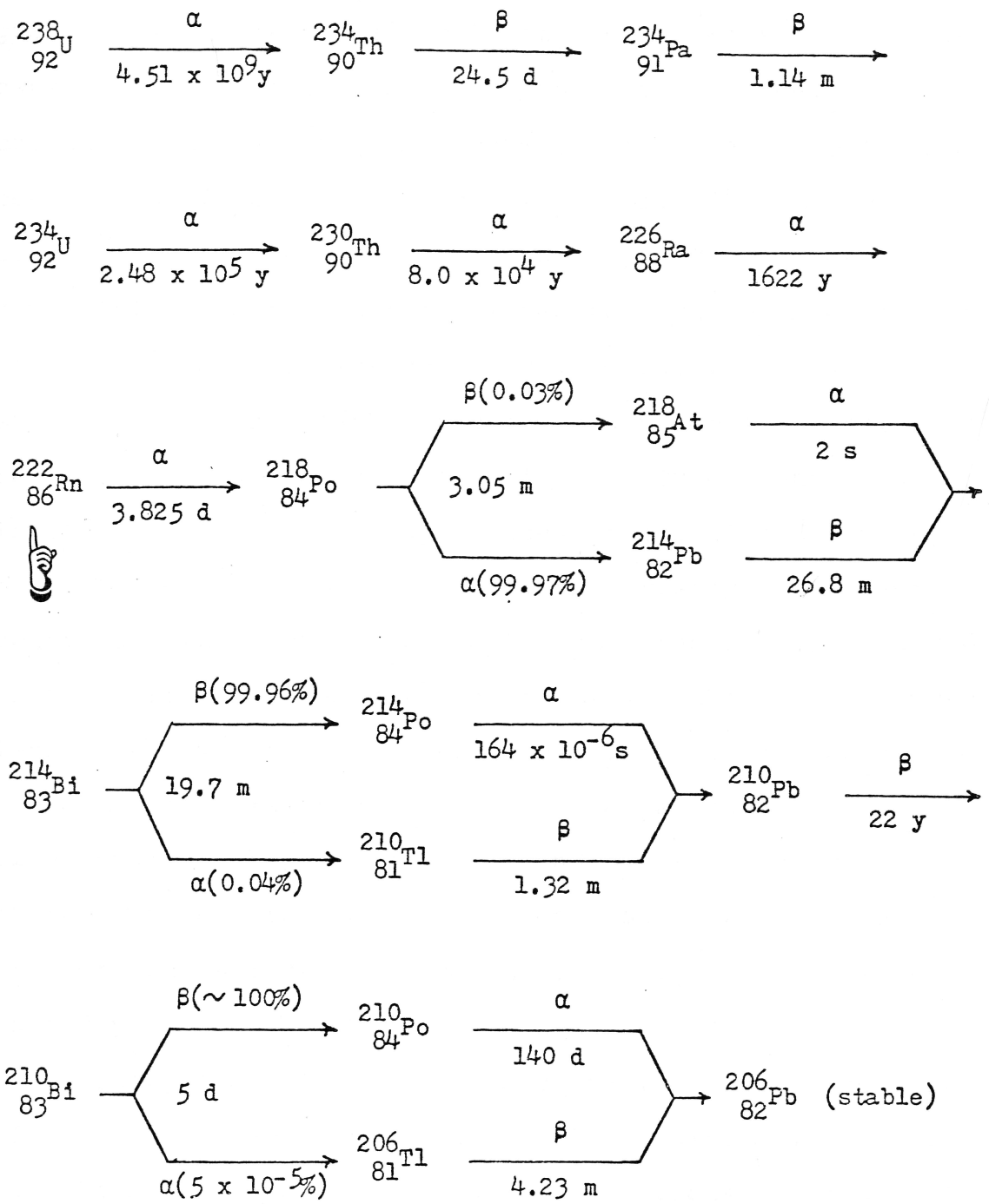

Figure 1-1: Uranium 238 decay series.

gradient. They hypothesised that soil cracks might be causing the rapid changes in the flux observed, because cracks have a higher permeability and diffusion coefficient than the surrounding soil. Changes in radon concentrations would occur rapidly in the cracks, and would influence the surface fluxes recorded, but might not affect the subsurface concentration gradients significantly since the cracks would be small compared to the surrounding volume of soil. Experiments which involved forcing air up through the soil and pouring a thin film of water on top showed the presence of discrete points of rapid air exit. Polygonal cracks were observed on the surface of the soil at the site. The cracks were less than a millimeter wide, spaced 5 to 10 cm apart, and probably not more than 10 cm deep. At an outcrop near the site, cracks and plant roots extending from the surface to at least 5 meters were observed, but it was unclear whether the structures were connected from the surface to this depth.

Schery and Siegel (in preparation) estimated the effects of cracks in the soil using analytical solutions for the porous media and assuming the cracks penetrated to fairly great depths where concentrations of radon have reached a maximum due to the balancing of production and decay rates. They described their calculations as "order of magnitude estimates for some limiting situations." However, from their results they were further convinced

that cracks would affect surface fluxes proportionally more than they would affect the subsurface concentration gradients. Also, they concluded that cracks could cause a net enhancement of flux for sinusoidal variations in pressure. Sinusoidal surface pressure variations of might be caused by fluctuations in wind speed or diurnal variations in atmospheric pressure. Schery's desire to quantify these theoretical results and explain his earlier experimental results created the need for a model with less limiting assumptions, and was the major impetus for this study.

The use of preexisting analytical solutions was considered first. Unfortunately, available solutions proved inadequate for the purposes of this study. Analytical solutions for solute transport in groundwater flowing in fractured rock have been derived by Neretnieks (1980) and Sudicky and Frind (1982). Typical assumptions for these models are illustrated in figure 1-2. Advection and dispersion were assumed in the crack, but in the soil only diffusion transverse to the crack was assumed. However, in the current study, concentration gradients in the soil are strong in the vertical direction, which will cause diffusion parallel to the cracks. Therefore, two-dimensional diffusion should be included in the soil for this model. The analytical models did not include advection in the porous media. Schery et. al (1984) calculated an average soil velocity of 1×10^{-4} cm/s from

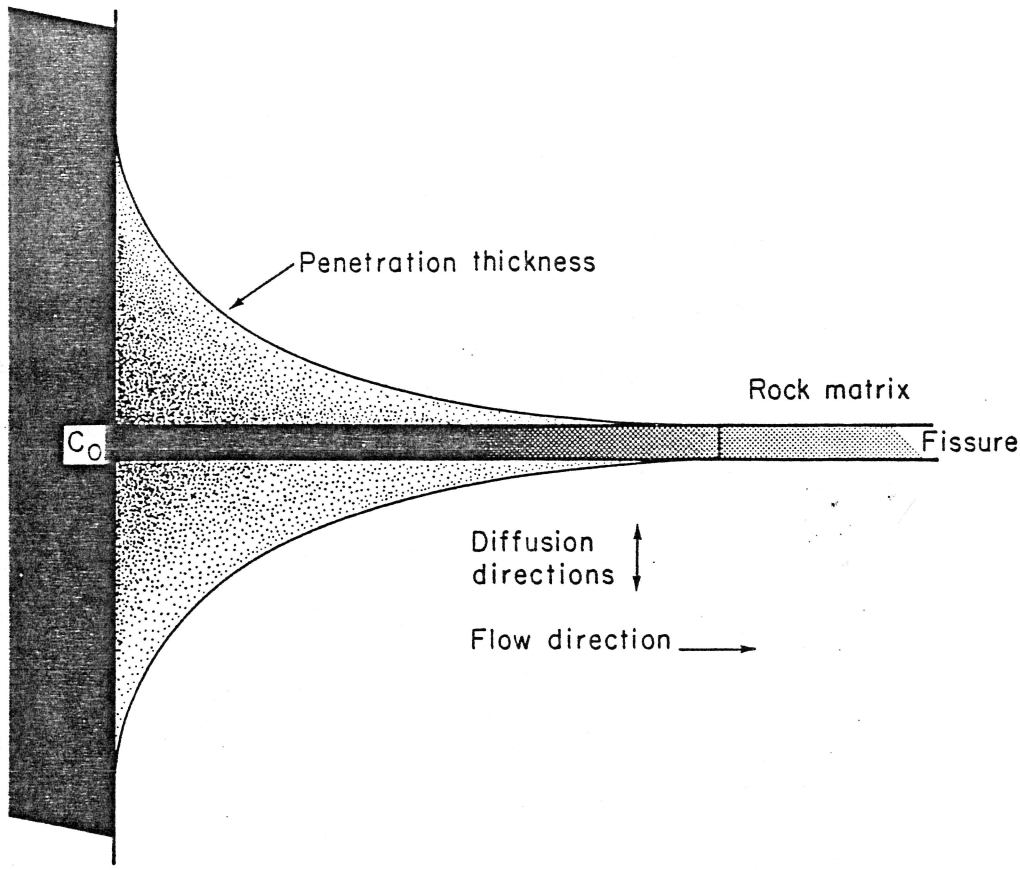

Figure 1-2: Schematic diagram of analytical solution for crack flow (Neretnieks,1980).

subsurface pressure gradients measured in the field, assuming a permeability equal to 2.7×10^{-8} cm^2 and a dynamic viscosity of 1.8×10^{-4} g/cm/s. This velocity is high enough to have a significant influence on the concentration profile, and thus both advection and diffusion in the soil must be included in the model.

The analytical models also assumed the cracks penetrate fully to a constant concentration boundary at depth. One goal of this study is to determine the effect of crack geometry, including depth into the soil, on radon flux density from the soil surface. For this reason, partially penetrating cracks need to be included in this model. Importantly, the effects of a transient flow field on partially penetrating crack would be two-dimensional and not uniform. So, two-dimensional advection in the soil must be included in this model.

Finally, the analytical solutions assume that at the top boundary, the concentration equals zero at a semi-infinite distance. A $dC/dx = 0$ boundary condition at the top of the crack would be more realistic, since as atmospheric pressure drops, the amount of radon transported out of the crack by advection is probably be large enough to raise the concentration above zero.

The lack of appropriate analytical solutions led next to the possibility of using existing numerical solutions. Recent finite-element solutions by Huyakorn et. al. (1983a and 1983b) and by Grisak and Pickens (1980a and

1980b) illustrate the two main approches to the numerical modeling of crack flow. The first method Huyakorn called the "double porosity" approach. In this method, the crack and soil equations were solved separately. A leakage term was included in the crack equations to account for solute lost or gained across the crack/matrix interface. The leakage term was estimated at each time step, then the crack equation was solved. Concentrations in the crack were used as a boundary for the porous-media equations. After solving the porous-media equations, the leakage term was determined by back substitution. The process was repeated until the solution converged. The method used by Grisak and Pickens has been called a "discrete fracture" approach by Huyakorn to distinquish it from his double porosity approach. The same convention will be used here. In this approach, the crack and porous media equations were solved simultaneously using a finite element approach simply by assigning different properties to the crack such as permeability, porosity, and diffusion coefficient. The crack was thus treated as an inhomogeneity in the porous media.

The use of available computer codes was considered, such as FTRANS (Intera,1985) which uses Huyakorn's approach. It was noted that the models had some of the limitations discussed above. For instance, most models only considered diffusion in the porous media transverse to the crack, and did not consider advective transport in

the porous media. These were considered serious limitations and a difficult one to correct in an unfamiliar model. It seemed simpler at the time to upgrade a finite-element model for two-dimensional advective-dispersive transport that the author had written. The discrete fracture approach was the easiest to include in the code since it only required giving different material properties to the crack, as opposed to Huyakorn's method, which would have nessesitated a new and separate equation for the crack.

1.2 PURPOSE

The purpose of this work is to develop a two-dimensional finite element model which simulates the effects of surface pressure changes on radon flux from cracked soil. Also, to investigate whether a model including soil with cracks will match the field data collected by Schery et. al. (1984) better than a one-dimensional model.

1.3 SCOPE OF PRESENT WORK

This work presents the theory and development of the finite element equations used in the FORTRAN computer code, CRACK, and then verifies the code to the extent allowed by available analytical solutions. Next, the sensitivity of the model to various soil and crack parameters and pressure perturbations is investigated.

The results of the sensitivity analysis are studied to determine if the field measurements of radon flux can be explained by a model including cracks. Also, the effects of atmospheric presure variations and changes in wind speed at ground surface are considered. Finally, suggestions are made for further field and modeling studies.

2. MATHEMATICAL MODEL

2.1 General Considerations and Assumptions

The model developed in section 2.2 simulates air flow caused by atmospheric pressure changes at the ground surface. Pressure gradients in the soil and cracks will drive the transport of radon gas, affecting the flux density of radon across the soil/air boundary.
The soil in the model is assumed to be homogeneous, isotropic, isothermal, and free of water down to the water table. The cracks in the model are evenly spaced, and of a uniform width and depth.

Figure 2-1 is a schematic diagram of the model, showing various components affecting transport. Flow and transport are two-dimensional in the soil, because the cracks do not extend all the way to the water table and pressure changes will result in a complex, nonuniform flow field. Flow and transport are one-dimensional in the crack, because the cracks are narrow and diffusion strong enough to assume that the radon is evenly mixed across the width of the crack.

The two-dimensional Cartesian coordiate system (in figure 2-1) consists of the x-direction, which is parallel to the soil/atmosphere boundary, and the z-direction, which is perpendicular to the soil/atmosphere boundary.

Molecular diffusion of radon-222 (D_d) is assumed to

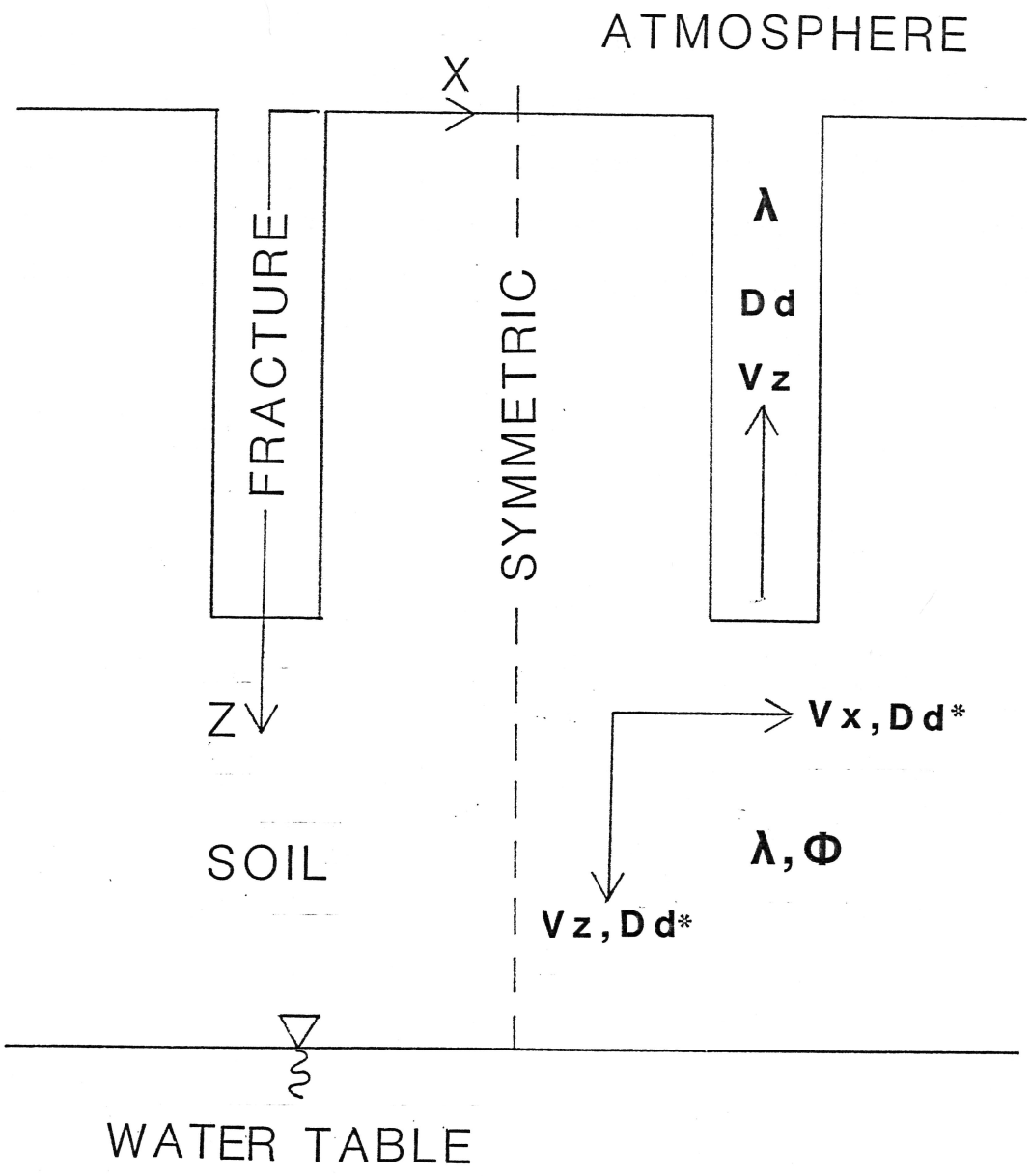

Figure 2-1: Two-dimensional model of soil with cracks.

D_d: diffusion coefficient in air
D_d^*: diffusion coefficient in soil
v: specific discharge velocity of air flow
λ: radioacitve decay coefficient of radon-222
ϕ: source constant for production of radon-222

be governed by Fick's Law. The flow of gas (v) is governed by Darcy's law. Radon decays with a half-life of 3.8 days, represented by the decay constant, λ . A constant rate of production for radon, ϕ, is ascribed to the soil; involving the assumtion that radon-producing radium-226 is evenly distributed in the soil (see figure 1-1).

2.2 Derivation of Governing Equations

2.2.1 The transport equation

The concentration of radon-222 gas in air (C) is defined as the number of atoms per unit volume of air. The porosity of a soil (n) is defined as the ratio of the volume of air space to the total volume of soil. Therefore, the concentration of radon gas in soil, or the number of atoms per unit bulk volume of soil is equal to nC.

The number of atoms transported per unit time per unit bulk cross-sectional area of soil is called the flux density. The diffusive flux density (Fd) is defined by Fick's Law for molecular diffusion in soil (Bear, 1979):

$$(2.2.1.1)\quad Fd_i = -(Dd^*)_{ij} \frac{\partial(nC)}{\partial x_j}$$

where: i = implies summation of index from 1 to 2
j = implies summation of index from 1 to 2
x_1 = x-direction coordinate
x_2 = z-direction coordinate
D_d^* = diffusion coefficient in soil (L^2/T)

The diffusion coefficient in soil is defined as (Bear, 1979):

$$(2.2.1.2)\quad Dd^*_{ij} = Dd\ \tau^*_{ij}$$

where: D_d = diffusion coefficient in air (L^2/T)
τ^*_{ij} = tortuosity of soil

The tortuosity of a soil is a scalar for isotropic soils and has been empiricallly determined to be between 0.01 and 0.66 (Bear, 1979).

The advective flux density, or the number of atoms transported per unit time per unit bulk cross-sectional area of soil due to gas flow is defined as (Bear, 1979):

(2.2.1.3) $Fa_i = v_i C$

where: v_i = specific discharge velocity of gas (L/T)
The specific discharge velocity may be defined as the volume of gas flowing per unit bulk cross-sectional area of soil per unit time.

The effects of mechanical dispersion are assumed to be negligible at the low flow velocities anticipated. According to Bear (1979), the condition for this assumption to be valid is that the Peclet number be less than one. The Peclet number is defined as $Pe = V d / D_d$, where d is some characteristic length of the soil. This characteristic length may be calculated from an empirical formula for intrinsic permeability: $k = c d^2$, where c is an empirical constant. Bear (1979) claims that a common value for the constant, c, is 100. When a permeability for the field soil is taken from Schery, et. al. (1984) of 2.7×10^{-8} cm^2, this yields a value for d of about 5×10^{-5} cm. Assuming an average air velocity in the soil of about 1×10^{-4} cm/s and D_d equal to 0.1 cm^2/s results in a Peclet number much less than one. Therefore, the assumption that molecular diffusion dominates over mechanical dispersion is a reasonable one.

Conservation of mass requires that the net number of

atoms transported into a unit volume of soil equal the change in the number of atoms stored in the volume, minus the number of atoms lost by radioactive decay, plus the number of atoms of radon-222 produced by decay of radium-226 in the soil.

The resulting continuity equation for the soil takes the form:

$$(2.2.1.4) \quad -\frac{\partial(nC)}{\partial t} = \frac{\partial F_i}{\partial x_i} + \lambda(nC) - n\phi$$

where: t = time
λ = ln(2)/half-life of radon-222 (T^{-1})
ϕ = production rate of radon per unit volume of soil pore space ($M/L^3/T$)
$F_i = Fd_i + Fa_i$ = total flux density

Substituting equations 2.2.1.1 and 2.2.1.3 into 2.2.1.4 gives:

$$(2.2.1.5) \quad \frac{\partial(nC)}{\partial t} = \frac{\partial}{\partial x_i}\left(Dd^* \frac{\partial(nC)}{\partial x_j}\right) - \frac{\partial}{\partial x_i}(v_i C) - n\lambda C + n\phi$$

The soil is assumed to be homogeneous and isotropic, with a scalar tortuosity (τ^*), making D_d^* a scalar:

$$(2.2.1.6) \quad \frac{\partial C}{\partial t} = Dd^* \frac{\partial^2 C}{\partial x_i^2} - \frac{\partial}{\partial x_i}\left(\frac{v_i}{n} C\right) - \lambda C + \phi$$

The specific discharge velocity is left inside the spatial partial derivative because the flow field is assumed to be nonuniform (see section 2.2.3).

For the transport equation in the crack perfect transverse mixing in the x-direction is assumed, which reduces the equation 2.2.1.6 to one dimension. Also, D_d is substituted for D_d^*, and a porosity of 1 is assumed in the

crack.

$$(2.2.1.7)\quad \frac{\partial C}{\partial t} = Dd\,\frac{\partial^2 C}{\partial z^2} - \frac{\partial}{\partial z}\left(\frac{v_z}{n}\,C\right) - \lambda C$$

where: z = z-direction spatial coordinate

2.2.2 Boundary conditions for transport equation

The boundary conditions for the transport equation are shown schematically in figure 2-2. At the top of the soil a first-type, or Dirichlet boundary condition of C=0 is imposed because this is close to the concentration measured at the top of the soil at the field site by Schery et. al. (1984). Also, the concentration of radon in the atmosphere is assumed to be zero. This boundary condition further implies that there is no advective flux across the top boundary, since the advective flux is calculated by equation 2.2.1.1.

At the top of the crack a second-type, or Neumann boundary condition of dC/dz=0 is imposed because advective transport is assumed to dominate and is strong enough to cause concentrations to rise above zero. This boundary condition means that there is no diffusive transport modelled across this boundary since the diffusive flux is calculated by equation 2.2.1.2.

The sides of the model are second-type boundaries, dC/dx=0, because they are axes of symmetry, either in the center of a crack or halfway between two evenly spaced and equal sized cracks. The concentrations should be the same

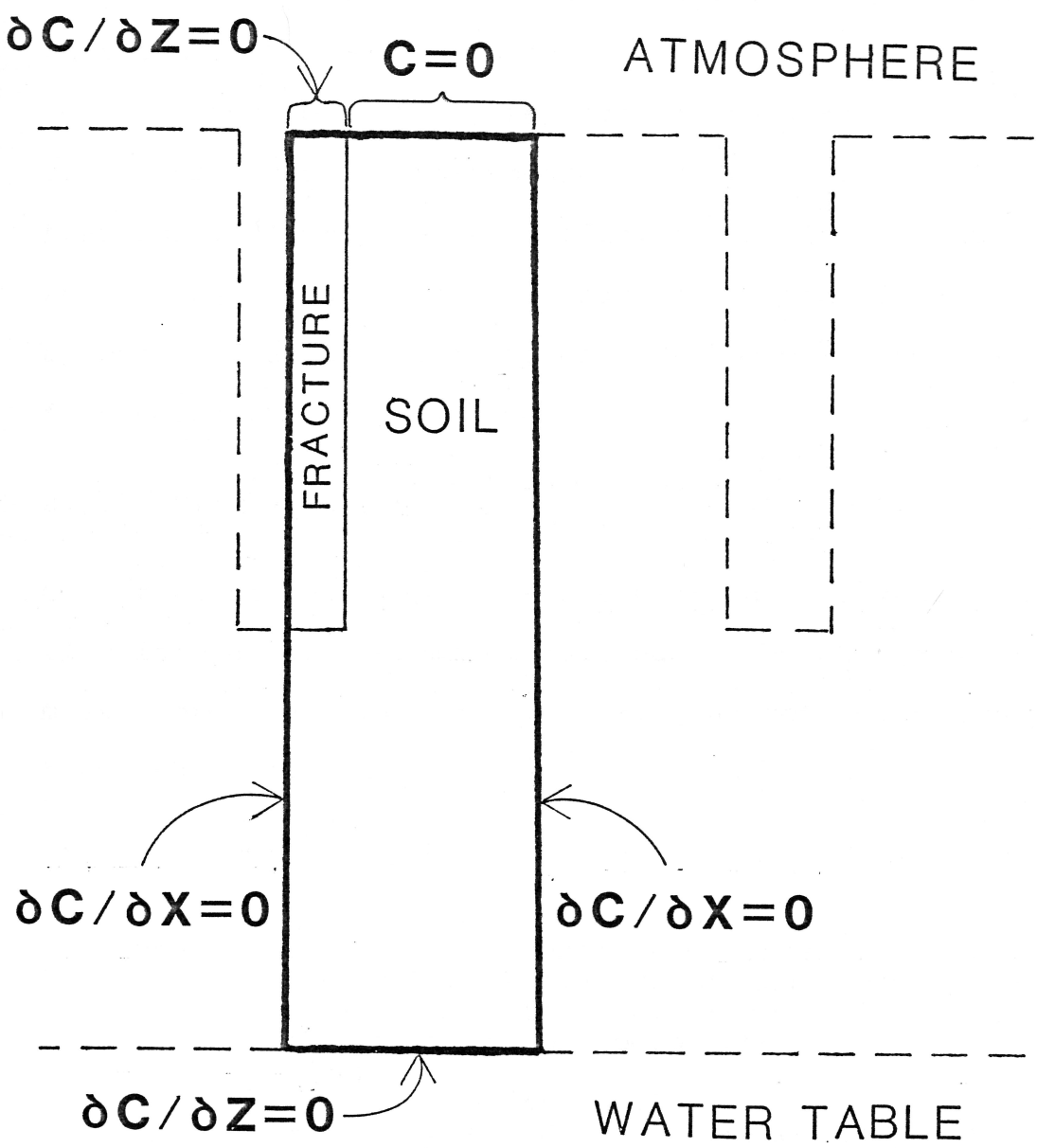

Figure 2-2: Boundary conditions for transport equation.

C: concentration of radon gas

on either side of the crack, therefore the gradient at that boundary is equal to zero.

The bottom boundary represents the water table which is assumed to be an impermeable barrier to gas flow and transport. Therefore the diffusive flux is set equal to zero using a second-type boundary condition, dC/dz=0. The advective flux is also zero on this boundary because the flow velocity is zero.

2.2.3 Flow equation

Conservation of mass requires that the net rate of fluid flow into a unit volume of soil equal the change of fluid mass stored within the volume. The continuity equation takes the form (Bear, 1979):

$$(2.2.3.1) \quad -\frac{\partial(n\rho)}{\partial t} = \frac{\partial(\rho v_i)}{\partial x_i}$$

where: i = implies summation of index from 1 to 2
j = implies summation of index from 1 to 2
x_1 = x-direction coordinate
x_2 = z-direction coordinate
n^2= porosity
ρ = gas density (M/L^3)
v_i = specific discharge velocity (L/T)

Darcy's law states (Bear, 1979):

$$(2.2.3.2) \quad v_i = -\frac{k_{ij}}{\mu}\left(\frac{\partial P}{\partial x_i} + \rho g \frac{\partial z}{\partial x_j}\right)$$

where: P = absolute gas pressure ($M/L^2/T$)
k = intrinsic permeability of soil (L^2)
μ = dynamic viscocity of air ($M/L/T$)
g = gravitational acceleration (L/T^2)

Combining the continuity equation and Darcy's Law gives:

$$(2.2.3.3) \quad \frac{\partial}{\partial t}(n\rho) = \frac{\partial}{\partial x_i}\left(\frac{k_{ij}}{\mu}\rho\left(\frac{\partial P}{\partial x_j} + \rho g \frac{\partial z}{\partial x_j}\right)\right)$$

Assuming an ideal gas, the equation of state is (Roller and Blum, 1981):

(2.2.3.4) $\rho = MP/RT$

where: M = molecular weight
R = universal gas constant
T = absolute temperature

For isothermal flow then:

(2.2.3.5) $\frac{\partial \rho}{\partial t} = \frac{M}{RT} \frac{\partial P}{\partial t}$

Substituting 2.2.3.4 and 2.2.3.5 into 2.2.3.3 gives:

(2.2.3.6) $\frac{\partial (nP)}{\partial t} = \frac{\partial}{\partial x_i} \left(\frac{k_{ij}}{\mu} P \frac{\partial P}{\partial x_j} \right) + \frac{\partial}{\partial x_i} \left(\frac{k_{ij}}{\mu} P \rho g \frac{\partial z}{\partial x_j} \right)$

Since the density of air is so small, the effect of gravity is assumed to be negligible. Also, n is assumed to be uniform in space and time because the soil is assumed to be homogeneous, isotropic, and incompressible, so the equation reduces to:

(2.2.3.7) $n \frac{\partial P}{\partial t} = \frac{\partial}{\partial x_i} \left(\frac{k_{ij}}{\mu} P \frac{\partial P}{\partial x_j} \right)$

Which, using the chain rule, can be rearranged to:

(2.2.3.8) $\frac{n}{P} \frac{\partial P^2}{\partial t} = \frac{\partial}{\partial x_i} \left(\frac{k_{ij}}{\mu} \frac{\partial P^2}{\partial x_j} \right)$

In the crack, we assume the porosity equals 1.0 and the permeability equals (Bear, 1979):

(2.2.3.9) $k_f = \frac{(\text{WIDTH OF CRACK})^2}{12}$

2.2.4 Boundary conditions for flow equation

The boundary conditions for the flow equation are illustrated in figure 2-3. The top boundary is a first-type boundary because it is at the soil surface; the pressure is prescribed as being the barometric pressure of the atmosphere at ground level. As mentioned in section 2.2.2, the side boundaries are axes of symmetry and are therefore flow divides. They are second-type boundaries, $dP/dx=0$. Again, the bottom boundary at the water table is considered to be impermeable to gas flow, so $dP/dz=0$.

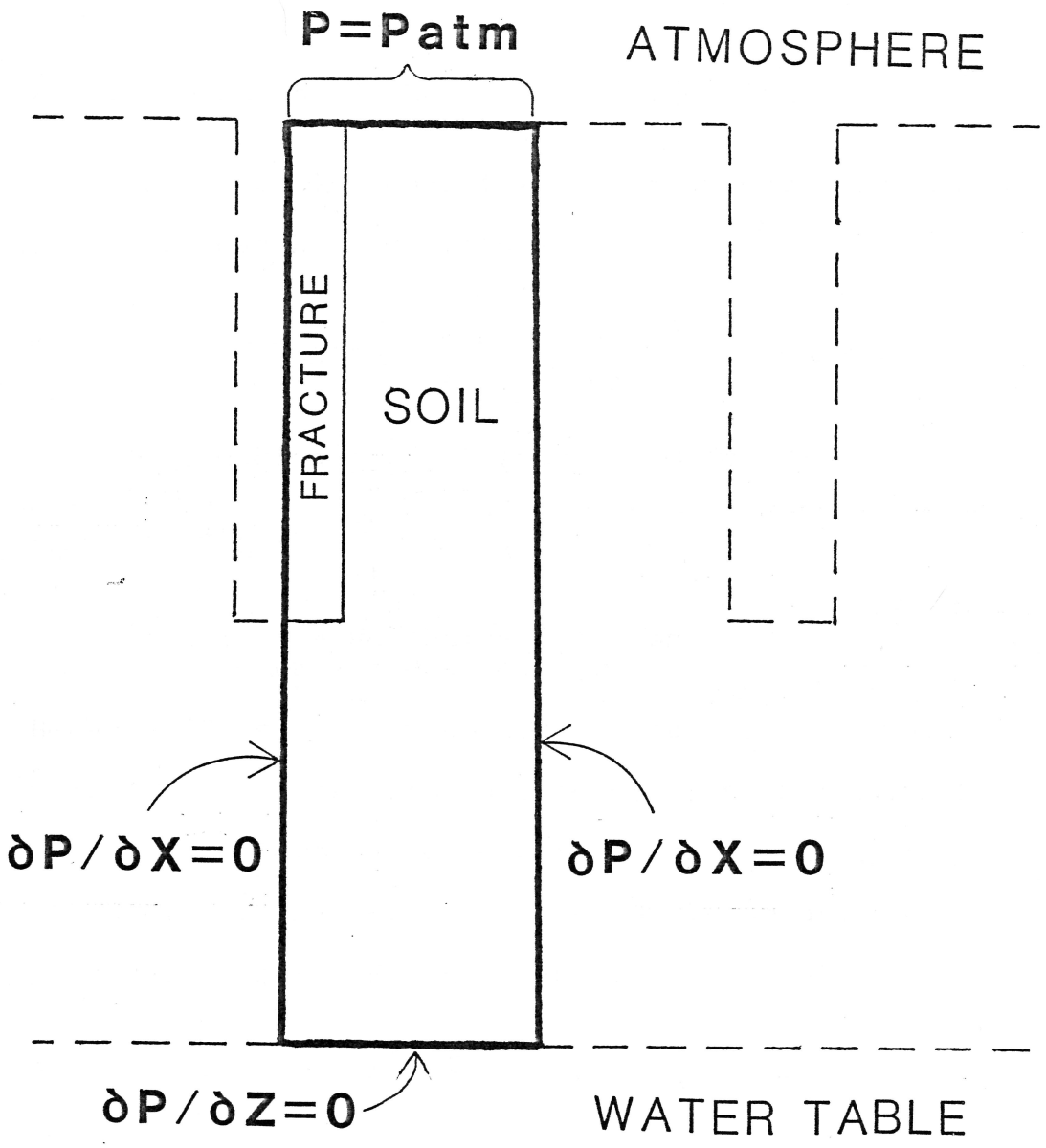

Figure 2-3: Boundary conditions for gas flow equation

P: absolute gas pressure

2.3 Solution by Galerkin Finite Element Method

2.3.1 Solution of the transport equation

The governing equation for transport of radon gas (2.2.1.6) can be rewritten as:

$$(2.3.1.1)\quad L(C) = \frac{\partial C}{\partial t} - Dd^* \frac{\partial^2 C}{\partial x_i^2} + \frac{\partial}{\partial x_i}\left(\frac{v_i}{n} C\right) + \lambda C - \phi = 0$$

Introducing a trial function $\hat{C}$ for C:

$$(2.3.1.2)\quad \hat{C}(x_i,t) = \sum_{J=1}^{nn} N_J(x_i)\, C_J(t)$$

where: N = weighting function
nn = number of nodes

Because $\hat{C}$ is only an approximation for C, substitution of $\hat{C}$ in (2.3.1.1) results in some error such that $L(\hat{C})\neq 0$.

The Galerkin method requires that the weighted integral of the error over the whole solution region must be equal to zero (Huyakorn and Pinder, 1983):

$$(2.3.1.3)\quad \int_R N_I\, L(\hat{C})\, dR = 0$$

where: R = solution region

This yields:

$$(2.3.1.4)\quad \int_R N_I \left[\frac{\partial \hat{C}}{\partial t} - Dd^* \frac{\partial^2 \hat{C}}{\partial x_i^2} + \frac{\partial}{\partial x_i}\left(\frac{v_i}{n} \hat{C}\right) + \lambda \hat{C} - \phi\right] dR = 0$$

Application of Green's theorem to the second derivative term gives:

$$(2.3.1.5)\quad \int_R \left(\frac{\partial \hat{C}}{\partial t} N_I + Dd^* \frac{\partial \hat{C}}{\partial x_i} \frac{\partial N_I}{\partial x_i} + \frac{\partial}{\partial x_i} \left(\frac{v_i}{n} \hat{C} \right) N_I + \lambda \hat{C} N_I - \phi N_I \right) dR$$

$$- \int_B \left(Dd^* \frac{\partial \hat{C}}{\partial x_i} N_I \vec{n}_i \right) dB$$

where: $\vec{n}_i$ = unit normal vector to boundary B

Since the boundary integral term in (2.3.1.5) only applies at boundary nodes, it will be left out of the discusion until section 2.3.2.

Substituting (2.3.1.2) for $\hat{C}$ in (2.3.1.5):

$$(2.3.1.6)\quad \int_R \left(\frac{\partial C_J}{\partial t} N_I N_J + Dd^* C_J \frac{\partial N_I}{\partial x_i} \frac{\partial N_J}{\partial x_i} + C_J N_I \frac{\partial}{\partial x_i} \left(\frac{v_i}{n} N_J \right) + \lambda C_J N_I N_J - \phi N_I \right) dR = 0$$

The time integral is solved using a standard finite difference approach:

$$(2.3.1.7)\quad \frac{\partial C_J}{\partial t} = \frac{C_J(t_{m+1}) - C_J(t_m)}{t_{m+1} - t_m} = \frac{C_J^{m+1} - C_J^m}{\Delta t}$$

where: C_{m+1}^m = concentration at previous time step
C^{m+1} = concentration at current time step
Δt = time increment

Substituting (2.3.1.7) into (2.3.1.6) and gathering terms yields:

$$(2.3.1.8)\quad \int_R \left(\left(\frac{1}{\Delta t} N_I N_J + Dd^* \frac{\partial N_I}{\partial x_i} \frac{\partial N_J}{\partial x_i} + N_I \frac{\partial}{\partial x_i} \left(\frac{v_i}{n} N_J \right) + \lambda N_I N_J \right) C_J^{m+1} \right) dR$$

$$= \int_R \left(\phi N_I + C_J^{m+1} \left(\frac{1}{\Delta t} N_I N_J \right) \right) dR$$

or, in matrix form:

$$(2.3.1.9) \quad [LHS]_{IJ} \{C^{m+1}\}_J = \{RHS\}_I$$

Stability of the solution may sometimes be ensured by weighting the solution towards the concentration at the previous time step, C^m. This may be accomplished by adding a time weighting factor, θ, to equation 2.3.1.9.

$$(2.3.1.10) \quad [LHS]_{IJ} \left(\theta\{C\}_J^{m+1} + (1-\theta)\{C\}_J^m\right) = \{RHS\}_I$$

where: θ = time weighting factor, between 0 and 1

Time weighting factors between 0.5 and 1.0 are unconditionally stable (Huyakorn and Pinder, 1983). A time weighting factor of 1.0 gives no weight to the previous time step, and is called a fully implicit time-stepping scheme. The time steps used for all simulations in chapter 4 were large enough for the fracture to have been essentially at steady state. For this reason, a fully implicit time weighting scheme was used, because weighting the solution towards the previous time step has no meaning in a steady-state solution. Accuracy of the solution was ensured by double precisioning most of the variables used in the solution. For the simulations done in the chapter 3, time weighting factors were used between 0.5 to 0.7. Accuracy of each solution was ensured by limiting the size of time steps, based on criteria from Huyakorn and Pinder, 1983.

The method of solving the matrix equations is

discussed in appendix C, along with all other aspects of coding the preceeding equations.

2.3.2 Solution of flow equations

The solution of the flow equation by the Galerkin finite element method is similar to that for the transport equation in section 2.3.1, except that there are fewer terms in the flow equation, and it is non-linear.

The governing equation for compressible, ideal gas flow may be rewritten as:

$$(2.3.2.1)\quad L(P) = \frac{n}{P}\frac{\partial P^2}{\partial t} - \frac{\partial}{\partial x_i}\left(\frac{k_{ij}}{\mu}\frac{\partial P^2}{\partial x_i}\right) = 0$$

Using the same techniques as in (2.3.1.2) through (2.3.1.5) gives:

$$(2.3.2.2)\quad \int_R \left(\frac{n}{P}\frac{\partial P_J^2}{\partial t} N_I N_J + \frac{k_{ij}}{\mu} P_J^2 \frac{\partial N_I}{\partial x_i}\frac{\partial N_J}{\partial x_i}\right) dR = 0$$

The equation is solved in terms of P^2; the P in the coefficient of the nonlinear time term is treated as the average pressure for all the nodes in an element.

Applying an implicit finite difference technique to the time derivative as in (2.3.1.7) yields:

$$(2.3.2.3)\quad \int_R \left(\frac{n}{P^{m+1}}\frac{1}{\Delta t} N_I N_J + \frac{k_{ij}}{\mu}\frac{\partial N_I}{\partial x_i}\frac{\partial N_J}{\partial x_i}\right) dR \cdot \left(P_J^{m+1}\right)^2 =$$

$$= \int_R \left(\left(P_J^m\right)^2 \frac{n}{P^{m+1}}\frac{1}{\Delta t} N_I N_J\right) dR$$

or, in matrix form:

$$(2.3.2.4)\quad [LHS(P^{m+1})]_{IJ}\,\{P^2\}_J^{m+1} = \{RHS(P^m, P^{m+1})\}_I$$

A time weighting factor may be added to equation 2.3.2.4, as in equation 2.3.1.10:

$$(2.3.2.5)\quad [LHS(P^{m+1})]_{IJ}\left(\theta\{P^2\}_J^{m+1} + (1-\theta)\{P^2\}_J^{m}\right) = \{RHS(P^{m},P^{m+1})\}_I$$

The flow equation is non-linear because the $[LHS]_{IJ}$ and $\{RHS\}_I$ are a function of P^{m+1}, the pressure at the current time step, which is unknown. Therefore, P^{m+1} must be solved for iteratively. A very simple method of iteration was used, called Picard iteration. For the first iteration, P^{m+1} was set equal to P^m, the pressure at the last time step. The equation was solved for P^{m+1}, and this value was used to solve the equation over and over again until the maximum normalized difference between values for two subsequent iterations was less than some prescribed tolerance (Huyakorn and Pinder, 1983):

$$(2.3.2.6)\quad \frac{\left(P_J^{k+1} - P_J^{k}\right)_{max_J}}{\left(P_J^{k+1}\right)_{max_J}}$$

where: P^{k+1} = pressure at current iteration
P^{k} = pressure at previous iteration

2.3.3 Numerical treatment of boundary conditions

The boundary integral term from (2.3.1.5):

$$(2.3.3.2)\quad \int_B \left(v_i\, C_J\, N_I\, \vec{n}_i\right) dB$$

represents the diffusive flux integrated across a boundary. At a second type boundary, where $dC/dX_i = 0$, this term simply vanishes.

At a first-type boundary, the concentration is forced equal to some specified value (see appendix C, subroutine BOUND1) and equation (2.3.1.5) does not have to be solved for concentrations at the nodes on this boundary. After the equations are solved for concentrations in the interior region, these concentrations may be substituted back into equation (2.3.1.5) at the boundary nodes to determine the diffusive flux boundary integral term (2.3.3.1). The advective flux across the top boundary of the crack may be calculated by integrating (2.2.1.3) across the boundary:

$$(2.3.3.1)\quad -\int_B \left(Dd^* \frac{\partial \hat{C}}{\partial x_i}\, N_I\, \vec{n}_i\right) dB$$

The total radon flux density across the top boundary of the model may be calculated by adding the advective flux integral from the top boundary of the crack and the diffusive flux integral from the top boundary of the soil and dividing by the total length of the top boundary. The calculation of the total radon flux density is an important performance measure in chapter 4.

There is one node situated on the top boundary at the interface between the soil and the crack. The node at this point is difficult to deal with numerically because it is located at the interface between a first-type (prescribed concentration) and second-type (prescribed diffusive flux) boundary. For the purposes of this discussion, the second-type boundary is considered to be to the left of the interface node, and the first-type boundary to the right. Wilson et. al. (1979) handled a node at the interface between first and second-type boundaries by making the node a first-type boundary (assigning it a prescribed value), but then subtracting the prescribed flux from the flux calculated by back substitution. Following suit, the interface node in this model was made a first-type boundary with a prescribed concentration of zero. Since the diffusive flux to the left of this point in the crack is prescribed as zero, no adjustment to the back-substitution calculations for diffusive flux is necessary.

The diffusive flux across the boundary at the interface node, calculated by back substitution, was noted to be very large. There is a contribution to this diffusive flux from all nodes directly surrounding the interface node. The back substitution equation may be broken down into components representing the relative contributions of each of these surrounding nodes. The relative magnitudes of these components indicate that the

large diffusive flux is almost exclusively due to the influence of the node in the crack which is directly to the left of the interface node. Because the concentration is fixed at zero at the top of the soil but not at the top of the crack, there is a strong horizontal concentration gradient from the crack to the soil at the interface node. In effect, the crack brings up higher concentrations of radon from deep in the soil, but before all of the radon can reach the top of the crack to escape by advection, much of it is drawn towards the zero concentration boundary at the top of the soil, and instead escapes by diffusion.

First and second-type boundaries are applied in the flow equation in exactly the same way as the transport equation.

2.4 Finite Element Grid

Figure 2-4 illustrates a typical finite element grid used for the simulations in this report. Note that the grid is very fine near the crack in the x-direction and near the surface in the z-direction. This is because concentration gradients are most likely to be strong in these areas. The grid increases in coarsness away from the origin in both directions in order to reduce the total number of elements used in the model.

Since concentration gradients will be strongest in and near the crack in the x-direction, it was necessary to determine how finely to grid the domain in this direction. The effect of increasing the number of elements in the crack in the x-direction is shown in figure 2-5. Including more than 3 elements in the crack in the x-direction caused no visible change in the flux density predicted, so 3 elements were used in the crack for all runs in this report.

Note that the bottom of the grid shown in figure 2-4 is at a depth of 1000 cm, whereas the water table, which is assumed to be the bottom of the model, is 3000 cm below ground surface. Gridding to a depth of 3000 cm required more elements, and hence larger arrays in the code, than New Mexico Tech's DEC-20 had the memory capacity for. Therefore, a simple modeling trick was used to cut off the grid at a reasonable depth, while still effectively extending the model down to the water table. The storage

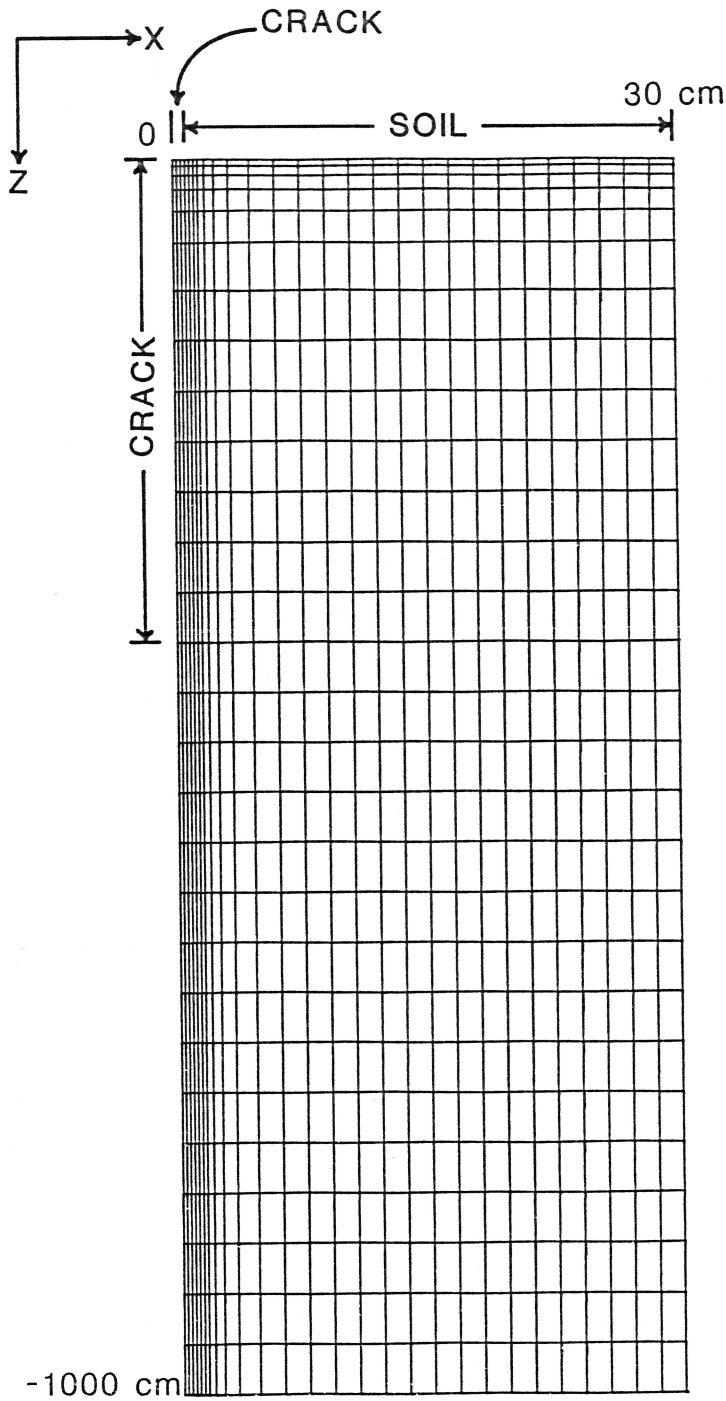

FIGURE 2-4: TYPICAL FINITE ELEMENT GRID.

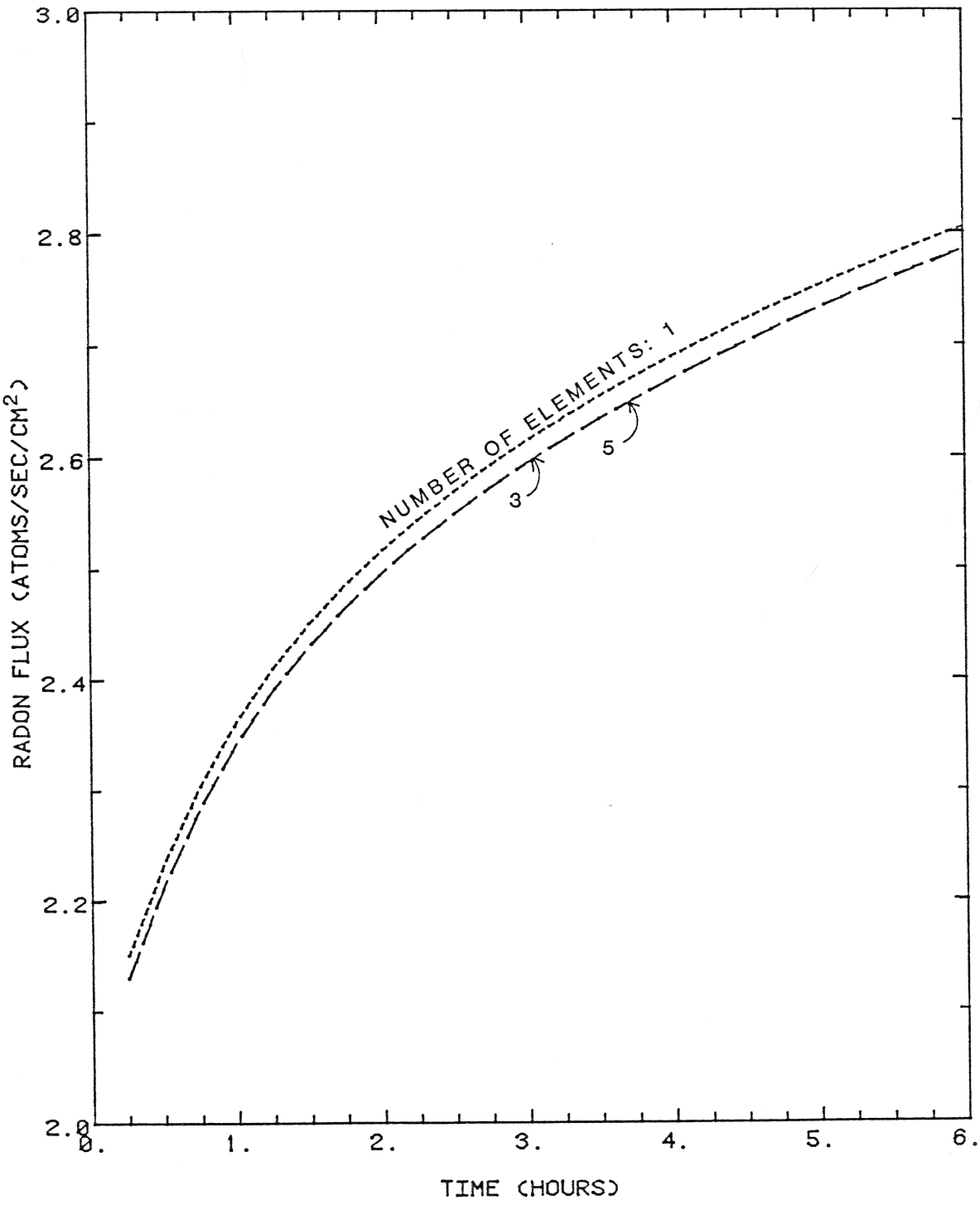

Figure 2-5: Effect of the number of elements in crack in x-direction. Test run is for parameters in tables 4-1, 4-2, and for cracks 400 cm deep, 0.06 cm wide, and 800 cm apart.

capacity of the portion of the model below a depth of 1000 cm was "lumped" into the bottom row of elements. This was accomplished by increasing the porosity of the bottom elements by the ratio of the vertical thickness of the portion of the model which was cut off to the vertical thickness of the bottom element just above the cut-off level. The permeability and diffusion coefficient of the bottom elements were decreased by the same amount, to prevent radon gas from escaping too quickly from the large reservoir of these elements. This approximation works because the soil properties at depths greater than 1000 cm are assumed to be uniform; also, the concentration of radon-222 approaches an asymptotic value of 25,000 atoms/cm^3 with depth below land surface. Also, because pressure and concentration gradients are linear deep in the soil.

Figure 2-6 presents a simulation which shows the effect of cutting off the model at different depths when water table is at a depth of 3000 cm. As the model is cut off at shallower depths, the predicted flux density increases. Since the lumped elements have a concentration of 25,000 atoms/cm^3; placing these elements above the depth where the actual concentration is very close to this value gives erroneous results. Cutting off the model at a depth of 500 cm increases the flux significantly because, in this example, the crack extends to a depth of 400 cm. Cutting off the model at a depth of 1000 cm gives slightly

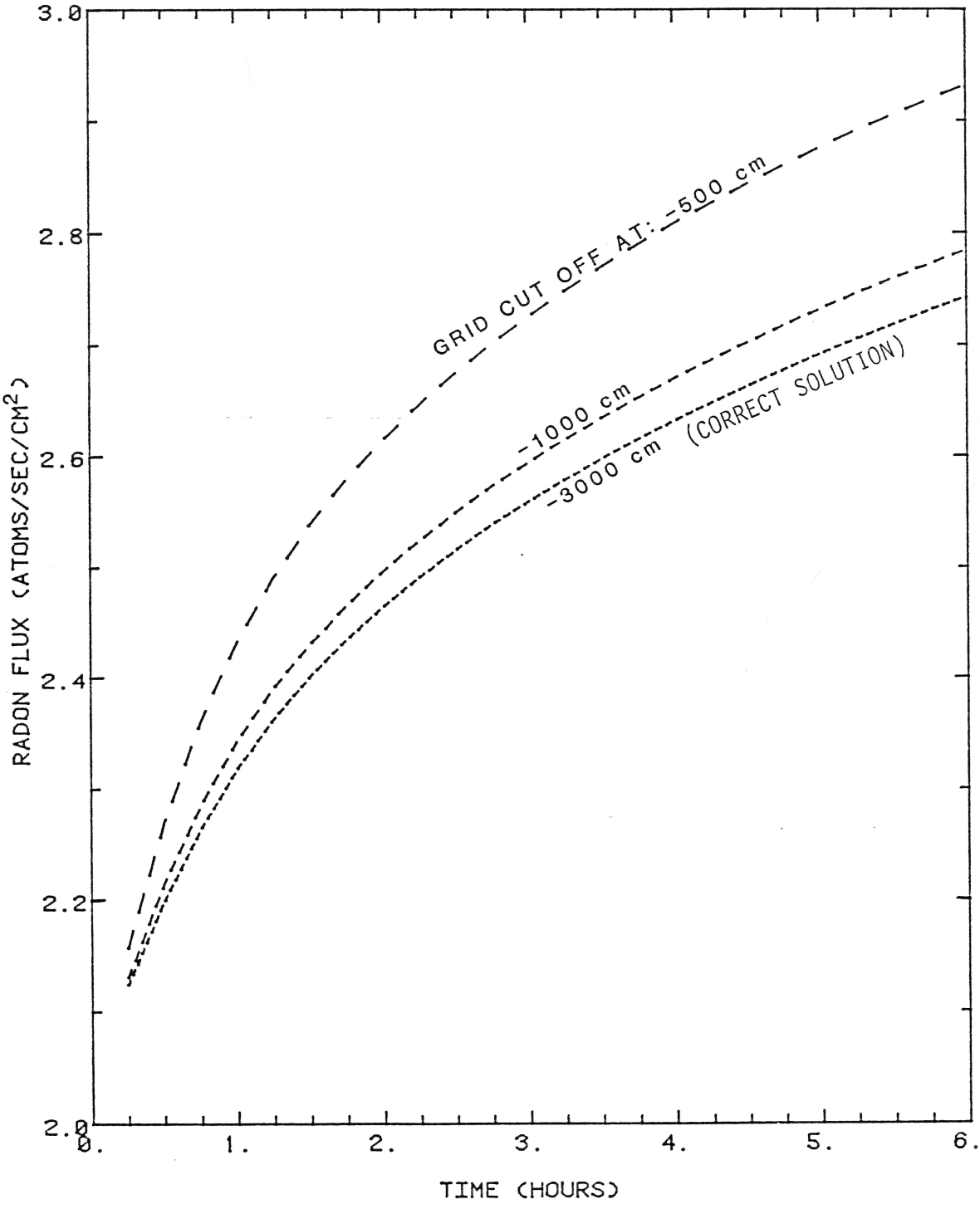

Figure 2-6: Effect of cutting grid off at different depths. Test run is for parameters in tables 4-1, 4-2, and for cracks 400 cm deep, 0.06 cm wide, and 800 cm apart.

higher fluxes than extending the grid down to the correct depth of 3000 cm. However, this difference was less than the field measurement error for radon flux density, 0.2 atoms/s/cm^2 (Schery et. al., 1984).

3. VERIFICATION OF NUMERICAL MODEL

Four test cases were run to verify the accuracy of the numerical model, CRACK, by comparing it to analytical solutions found in the literature. The model consists of two main parts, a flow code and a transport code. The first two test cases verify the transport code and the last two verify the flow code.

3.1 1-D Advection, Dispersion, Decay and Source.

The solute transport code was compared to a one-dimensional analytical solution of the advection-dispersion equation with radioactive decay and a linear source term. The governing equation is:

$$(3.1.1)\quad \frac{\partial C}{\partial t} = Dd^* \frac{\partial^2 C}{\partial z^2} - \frac{v_z}{n}\frac{\partial C}{\partial z} - \lambda C + \phi$$

where: C = concentration of radon (M/L^3)
D_d^* = coeff. of diffusion of radon in soil (L^2/T)
V_z = discharge velocity of air in soil (L/T)
n = porosity of soil
λ = radioactive decay constant of radon (T_3^{-1})
ϕ = rate of radon production in soil $(M/L^3/T)$

The steady-state analytical solution was taken from Clements (1974):

$$(3.1.2)\quad C = C^{\infty}\left[1 - \exp\left(\left(\frac{v_z/n}{2Dd^*} + \left(\frac{(v_z/n)^2}{4(Dd^*)^2} + \frac{\lambda}{Dd^*}\right)1/2\right)z\right)\right]$$

where: C^{∞} = concentration of radon at depth (M/L^3)

The numerical model was compared to the analytical solution with the data shown in figure 3-1. The model ran

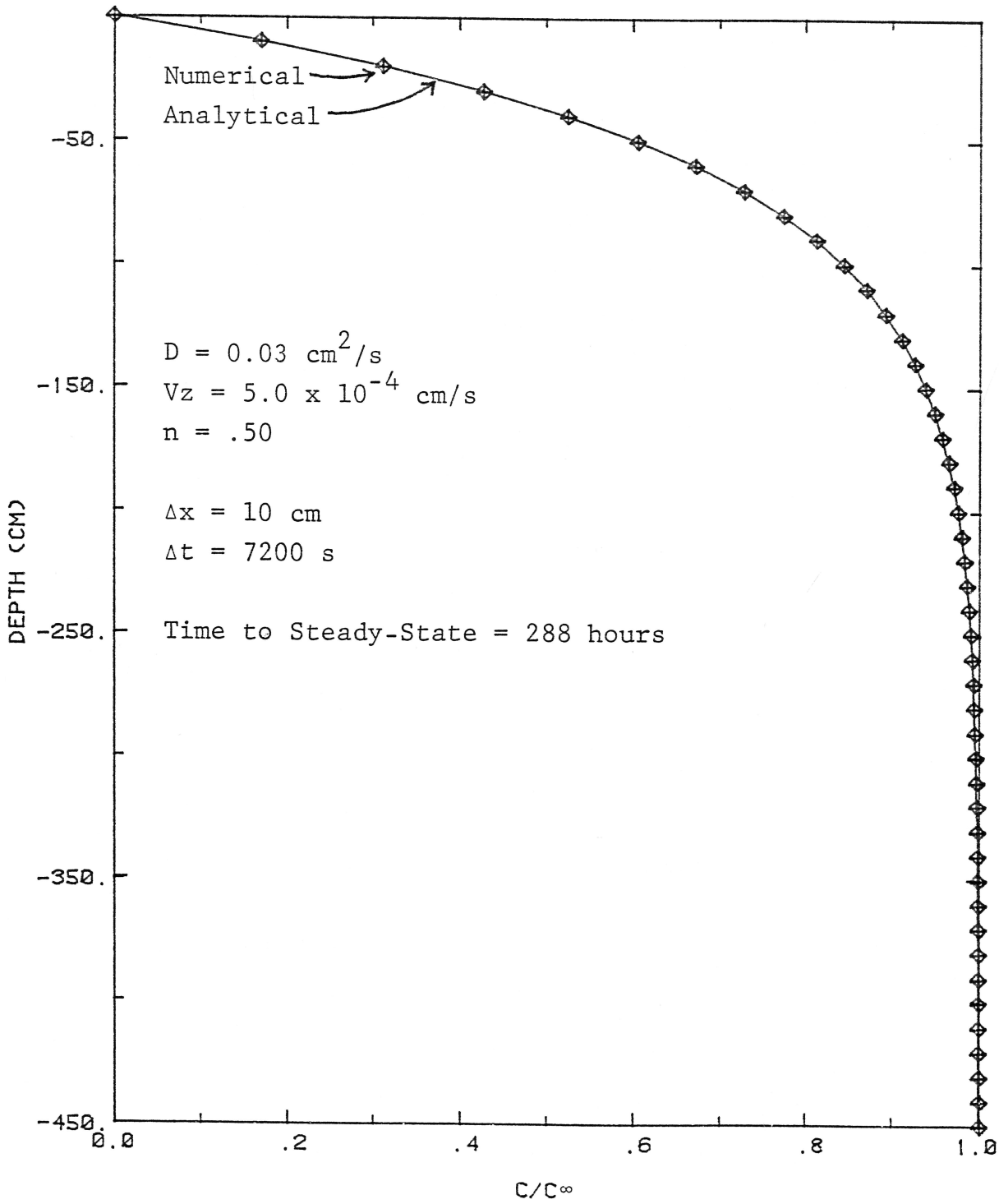

FIGURE 3-1: Comparison of Galerkin finite element solution to steady-state analytical solution for advective-dispersive equation with decay and source.

288 simulation hours before it reached steady-state. There is excellent agreement between the two solutions.

Stability of the solution was ensured by using a time weighting factor, θ, of 0.5. Using this time weighting factor is termed the Crank-Nicholson scheme, which weights the solution by half towards the solution at the previous time step. This time weighting factor is unconditionally stable. Accurate time steps were chosen using the formulas (Huyakorn and Pinder, 1983):

$$(3.1.3) \quad \frac{(v_z/n)\, z}{2} \leq D_d^*$$

$$(3.1.4) \quad \Delta t \leq \left[\frac{(v_z/n)}{2\Delta z} + \frac{D_d^*}{\Delta z^2} \right]$$

where: Δz = smallest element dimension

3.2 Matrix Diffusion from a Single Crack

The transport code was tested in two dimensions for the case of a single, vertical crack with vertical advection, dispersion and decay. The crack is contained in a soil matrix block with horizontal dispersion and decay. The governing equation for the crack is:

$$(3.2.1) \quad \frac{\partial C}{\partial t} = Dd \frac{\partial^2 C}{\partial z^2} - \frac{v_z}{n} \frac{\partial C}{\partial z} - \lambda C + \frac{nDd^*}{b} \frac{\partial C}{\partial x} \Big|_{x=b}$$

where: b = boundary between soil and crack

The governing equation for transport in the soil matrix is:

$$(3.2.2) \quad \frac{\partial C}{\partial t} = Dd^* \frac{\partial^2 C}{\partial x^2} - \lambda C$$

A steady-state analytical solution by Sudicky and Frind (1982) was used for comparison. The solution for transport in the crack is:

$$(3.2.3)\quad C_C = C^{\infty} \exp\left[\frac{(v_z/n)z}{2D}\left[1 - \left(1 + \frac{4}{\gamma}(1+\beta)\right)^{1/2}\right]\right]$$

where: $\beta = n\,Dxx^{1/2}/\lambda^{1/2}b \cdot \tanh(\sigma\lambda^{\frac{1}{2}})$
$\gamma = (v/n)^2/\lambda Dzz$

The analytical solution for transport in the soil matrix is:

$$(3.2.4)\quad C_S = C_C\left[\frac{\cosh(G\lambda^{1/2}(B-x)}{\cosh(\sigma\lambda^{1/2})}\right]$$

where: $G = Dxx^{-1/2}$
$\sigma = G(B-b)$
$B = 1/2$ of crack spacing

A steady-state solution was obtained by using one large time step of 10^{35} seconds. Good agreement can be seen in figure 3-2 for various profiles in the x and z-directions.

3.3 1-D linearized gas flow

The govering equation for one-dimensional gas flow is (Huyakorn and Pinder, 1983):

$$(3.3.1)\quad \frac{\partial}{\partial x}\left(\frac{k}{\mu} P \frac{\partial P}{\partial x}\right) = n \frac{\partial P}{\partial t}$$

where: P = absolute pressure
k = intrinsic permeability (L^2)
μ = dynamic viscosity of air

The solution is linearized by assuming that P on the

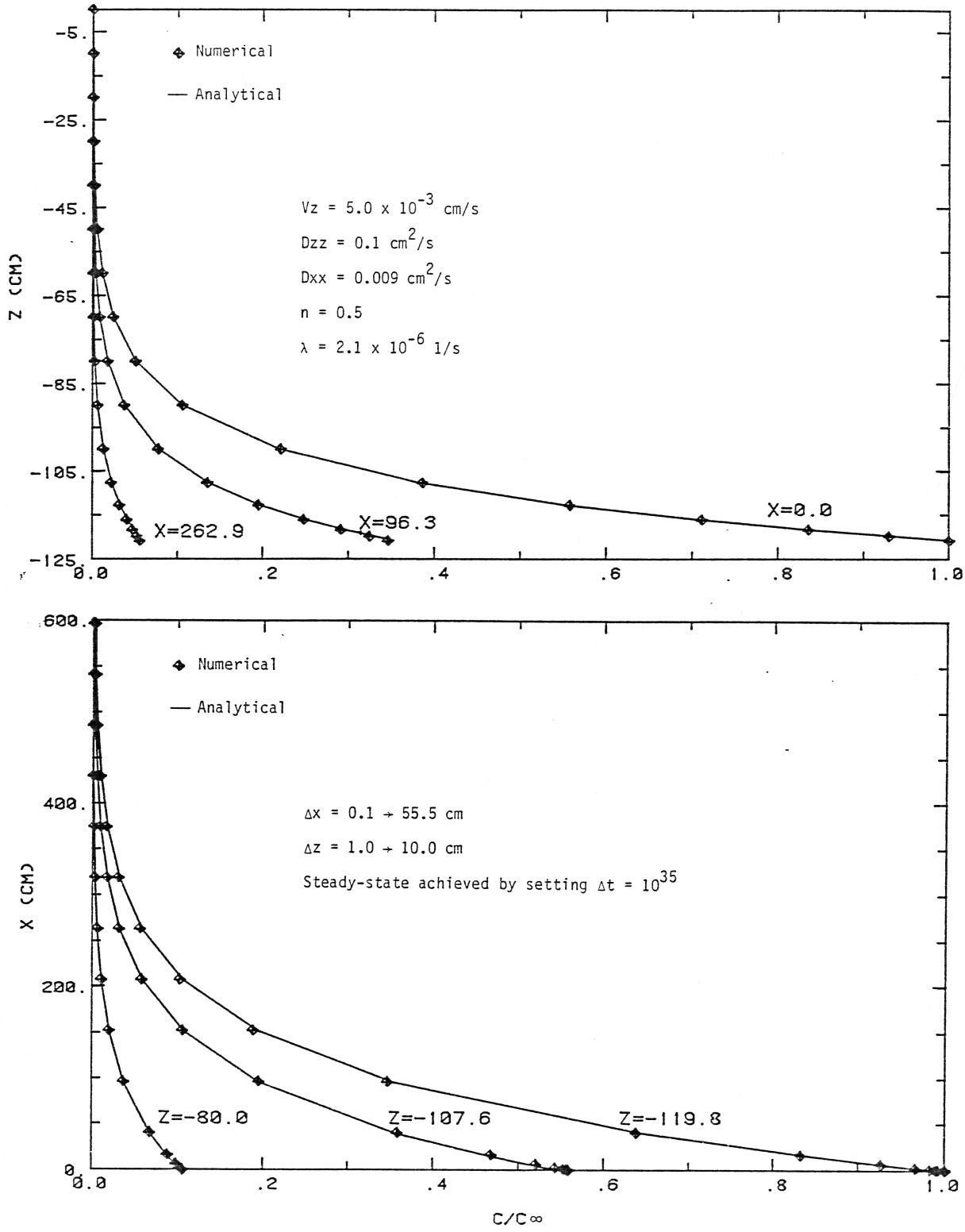

Figure 3-2: Comparison of Galerkin numerical solution to a steady state analytical solution for matrix diffusion from a single crack (analytical solution is calculated only at same points as numerical solution).

left-hand side of the equation equals the pressure at the last time step yielding:

$$(3.3.2)\quad \frac{\partial^2 P}{\partial x^2} = \frac{n\ \mu}{P_p k}\frac{\partial P}{\partial t}$$

where: P_p = pressure at previous time step

The numerical model was compared to a transient analytical solution for a semi-infinite domain (Carslaw and Jaeger, 1959):

$$(3.3.3)\quad P = P_0 + P_L\ \mathrm{erfc}\left(\frac{x}{\sqrt{4(k/\mu)(P_p/n)t}}\right)$$

where: $P_o = P(X,t=0) = 1.0$
$P_L^o = P(X=0,t) = 2.0$

Good agreement between the two methods can be seen in figure 3-3. A time weighting factor of 0.7 was used which is unconditionally stable. Accuracy of the solution was ensured by limiting the time step size by the criteria (Huyakorn and Pinder, 1983):

$$(3.3.4)\quad \Delta t \leq \Delta x^2 \frac{n\ \mu}{P_p k}$$

where: Δx = smallest element dimension

3.4 2-D Linear Flow from Intersecting Constant Pressure Boundaries

This case was chosen to verify two-dimensional flow from the side and top boundary. The governing equation for 2-D gas flow is similar to equation (3.3.2), above:

$$(3.4.1)\quad \frac{\partial^2 P}{\partial x^2} + \frac{\partial^2 P}{\partial z^2} = \frac{n\ \mu}{P_p k}\frac{\partial P}{\partial t}$$

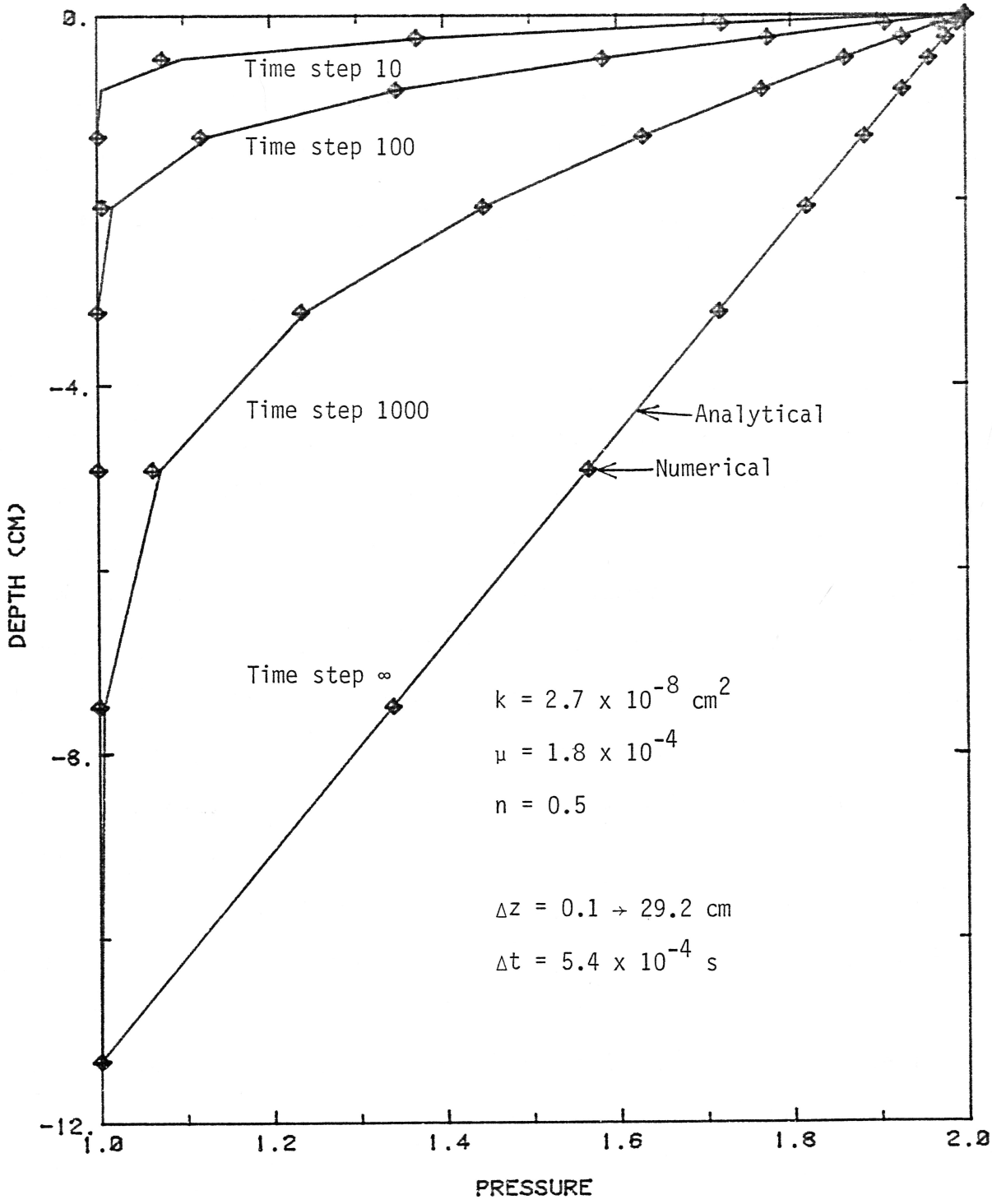

Figure 3-3: Comparison of numerical solution for pressure equation to a one-dimensional transient analytical solution for linear flow (analytical solution is calculated only at same points as numerical solution).

The analytical solution for a semi-infinite domain was taken from Carslaw and Jaeger (1959):

$$(3.4.2)\quad P = P_0 + P_L \left[1 - \operatorname{erf}\left(\frac{x}{\sqrt{4\,(k/\mu)(P_p/n)t}} \right) \operatorname{erf}\left(\frac{z}{\sqrt{4\,(k/\mu)(P_p/n)t}} \right) \right]$$

where: $P_o = P(x,z,t=0)$
$P_L^o = P(x,z=0,t) = P(x=0,z,t)$

The pressure in the crack and at the surface where set to a constant of 2.0 while the initial condition in the soil matrix was a pressure of 1.0. Figures 3-4a through 3-4c show profiles in the x and z-directions at early, intermediate and late times. The numerical solution shows better agreement at later times. The same stability and accuracy criteria were used as in section 3.3. There is inaccuracy at early times from truncation errors inherent in attempting to model the movement of a sharp pressure front.

It was not necessary to verify the flow equations against an analytical solution for crack flow. The linear flow equation is actually a simpler version of the transport equation; the permeability term of the flow equation is analogous to the diffusion term of the transport equation.

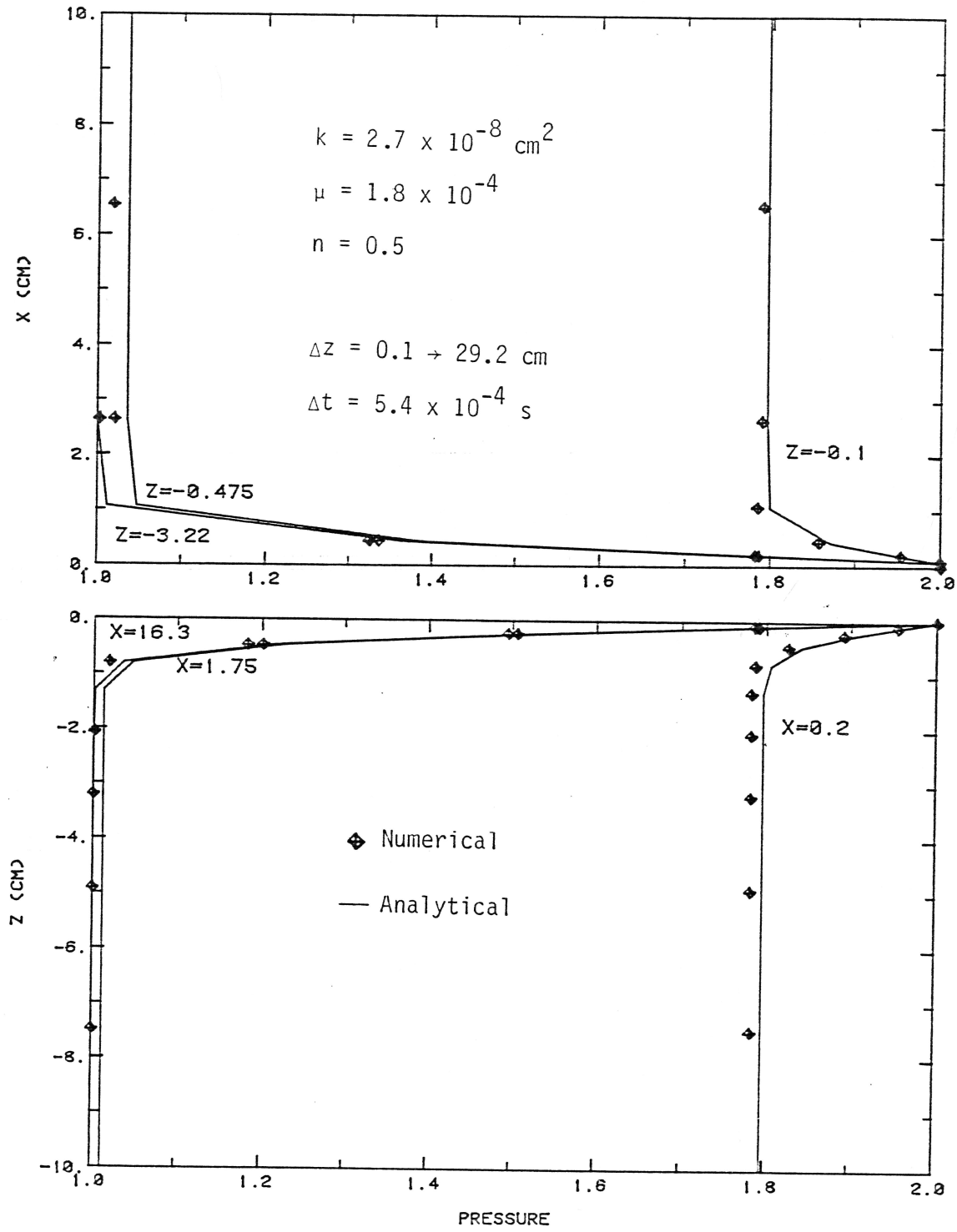

Figure 3-4a: Comparison of numerical solution for pressure to a two-dimensional analytical solution for linear flow between 2 intersecting constant pressure boundaries. Time step 10.

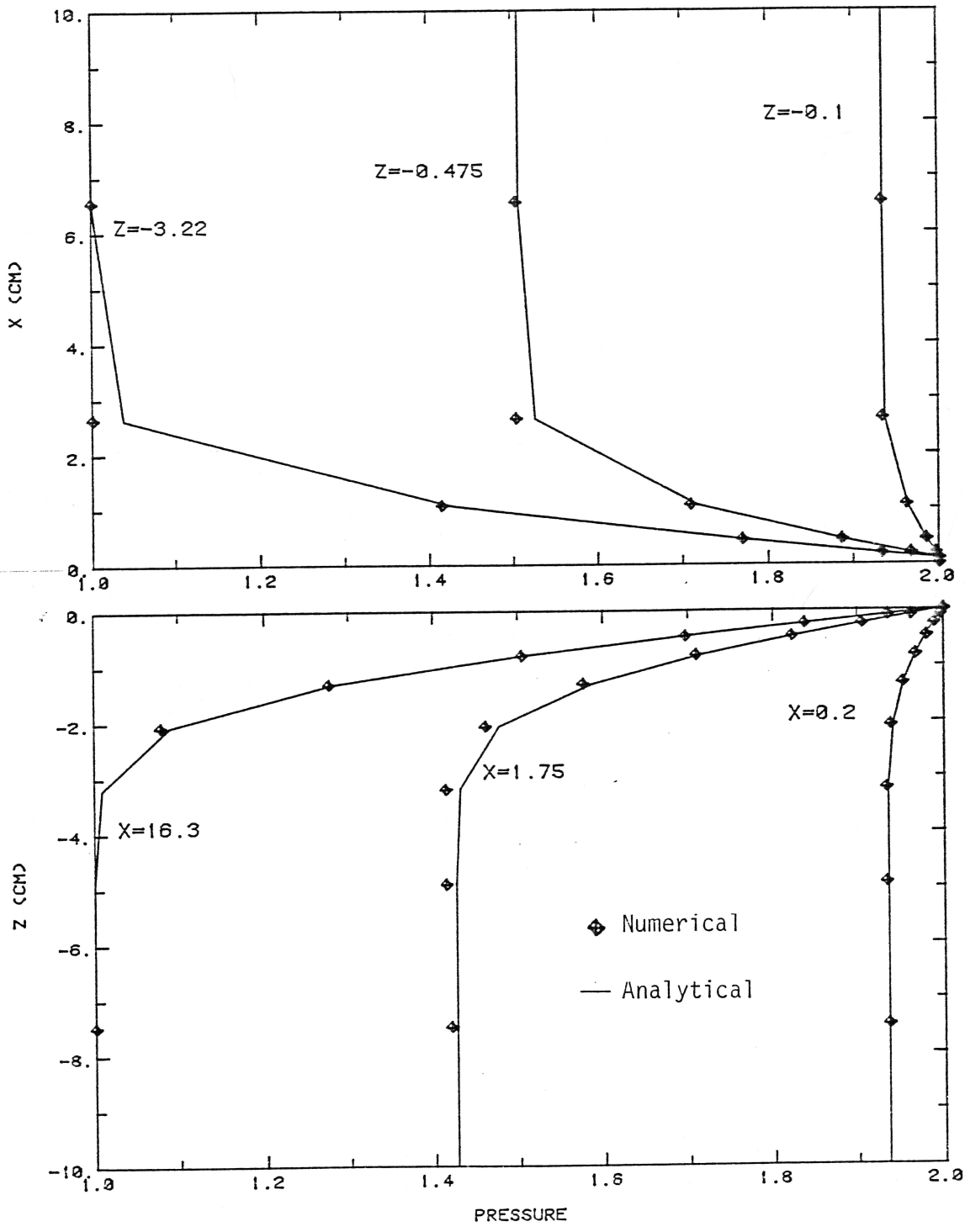

Figure 3-4b: Comparison of numerical solution for pressure to a two-dimensional analytical solution for linear flow between 2 intersecting constant pressure boundaries. Time step 100.

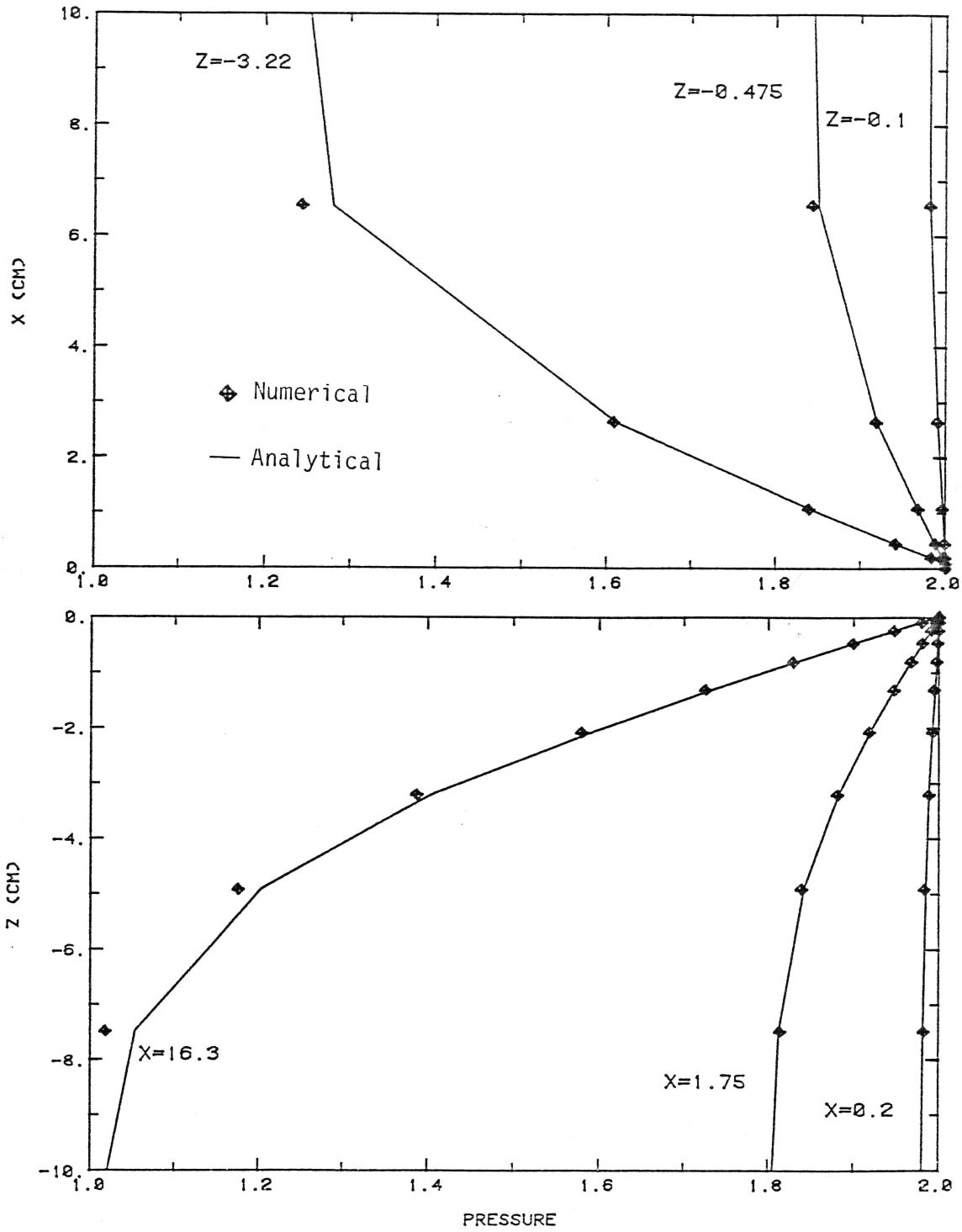

Figure 3-4c: Comparison of numerical solution for pressure to a two-dimensional analytical solution for linear flow between 2 intersecting constant pressure boundaries. Time step 1000.

4. SENSITIVITY OF MODEL TO VARIOUS PARAMETERS

The objective of this chapter is to vary the input parameters of the model to better understand how cracks in soil may affect radon flux densities. First the crack geometry is varied including crack width, spacing and depth. Next, the soil parameters are perturbed including porosity, intrinsic permeability, and diffusion coefficient. Finally, the effect of decreasing, increasing, and sinusoidally varying the atmospheric pressure conditions with time are tested. Certain paramters were kept constant for all runs in this report; they are summarized in the following table:

Table 4-1: Constant parameters for all runs

Air dynamic viscosity	1.8×10^{-4} g/cm/s
Radon diffusion coefficient in air (D_d)	0.1 cm^2/s
Radon decay constant	2.1×10^{-6} s^{-1}
Radon production rate	5.25×10^{-2} atoms/cm^3/s
Depth to watertable	30 meters
Initial atmospheric pressure (Po)	85,000. Pascals

The air and radon parameters were taken from Schery et. al. (1984). The depth to watertable is an estimate

for Schery's field site. The initial atmospheric pressure is a common one for the field site.

The production rate of radon per unit volume of soil pore space, ϕ, was determined for the soil at the field site of Schery et. al. (1984), by observing that the radon concentrations asymptotically reach a maximum value of 25,000 atoms/cm^3 with depth. Far below the surface, where radon-222 escape is negligible, the rate of radioactive decay must be balanced by the production rate. This requires that $C^{\infty} = \phi / \lambda$, where C^{∞} is the radon-222 concentration deep in the soil. Knowing that the decay constant for radon, λ, equals 2.1×10^{-6} s^{-1} yields a value of 5.25×10^{-2} atoms/cm^3/s for the production rate.

All runs were started from steady-state pressure and concentration conditions. For pressures, the steady-state conditions are the soil and cracks being at atmospheric pressure. In other words, velocities are zero, and there is no advection. The steady-state concentration profile incorporates the effects of diffusion, decay, production, and boundary conditions in equilibrium with one another. Equilibrium conditions will vary slightly based on the width and depth of the crack. Figure 4-1 shows a steady-state diffusive profile for cracks 400 cm deep, .06 cm wide, and spaced 800 cm apart. The concentraton gradient is strongest near the surface. Notice that the concentration profile reaches an asymptotic value with depth of 25,000 atoms/cm^3 of soil

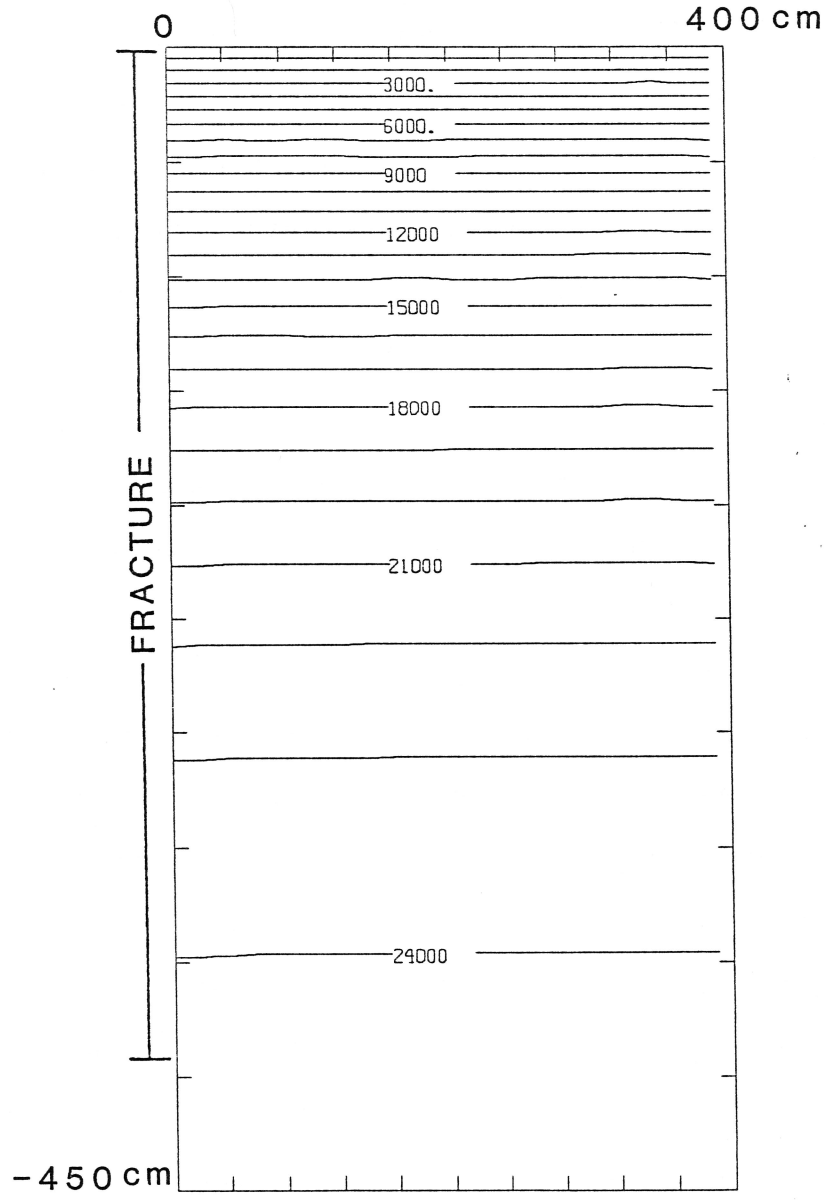

Figure 4-1: Steady-state concentration profile for soil with cracks 400 cm deep, 0.06 cm wide, and 800 cm apart.

air space.

As an introduction to this section, a generic simulation is presented to show the effects of atmospheric pressure changes over time. Showing the transient effects is important because all other runs in this section are illustrated at the last time step only. This simulation uses the parameters in tables 4-1 and 4-2 (see page 54), and cracks 400 cm deep, 0.06 cm wide, and spaced 800 cm apart. This crack configuration is used extensively in the following sections. The atmospheric pressure was decreased at a rate of 90 Pa/hr, using time steps of 900 seconds, or one-quarter hour. Figure 4-2a shows that the subsurface pressure gradient field is the same for each time step. In other words, the pressures are in a quasi-steady-state. The pressure gradients are generally towards the surface and crack, but are strongest near the bottom of the crack. The pressure gradients drive radon into the crack, where velocities are higher due to the crack's higher permeability. Radon concentrations thereby increase steadily with time in the crack (figure 4-2b). The difference in concentrations is much greater between 0.5 hours and 1.0 hours than between 1.0 hours and 2.0 hours. This indicates that changes in radon concentrations are rapid at first, eventually reaching some equilibrium. Figure 4-2c shows how the total radon flux density increases with time as the atmospheric pressure decreases. The increase in flux is nonlinear for

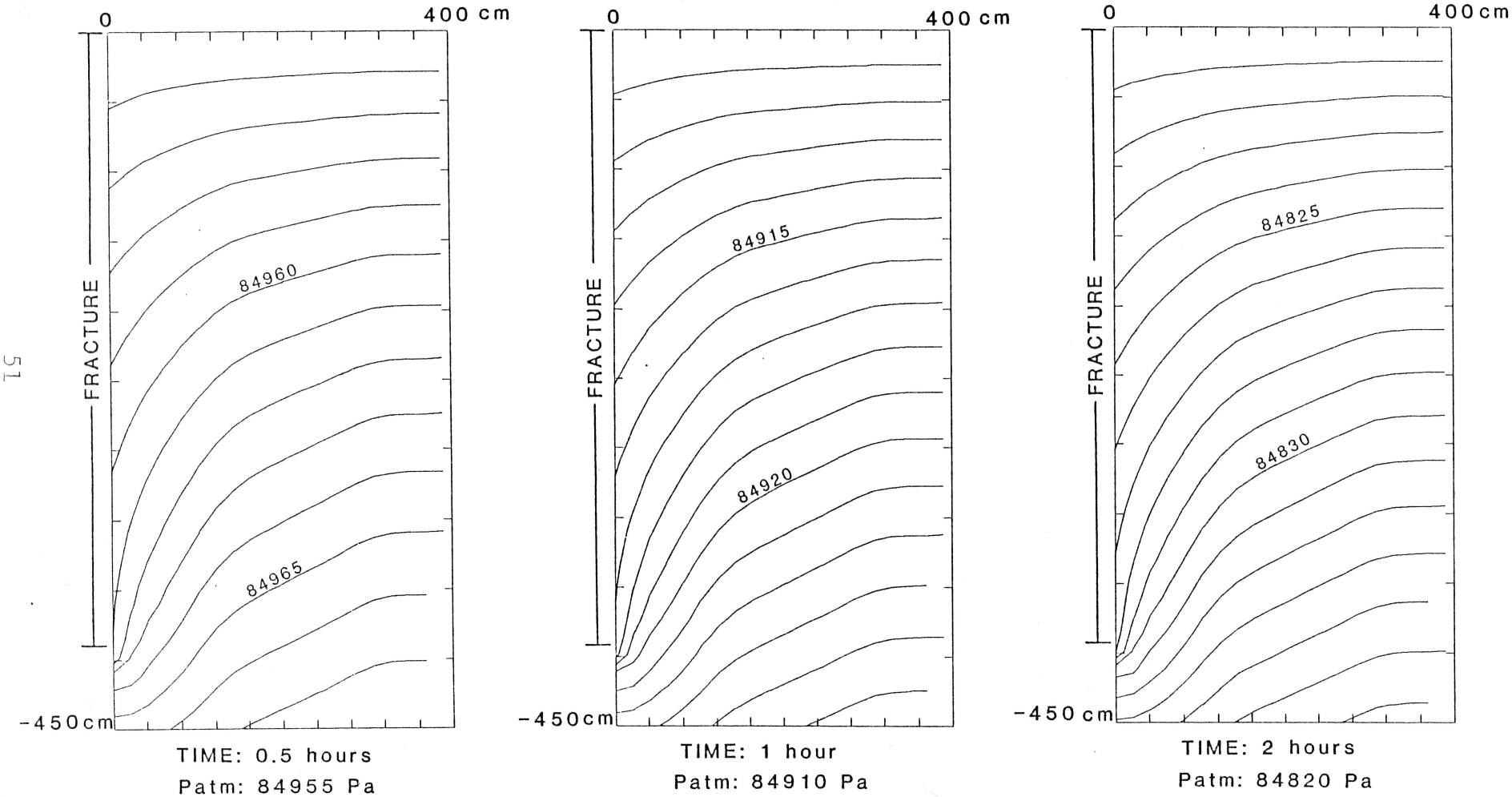

Figure 4-2a: Effect of decreasing atmospheric pressure with time at a rate of 90 Pa/hr on gas pressures (Pascals) in soil with cracks 400 cm deep, 0.06 cm wide, and 800 cm apart.

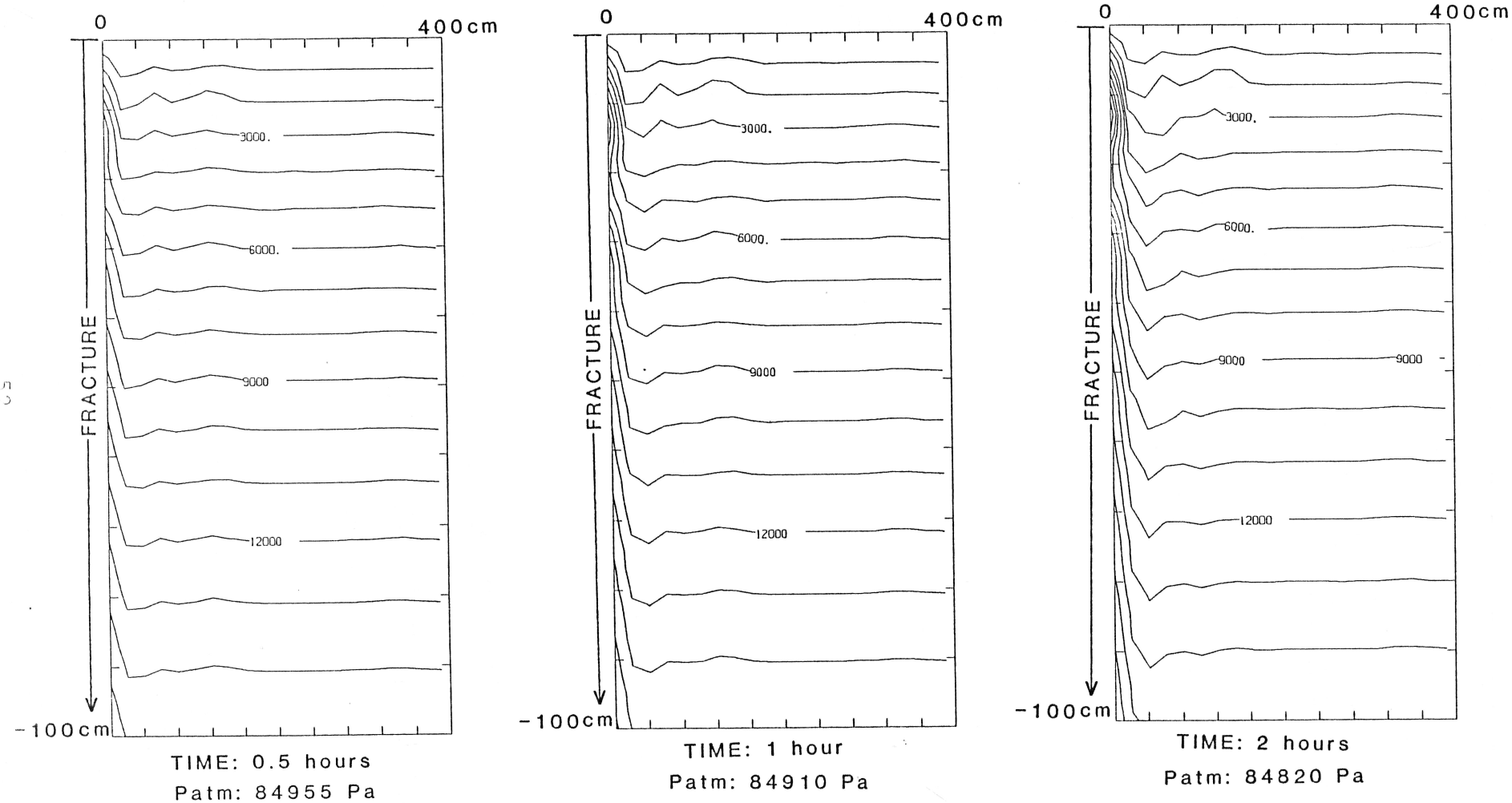

Figure 4-2b: Effect of decreasing atmospheric pressure with time at a rate of 90 Pa/hr on radon concentrations ($atoms/cm^3$) in soil with cracks 400 cm deep, 0.06 cm wide, and 800 cm apart.

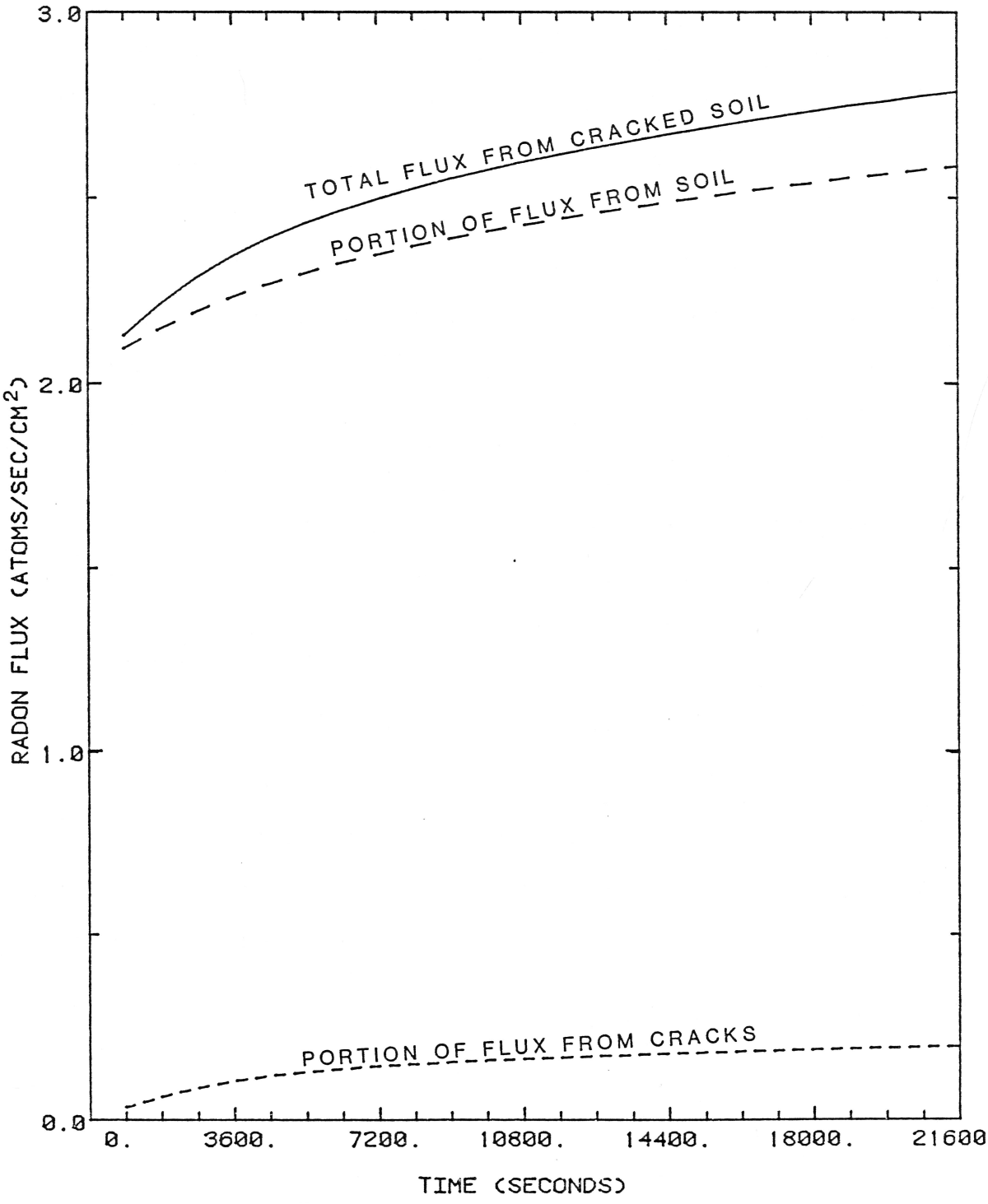

Figure 4-2c: Effect of decreasing atmospheric pressure with time at a rate of 90 Pa/hr on radon flux from soil with cracks 400 cm deep, 0.06 cm wide, and 800 cm apart.

the first hour or two, while radon concentrations are still increasing. Thereafter, once radon concentratons have reached equilibrium, the increase in flux per unit time is constant, proportional to the decrease in atmospheric pressure. The portion of flux from the crack and the portion from the soil are also shown in figure 4-2c. The portion of flux from the crack is much smaller because the cracks are very small compared to the surrounding soil. In mathematical terms, to calculate the portion of flux density from the crack, the advective flux integral (2.3.3.2) has been divided by the crack width.

4.1 Crack Geometry

Cracks of different depths, widths, and spacings were modeled to see how much total flux density could be enhanced in comparison to one-dimensional soil model. All other parameters were kept constant for the runs in this section, and are summarized in table 4-2.

Table 4-2: Constant parameters for runs in Section 4.1

Soil porosity (n)	0.35
Soil intrinsic permeability (k)	2.7×10^{-8} cm^2
Radon diffusion coefficient in soil (D_{d*})	2.6×10^{-2} cm^2/s
Change in atmospheric pressure per unit time (dPatm/dt)	-90. Pa/hr
Time increment (Δt)	900. seconds

The soil and radon parameters were taken from Schery et. al. (1984). The change in atmospheric pressure per unit time is a common one seen at the Schery field site. The choice of the time increment was discussed before.

The percent increase between the results of the cracked soil model and a one-dimensional soil model after six hours of simulation time were used for comparison. The one-dimensional model uses the same governing equations and boundary conditions developed in chapter 2, except that no cracks are included in the soil. The one-dimensional model also uses very similar initial conditions those shown in figure 4-1, except that concentrations are assumed to be uniform in the (horizontal) x-direction. The results of the one-dimensional model are shown in various locatons throughout section 4.1. For instance, the flux densities predicted by the one-dimensional model are shown in figure 4-6c (page 65) and are labelled "NO CRACKS". The pressures and concentrations predicted by the one-dimensional model essentially the same as those shown in figures 4-7a and 4-7b (pages 67 and 68). The formula for calculating the percent increase between the model with cracks and the model without cracks (all other parameters being equal) is:

$$(4.1)\quad \frac{\text{flux from model w/ cracks - flux from 1-D model}}{\text{flux from 1-D model}} \times 100$$

Results were compared at a time of 6 hours. At this time,

flux densities predicted by the model seemed to be increasing at a fairly constant rate.

4.1.1 Crack spacing

The effect of crack spacing on a relatively shallow crack (30 cm) can be seen in figure 4-3. As cracks are spaced closer together, the flux density increases. The increases in flux in comparison to a one-dimensional model are very small, up to 1.5 percent.

In Figure 4-4a, when cracks are spaced far apart, say 200 cm, the pressure decrease in the crack only spreads into the soil out to a distance of about 30 cm. As cracks are spaced closer together, 56 cm for instance, the pressure decreases in adjacent cracks touch. When the cracks are very closely spaced, 16 cm apart, the pressure decreases extend past the midpoint between adjacent cracks, enhancing the total decrease of pressure in the soil.

Close crack spacing results in the reduction in pressure gradients towards the surface and crack, yielding lower velocities, and hence less advective transport of radon into the crack. As a result, as cracks are more closely spaced, concentrations in the crack decrease (figure 4-4b). However, figure 4-4c shows that flux density increases as cracks are more closely spaced. Although concentrations in the crack are decreasing, having a greater number of cracks per unit area causes an

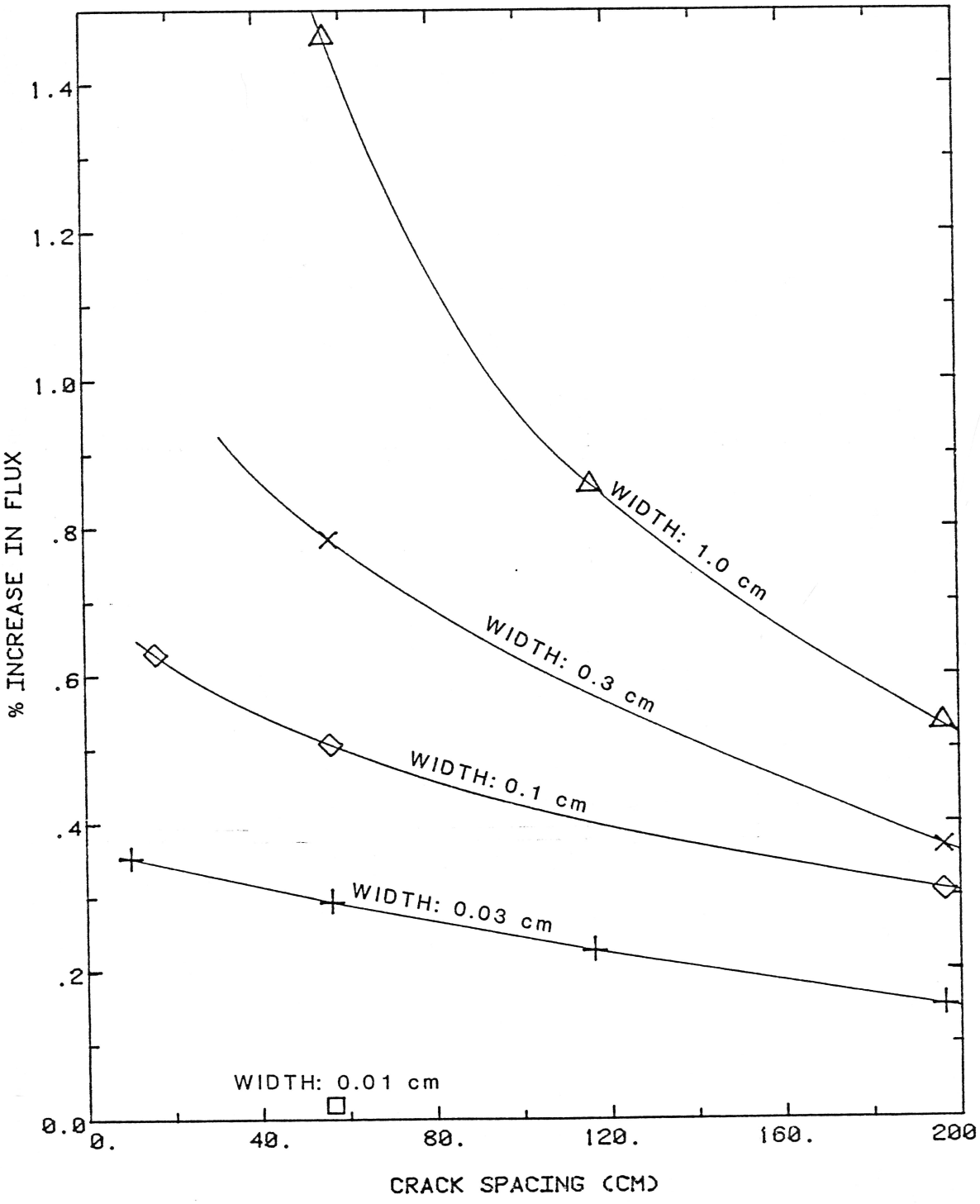

Figure 4-3: Effect of spacing and crack width on percent difference in flux density between soil with 30 cm deep cracks and soil without cracks after 6 hours of decreasing atmospheric pressure.

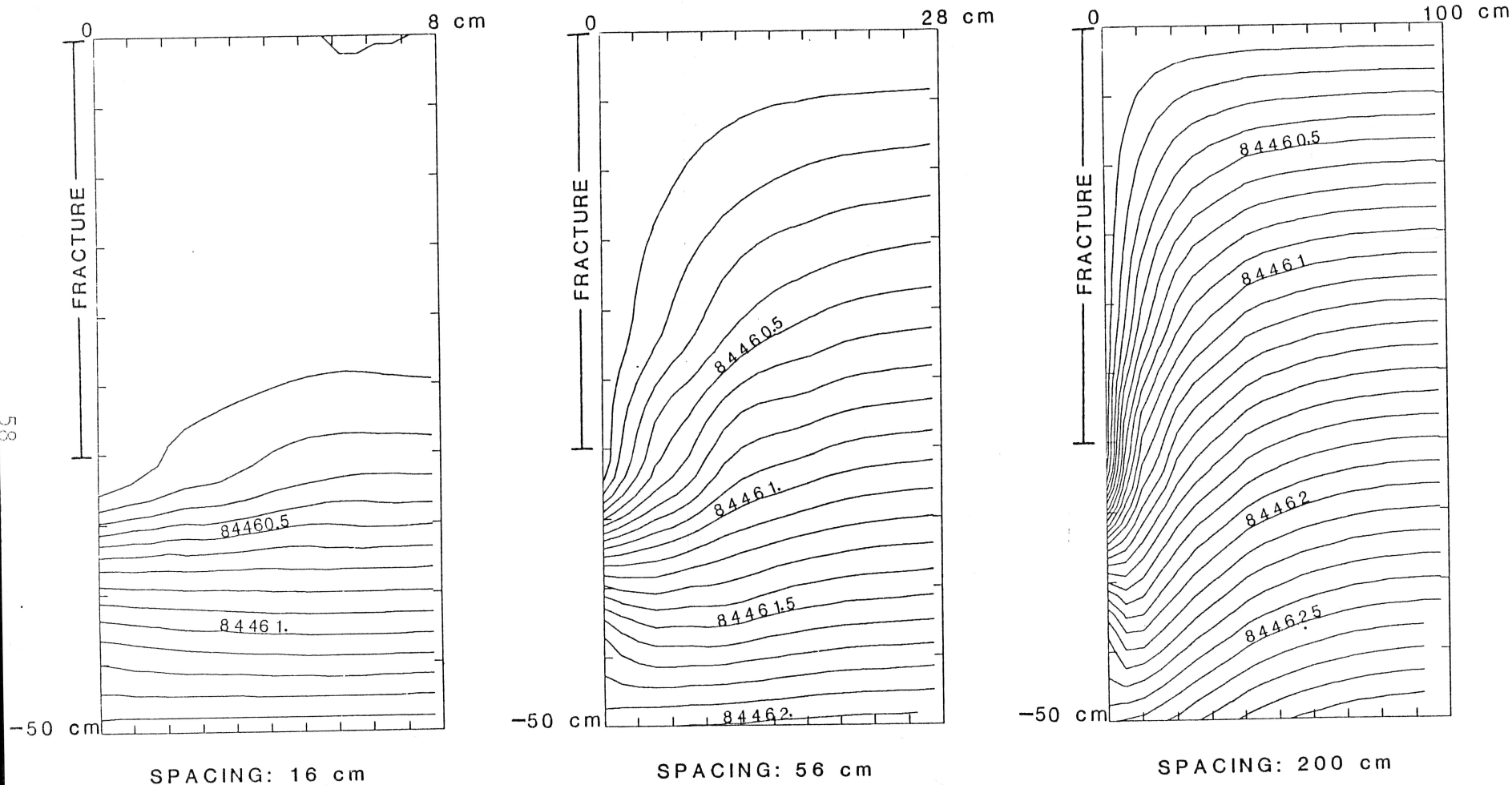

Figure 4-4a: Effect of crack spacing on gas pressures (Pascals) in soil with cracks 30 cm deep and .1 cm wide after 6 hours of decreasing atmospheric pressure. (Note: horizontal scale varies).

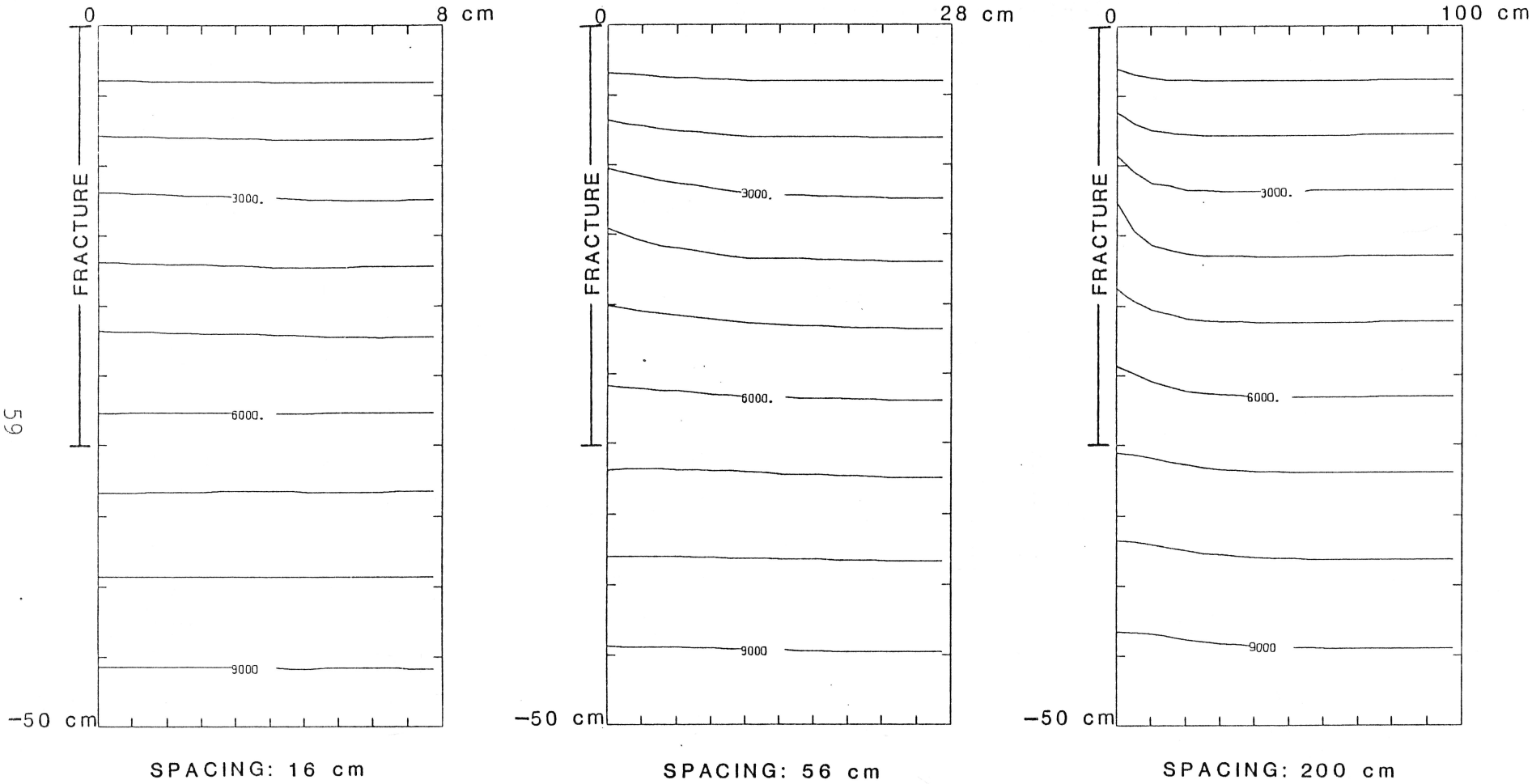

Figure 4-4b: Effect of crack spacing on radon concentrations (atoms/cm^3) in soil with cracks 30 cm deep and .1 cm wide after 6 hours of decreasing atmospheric pressure. (Note: horizontal scale varies).

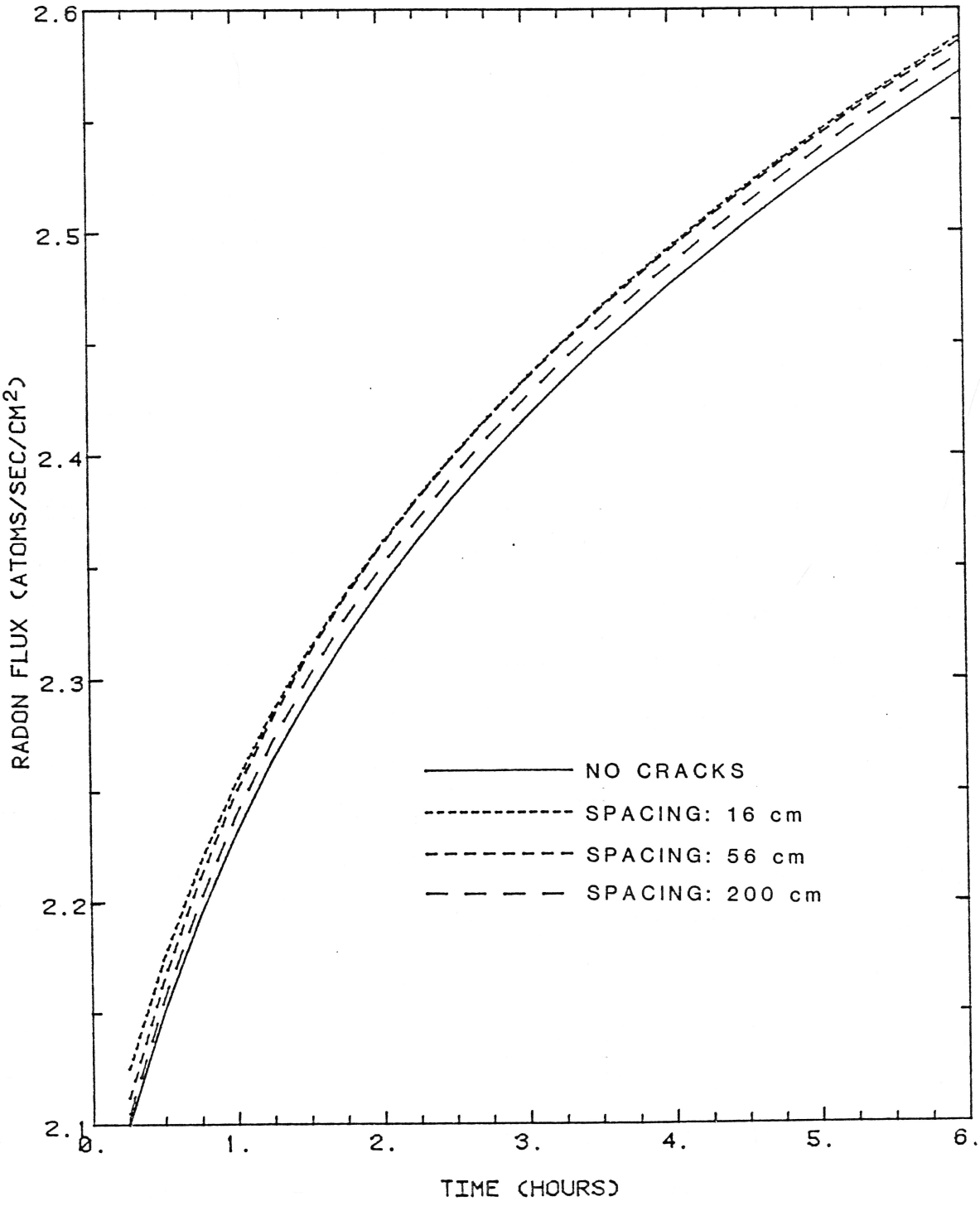

Figure 4-4c: Effect of crack spacing on radon flux density from soil with cracks 30 cm deep and .1 cm wide during 6 hours of decreasing atmospheric pressure.

increase in flux.

Figure 4-5 shows that effects of spacing for a relatively deeper crack (400 cm) are different from those for a shallow crack. The increases in flux are also much larger for a deep crack than for a shallow one. Closer spacing causes an increase in flux density until the cracks interfere, then it decreases sharply. It appears that if spacing is greater than depth, then fluxes increase with closer crack spacing. This is the same result seen for a shallow crack. However, if spacing is approximately less than depth, fluxes decrease with closer crack spacing. Figure 4-6a shows again that the closer cracks are spaced, the weaker are the pressure gradients towards the crack. Also, in figure 4-6b closer spacing again results in lower concentration gradients near the crack and surface. Lower pressure and concentration gradients oppose the effect of closer crack spacing, which is to increase the flux density. In figure 4-6c instead of the flux density for cracks spaced at 200 cm being greater than for 400 cm, it is actually less than the flux density for 800 cm. A limit is reached when crack spacing is less than crack depth (400 cm), and the effects of reduced pressure and concentration gradients cause the flux density to decrease.

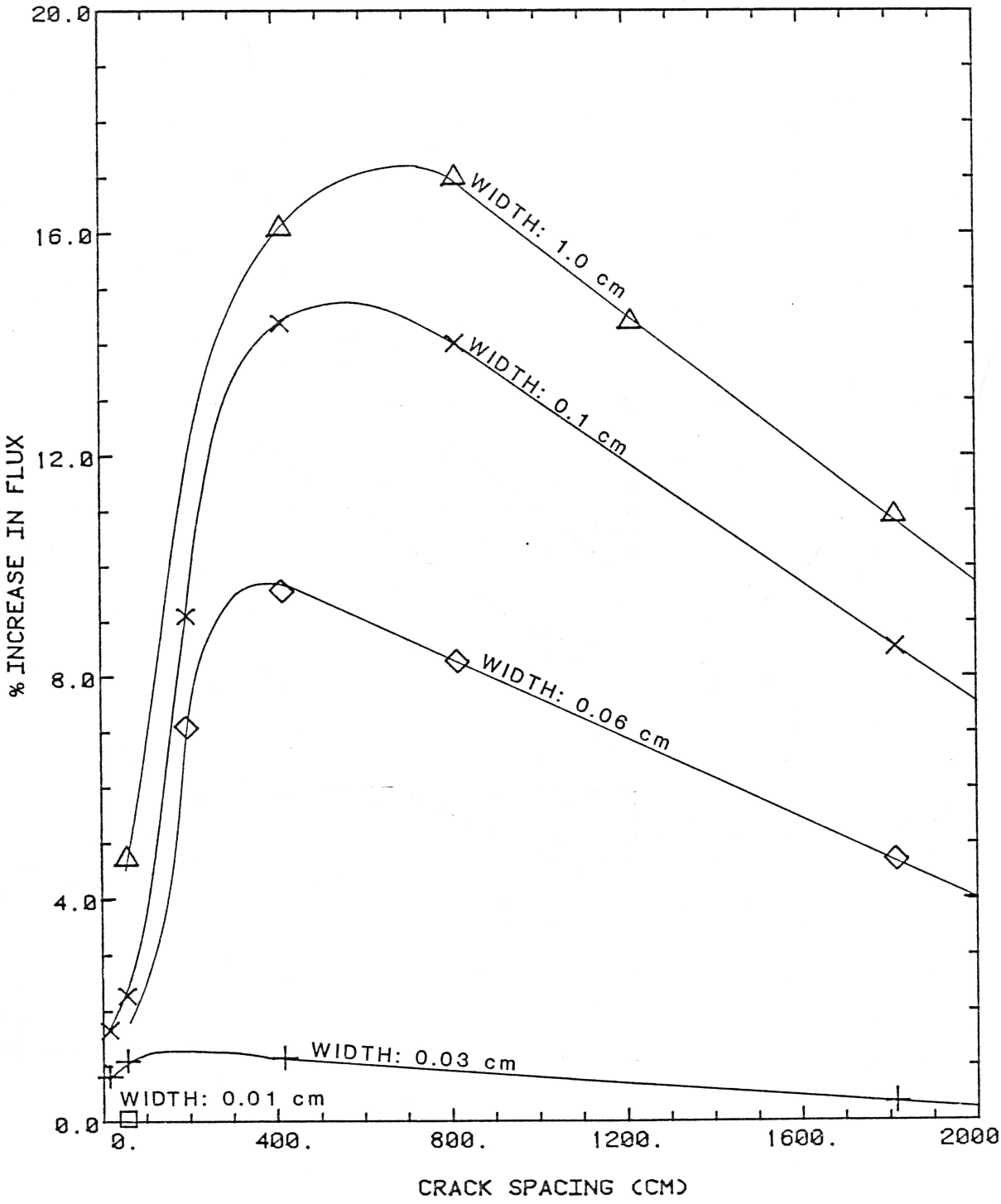

Figure 4-5: Effect of crack width and spacing on percent difference in flux density between soil with 400 cm deep cracks and soil without cracks after 6 hours of decreasing pressure.

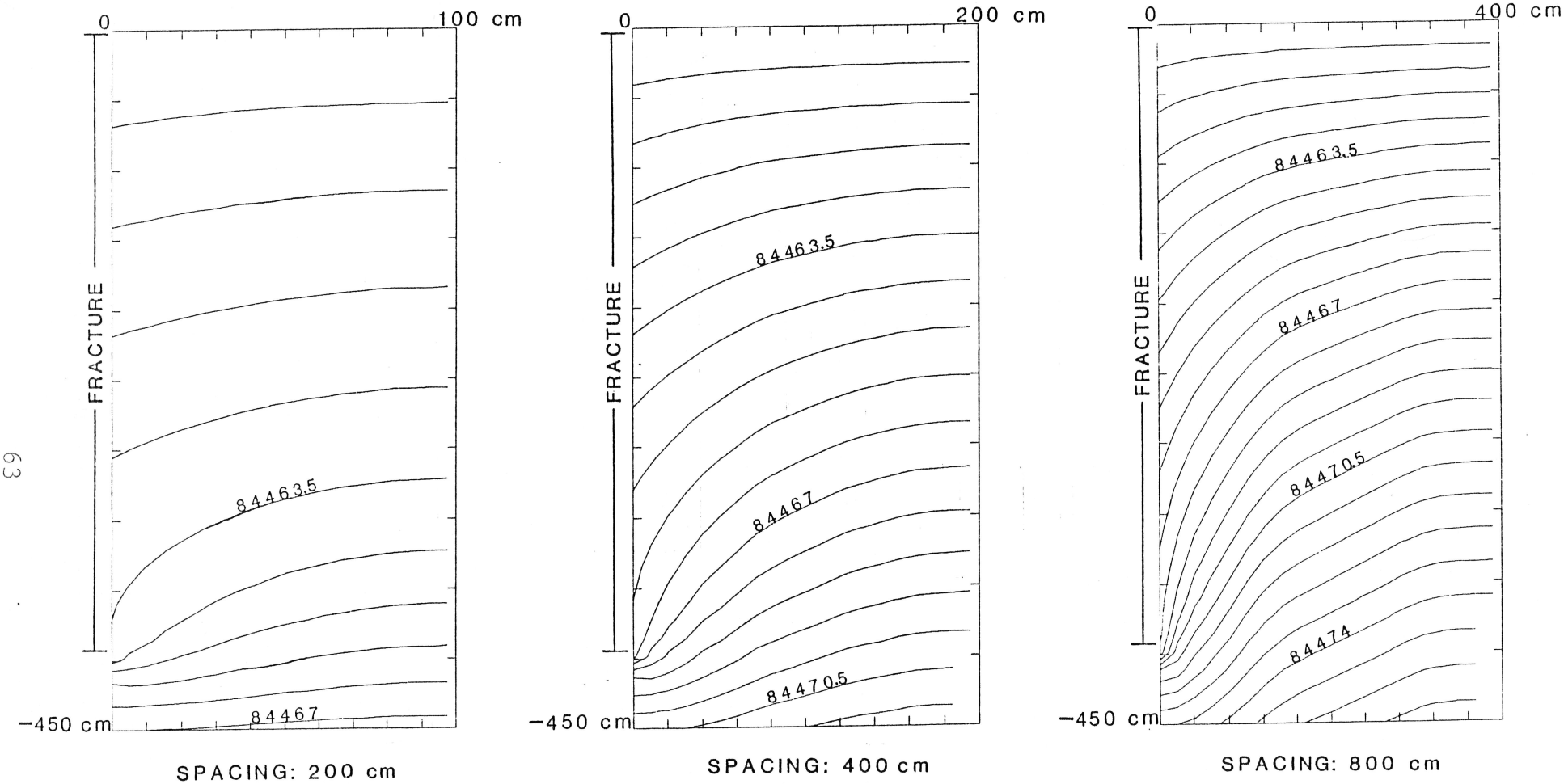

Figure 4-6a: Effect of crack spacing on gas pressures (Pascals) in soil with cracks 400 cm deep and .06 cm wide after 6 hours of decreasing atmospheric pressure. (Note: horizontal scale varies).

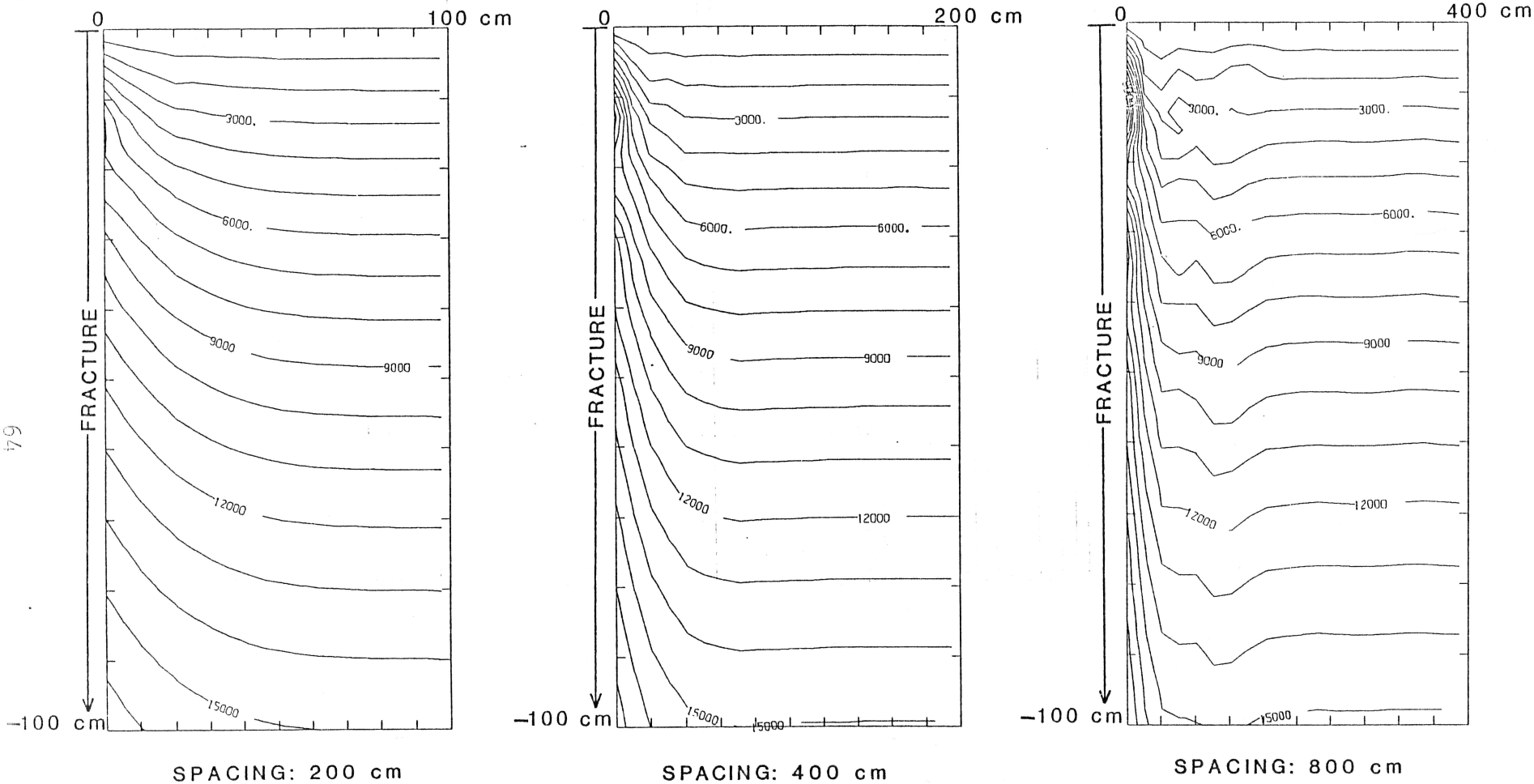

Figure 4-6b: Effect of crack spacing on radon concentrations ($atoms/cm^3$) in soil with cracks 400 cm deep and .06 cm wide after 6 hours of decreasing atmospheric pressure. (Note: horizontal scale varies).

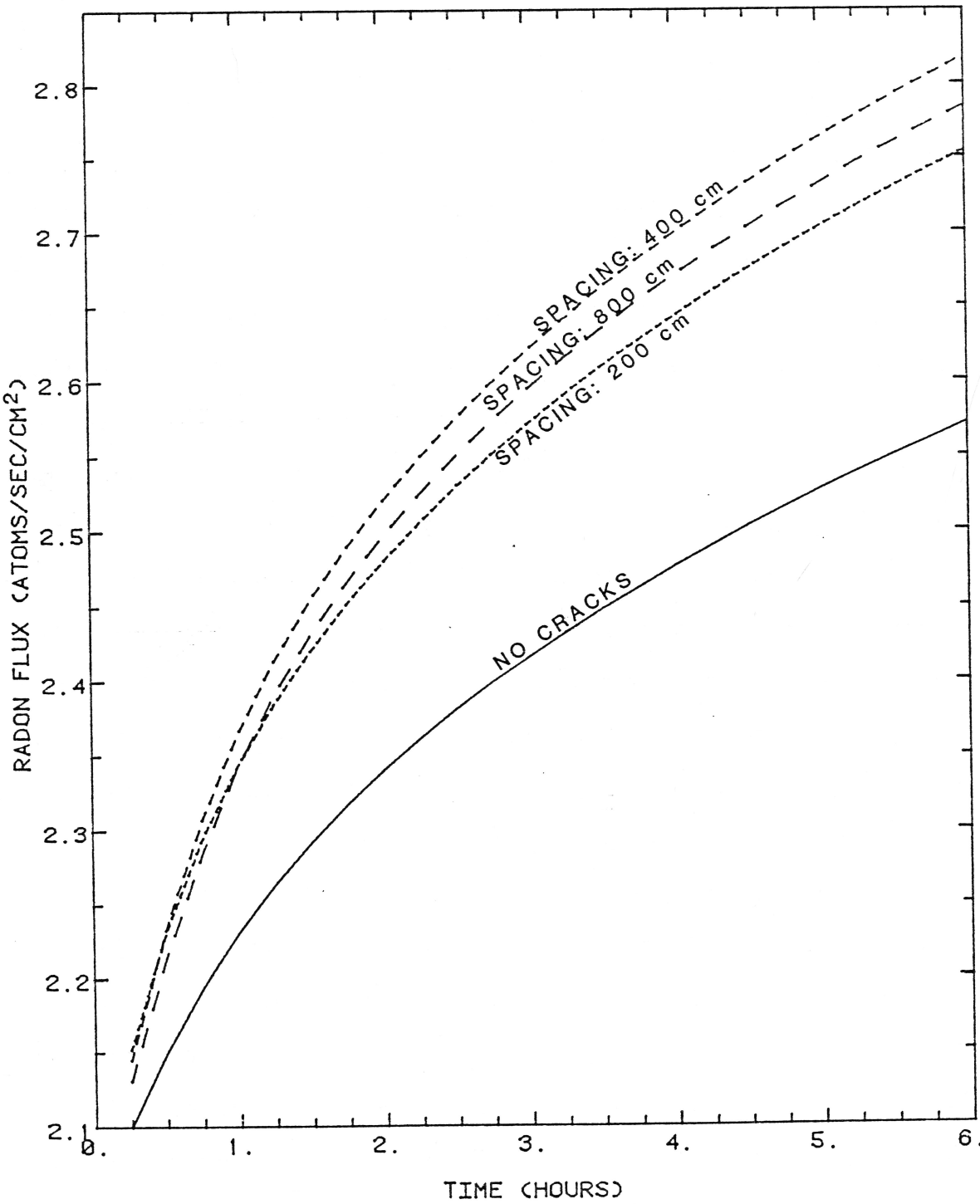

Figure 4-6c: Effect of crack spacing on radon flux density from soil with cracks 400 cm deep and .06 cm wide during 6 hours of decreasing atmospheric pressure.

4.1.2 Crack width

Figure 4-3 shows the effects of crack width on the percent increase in flux density in comparison to the one-dimensional model for a relatively shallow crack (30 cm). As the crack width increases, so does the flux density. There seems to be a logarithmic dependence on width. The increase in flux becomes more nonlinear as the crack width increases; the permeability of the crack is equal to the square of crack width divided by 12, according to equation 2.2.3. As seen in figure 4-7a, a crack 0.01 cm wide (permeability = 8.3×10^{-6} cm^2) has almost no effect on the pressure gradients, while a crack 0.03 cm wide (permeability = 7.5×10^{-5} cm^2) allows surface pressures to drop nearly to the bottom of the crack. Pressure contours in soil with a 1.0 cm wide crack (permeability = 8.3×10^{-2} cm^2) look similar to those for a 0.03 cm crack; once the crack is wide enough to allow surface pressure to drop essentially to the bottom, increasing the crack width further will make little difference in the pressure contours in the soil.

Increasing the width from 0.01 cm to 0.03 cm causes concentrations to increase slightly in the crack (figure 4-7b) due to the increase in pressure gradients towards the crack. However, a 1.0 cm wide crack causes concentrations to actually decrease towards the crack. The diffusion coefficient in the crack is four times greater than the diffusion coefficient in the soil. The

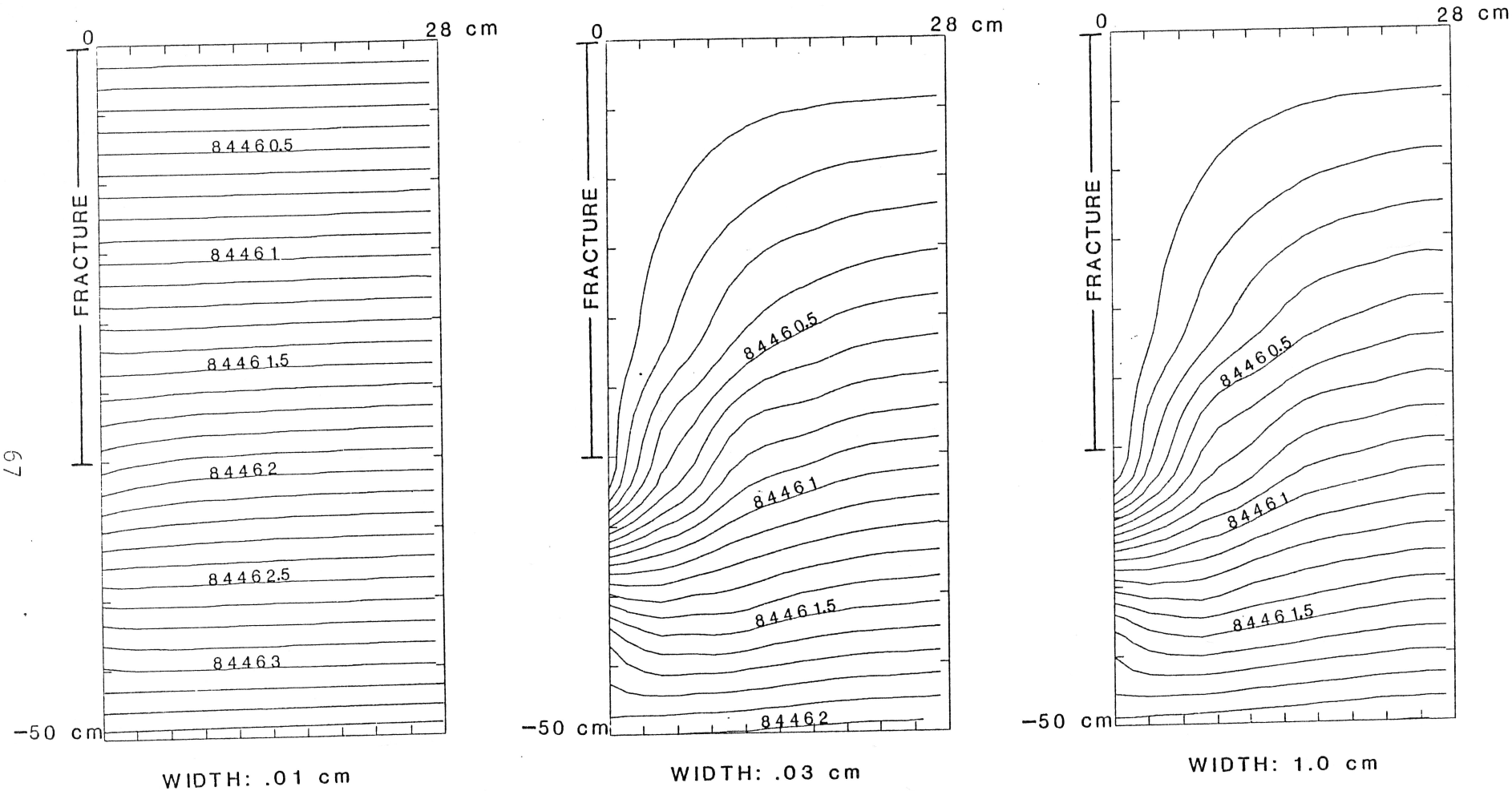

Figure 4-7a: Effect of crack width on gas pressures (Pascals) in soil with cracks 30 cm deep and spaced 56 cm apart after 6 hours of decreasing atmospheric pressure.

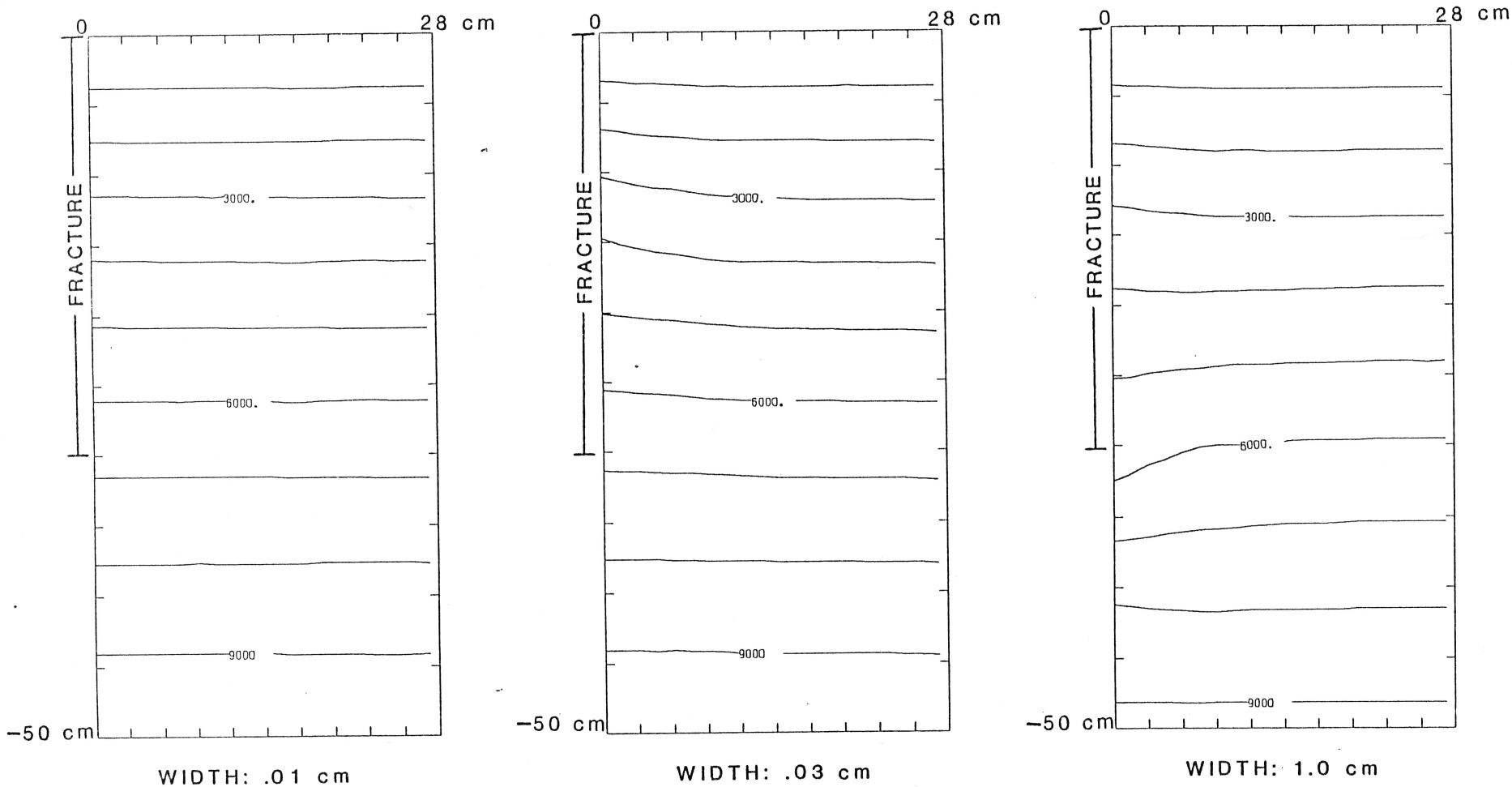

Figure 4-7b: Effect of crack width on radon concentrations (atoms/cm^3) in soil with cracks 30 cm deep and spaced 56 cm apart after 6 hours of decreasing atmospheric pressure.

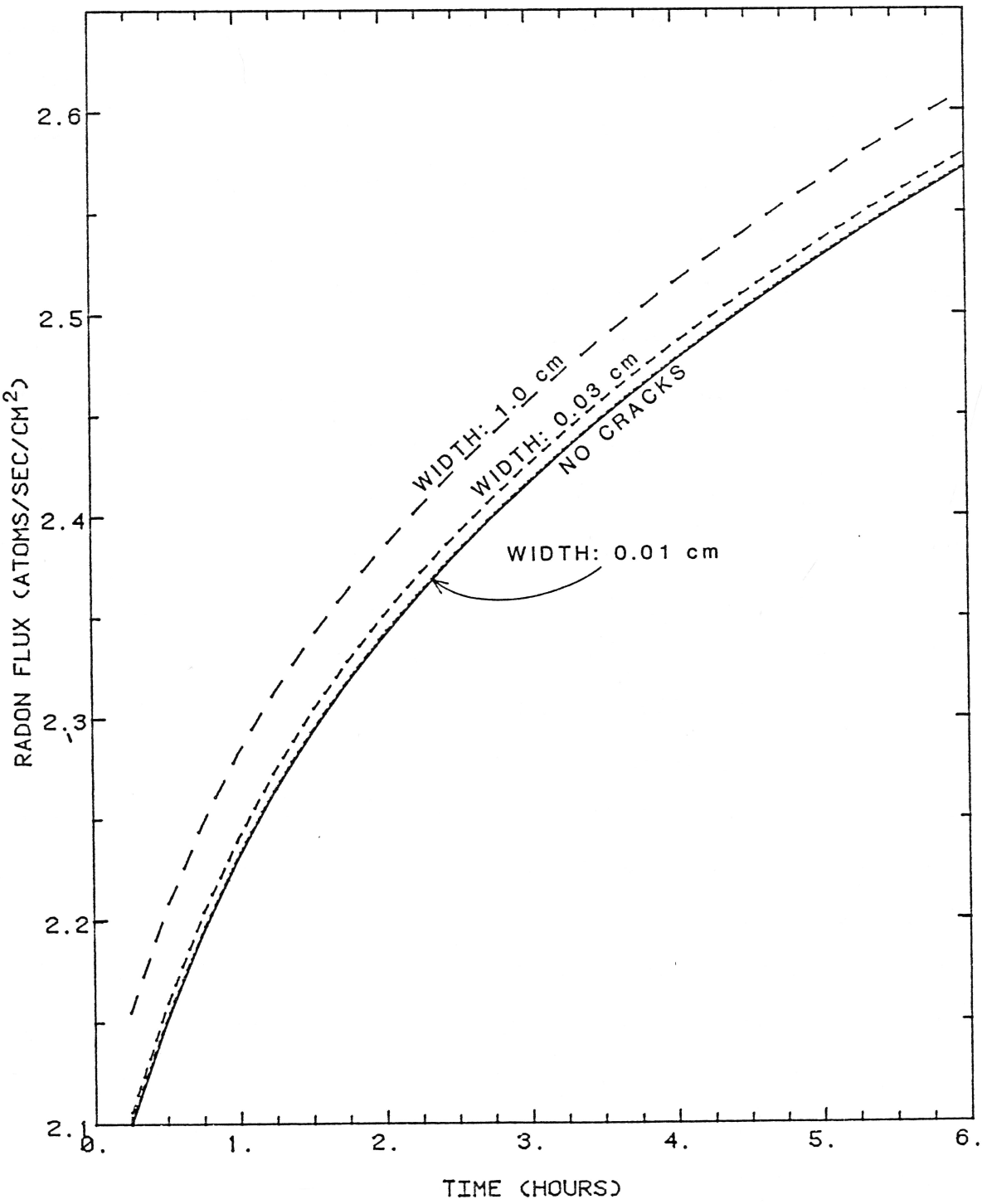

Figure 4-7c: Effect of crack width on radon flux density from soil with cracks 30 cm deep and spaced 56 cm apart during 6 hours of decreasing atmospheric pressure.

larger crack diffusion coefficient moves radon more quickly to the surface, lowering concentrations in the crack and adjacent soil. A 0.01 cm crack, which did not affect the pressure and concentration profiles, also does not increase the radon flux density in comparison to a 1-D model (figure 4-7c). Even though the crack permeability for a width of 0.01 cm is 300 times greater than that of the surrounding soil, a 0.01 cm crack is essentially part of the soil. A 0.03 cm crack shows a slight increase in flux density, and a 1.0 cm crack shows a significant increase in flux density, largely due to wider cracks covering more area with a larger diffusion coefficient.

In figure 4-5, it can be seen that increasing the width of a relatively deep crack (400 cm) causes an increase in percent change in flux density compared to a one-dimensional model. In figure 4-8a, as crack width increases pressures in the crack decrease, approaching surface pressure, because the permeability of the crack increases with the square of the crack width. The gradients in the soil toward the crack become stronger, causing concentrations around the crack to increase (figure 4-8b). However, this effect is counteracted by the vertical pressure gradient in the crack becoming weaker with increasing width. The flux density becomes larger with an increase in width (figure 4-8c), mediated by the opposing affects of stronger gradients in the soil towards the crack and weaker gradients in the crack.

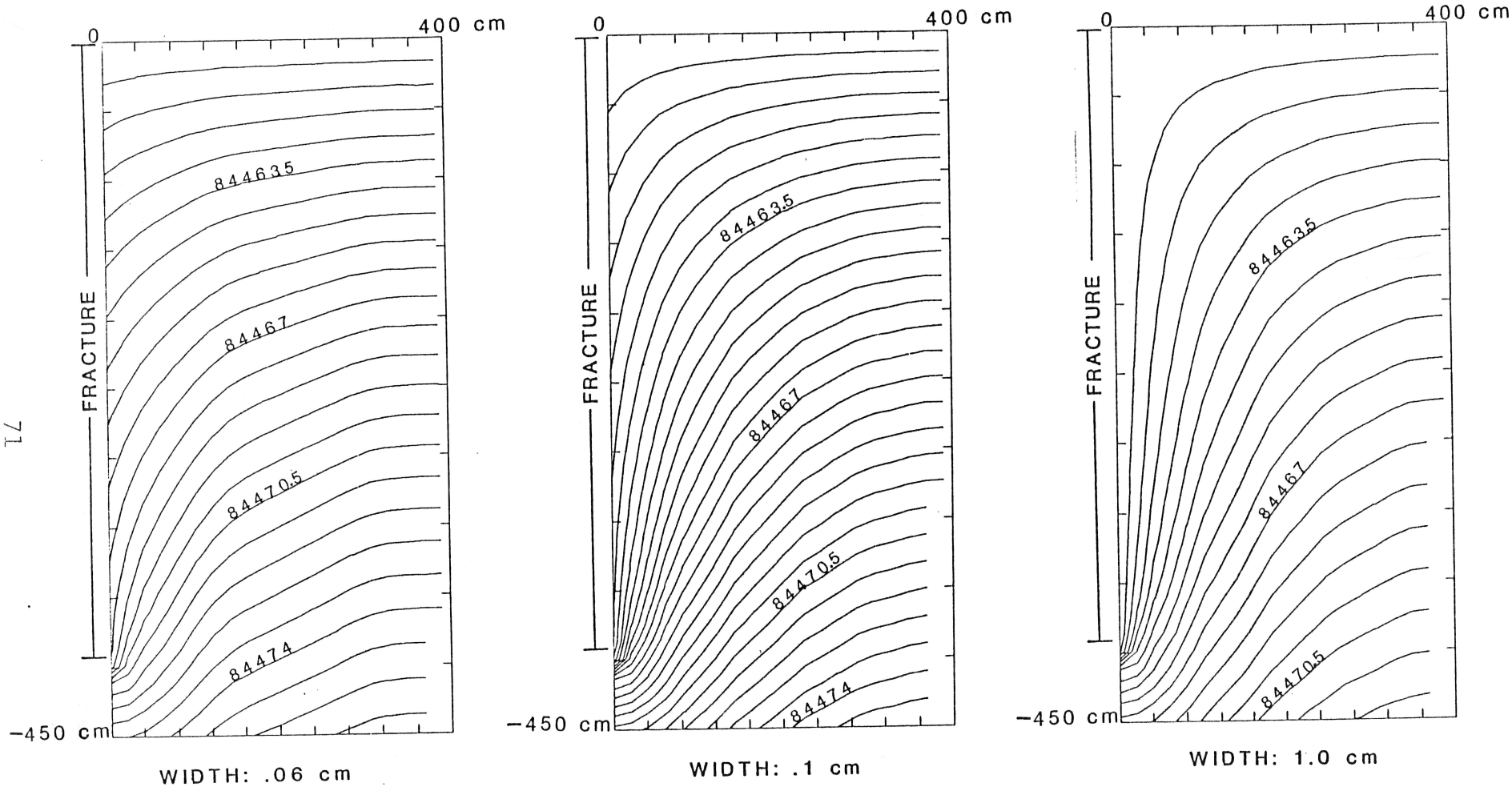

Figure 4-8a: Effect of crack width on gas pressures (Pascals) in soil with cracks 400 cm deep and spaced 800 cm apart after 6 hours of decreasing atmospheric pressure.

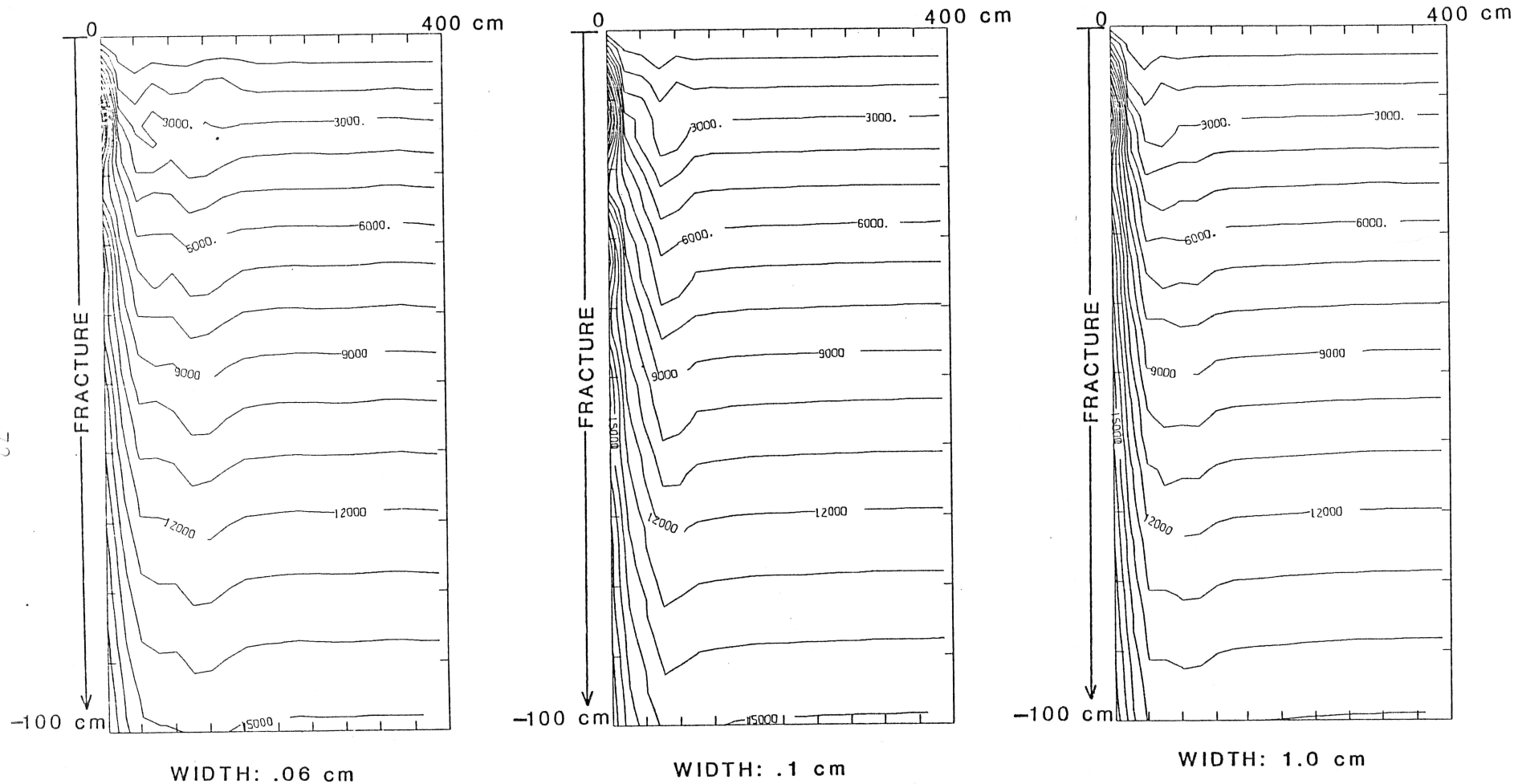

Figure 4-8b: Effect of crack width on radon concentrations (atoms/cm^3) in soil with cracks 400 cm deep and spaced 800 cm apart after 6 hours of decreasi atmospheric pressure.

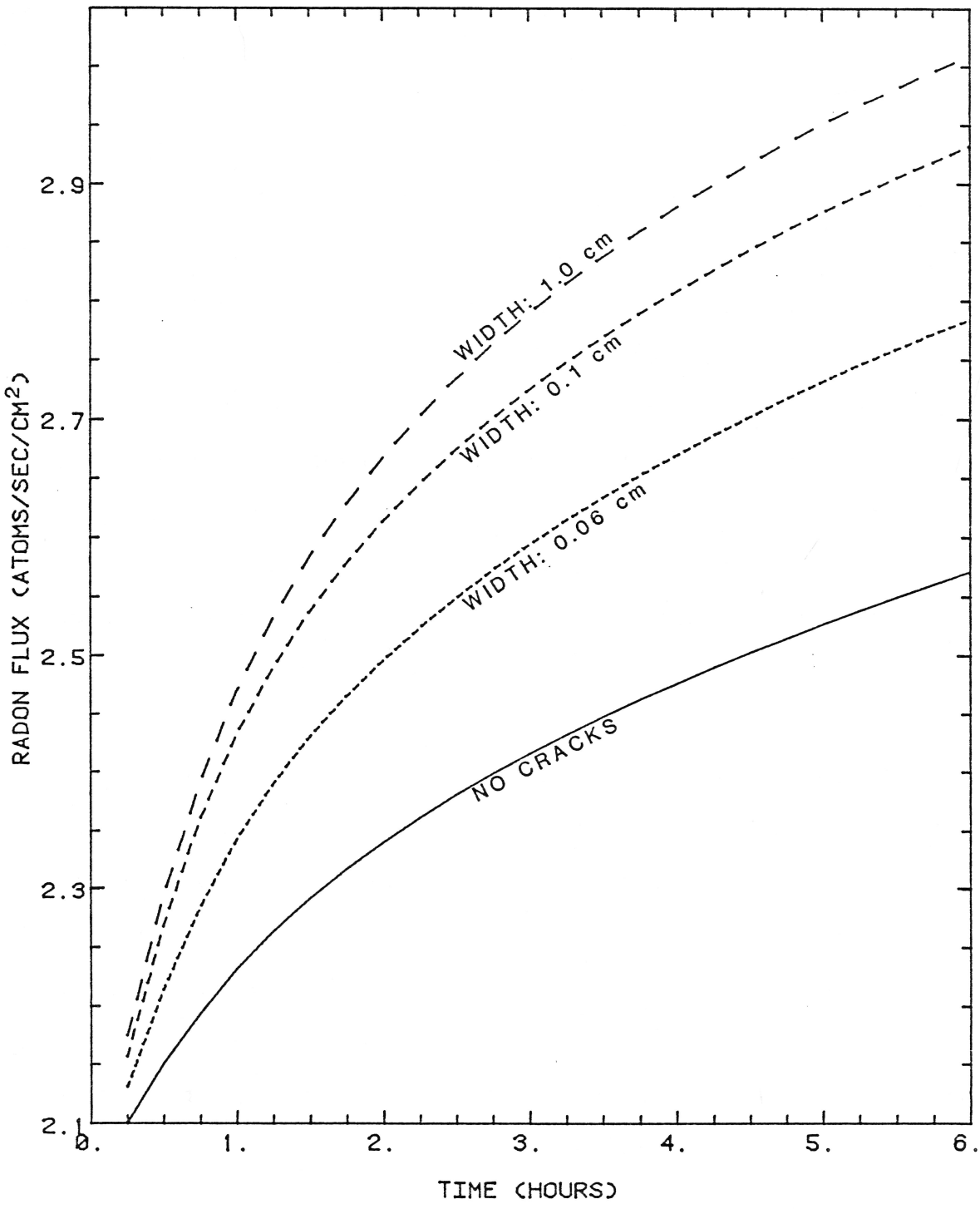

Figure 4-8c: Effect of crack width on radon flux density from soil with cracks 400 cm deep and spaced 800 cm apart during 6 hours of decreasing atmospheric pressure.

4.1.3 Crack depth

The effect of increasing crack depth is shown in figure 4-9a, where an increase in depth results in an increase in flux density compared to a 1-D model. However, the increase in flux density is not proportional to crack depth, but approaches an asymptotic value.

As the crack deepens, pressures decrease in the crack and pressure gradients in the soil curve towards the crack (figure 4-9b). Note that the highest gradients in the soil towards the crack are near the bottom of the crack. Most radon will be driven into the crack near its bottom. Also, the velocities in the crack decrease towards the bottom. As the crack deepens, lower velocities are at the bottom.

The crack brings up radon from higher concentrations at depth, and the concentrations near the surface increase (figure 4-9c) and so do the radon fluxes (figure 4-9d). However, the velocities at the bottom of the crack are becoming slower with depth. Therefore, even though the bottom of the crack may be intercepting higher radon concentrations, the rate at which the radon is brought to the surface is decreasing. As a result, the radon flux density becomes larger with increasing crack depth, but reaches an asymptotic value. This effect is also partially due to radon concentrations approaching an asymptotic value with depth (see figure 4-1).

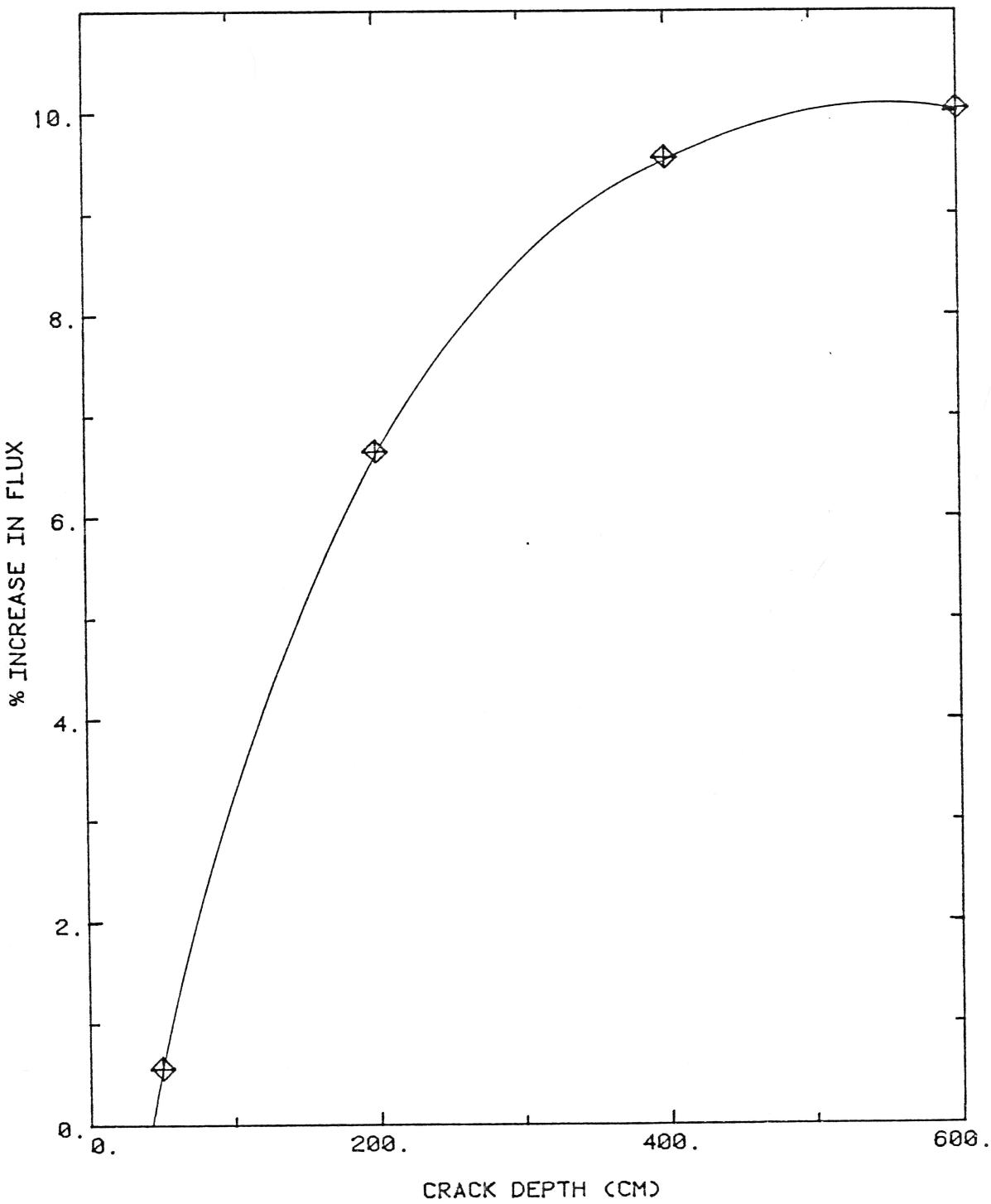

Figure 4-9a: Effect of crack depth on percent difference in flux density between soil with cracks spaced 400 cm apart and 0.06 cm wide and soil without cracks after 6 hours of decreasing pressure.

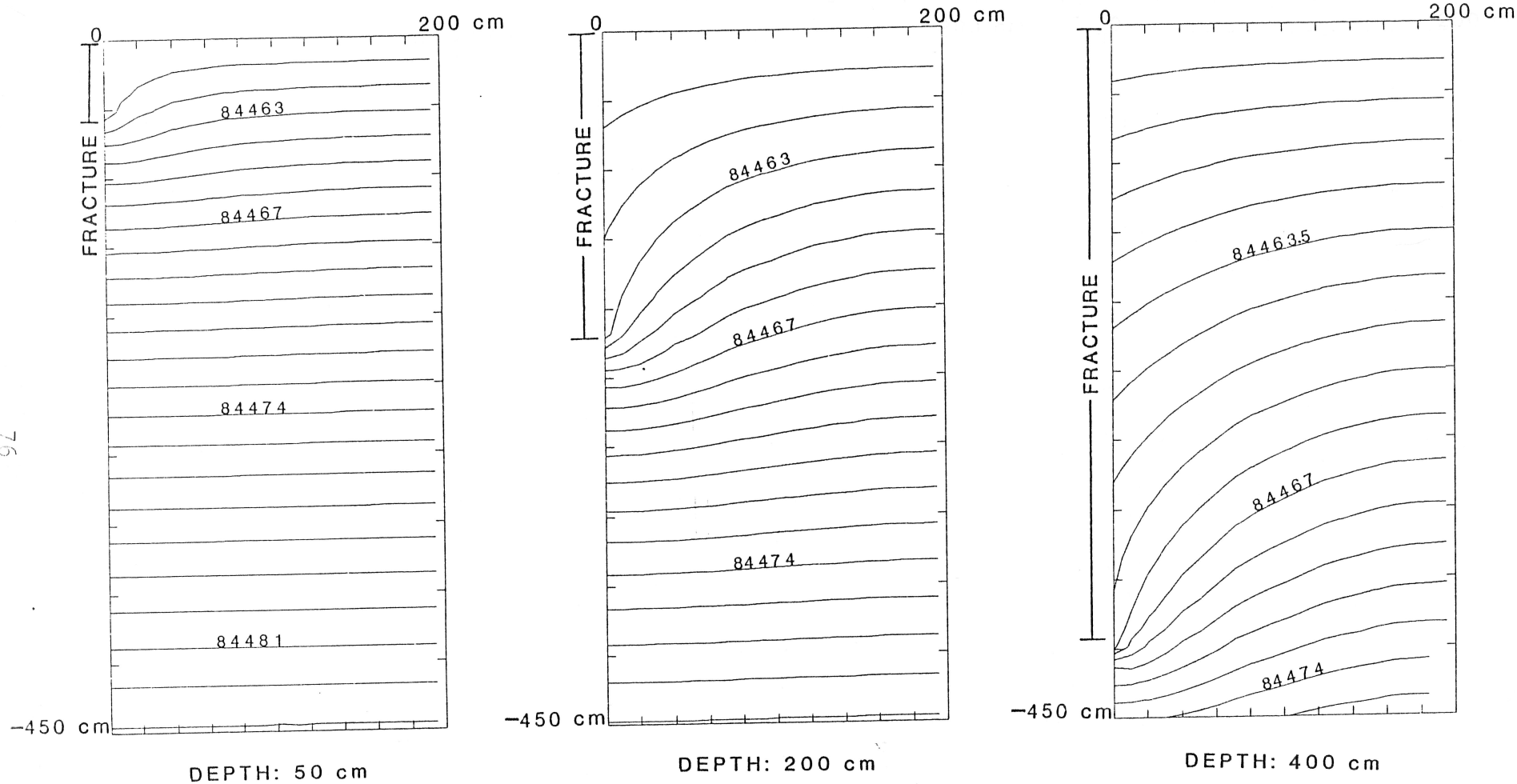

Figure 4-9b: Effect of crack depth on gas pressures (Pascals) in soil with cracks 0.06 cm wide and spaced 400 cm apart after 6 hours of decreasing atmospheric pressure.

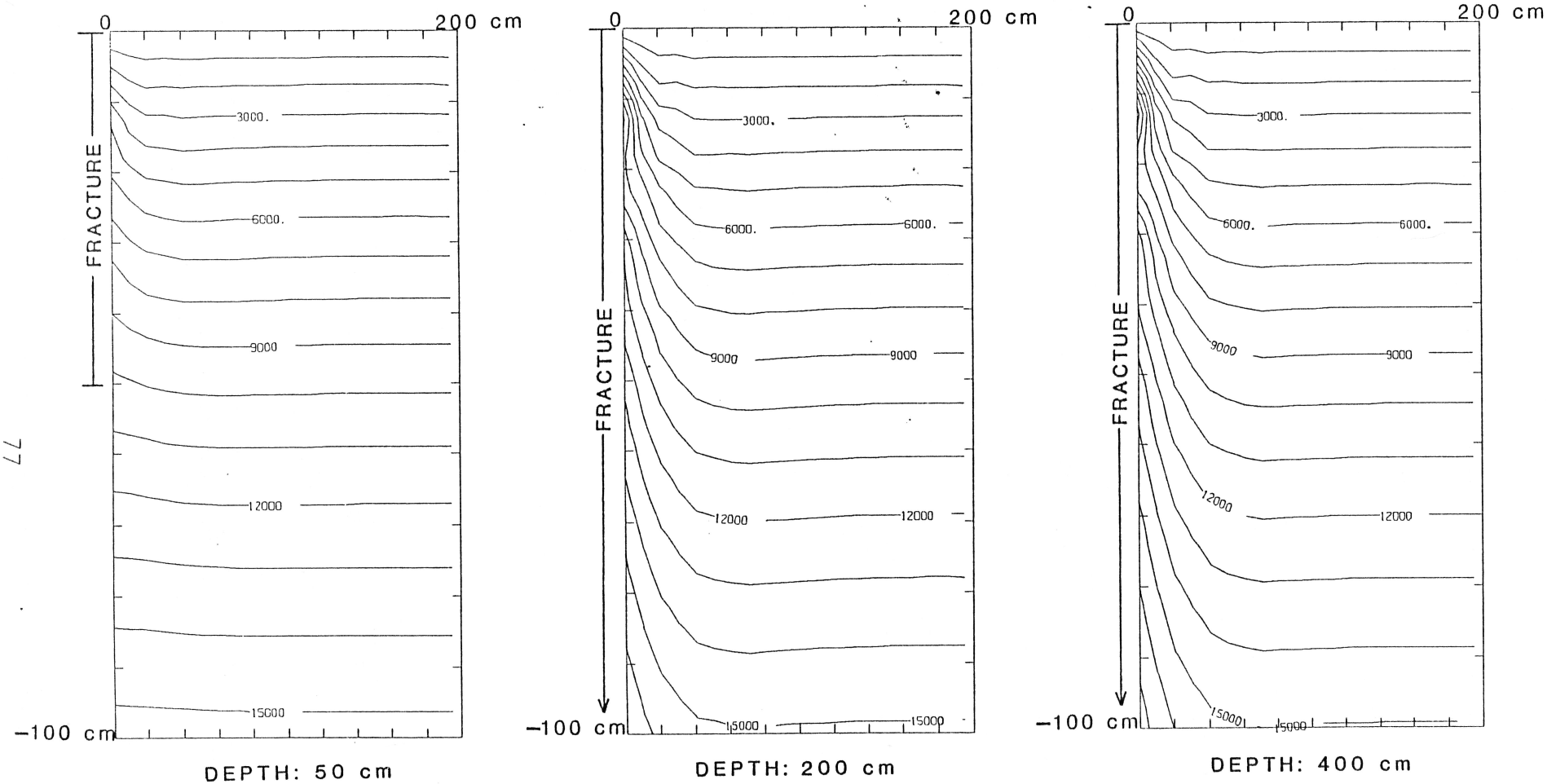

Figure 4-9c: Effect of crack depth on radon concentrations (atoms/cm^3) in soil with cracks 0.06 cm wide and spaced 400 cm apart during 6 hours of decreasing atmospheric pressure.

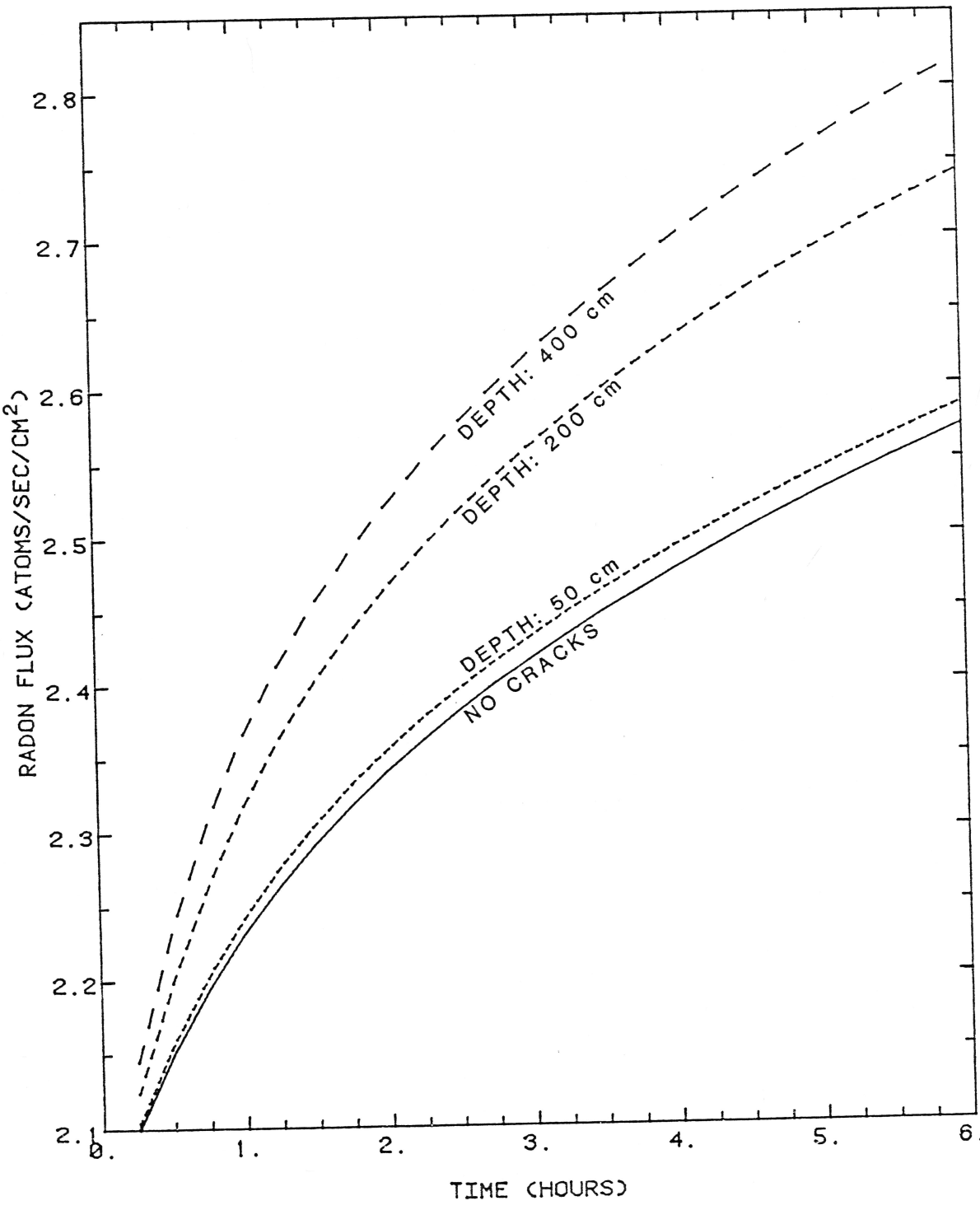

Figure 4-9d: Effect of crack depth on radon flux density from soil with cracks 0.06 cm wide and spaced 400 cm apart after 6 hours of decreasing atmospheric pressure.

4.2 Soil Type

Soil parameters used in the previous section were taken from Schery et. al. (1984). The effect of choosing different parameters contributes to an understanding of the effect of cracks in different types of soils. Certain parameters were kept constant for all runs in this section and are listed in table 4-3.

Table 4-3: Constant parameters for section 4.2

Crack spacing	800 cm
Crack width	0.6 cm
Crack depth	400 cm
Change in atmospheric pressure per unit time (dPatm/dt)	-90. Pa/hr
Time increment (Δt)	900. seconds

4.2.1 Porosity

The porosity of the soil (n) was varied while keeping the permeability (k) equal to 2.7×10^{-8} cm^2 and the radon diffusion coefficient in soil (D_d*) equal to 2.6×10^{-2} cm^2/s. In figure 4-10a, it can be seen that the pressure gradient is directly proportional to the porosity. Increasing soil porosity increases the gas storage capacity of the soil for changes in pressure, and pressure decreases do not move as far down into the soil.

Moreover, from Darcy's Law (2.2.3.2) the specific

discharge velocity is directly proportional to the pressure gradient. Therefore, the specific discharge velocity is directly proportional to the porosity. However, in the governing equation for transport (2.2.1.6), the specific discharge velocity (v) is the only term divided by the porosity. Therefore, changing porosity has no effect on the concentration maps (figure 4-10b).

However, the diffusive flux density (equation 2.2.1.1) is proportional to the porosity (figure 4-10c). Therefore, the flux density increases with an increase in porosity. Also, for larger porosities the flux density increases more per unit time. The pressure gradient in the crack increases proportionally to the porosity of the soil, resulting in more advective flux out of the crack.

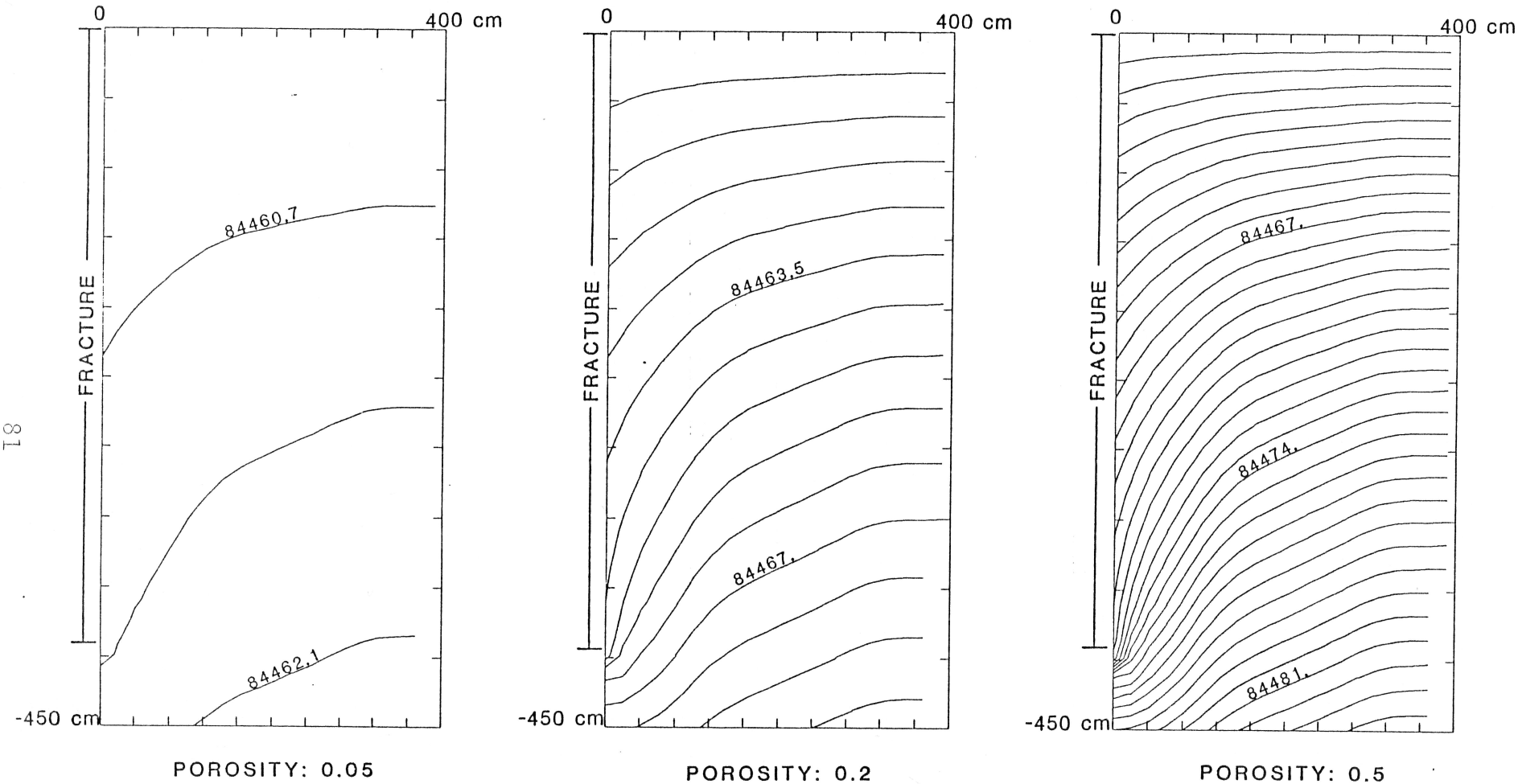

Figure 4-10a: Effect of soil porosity on gas pressures (Pascals) in soil with cracks 400 cm deep, 0.06 cm wide and spaced 800 cm apart after 6 hours of decreasing atmospheric pressure.

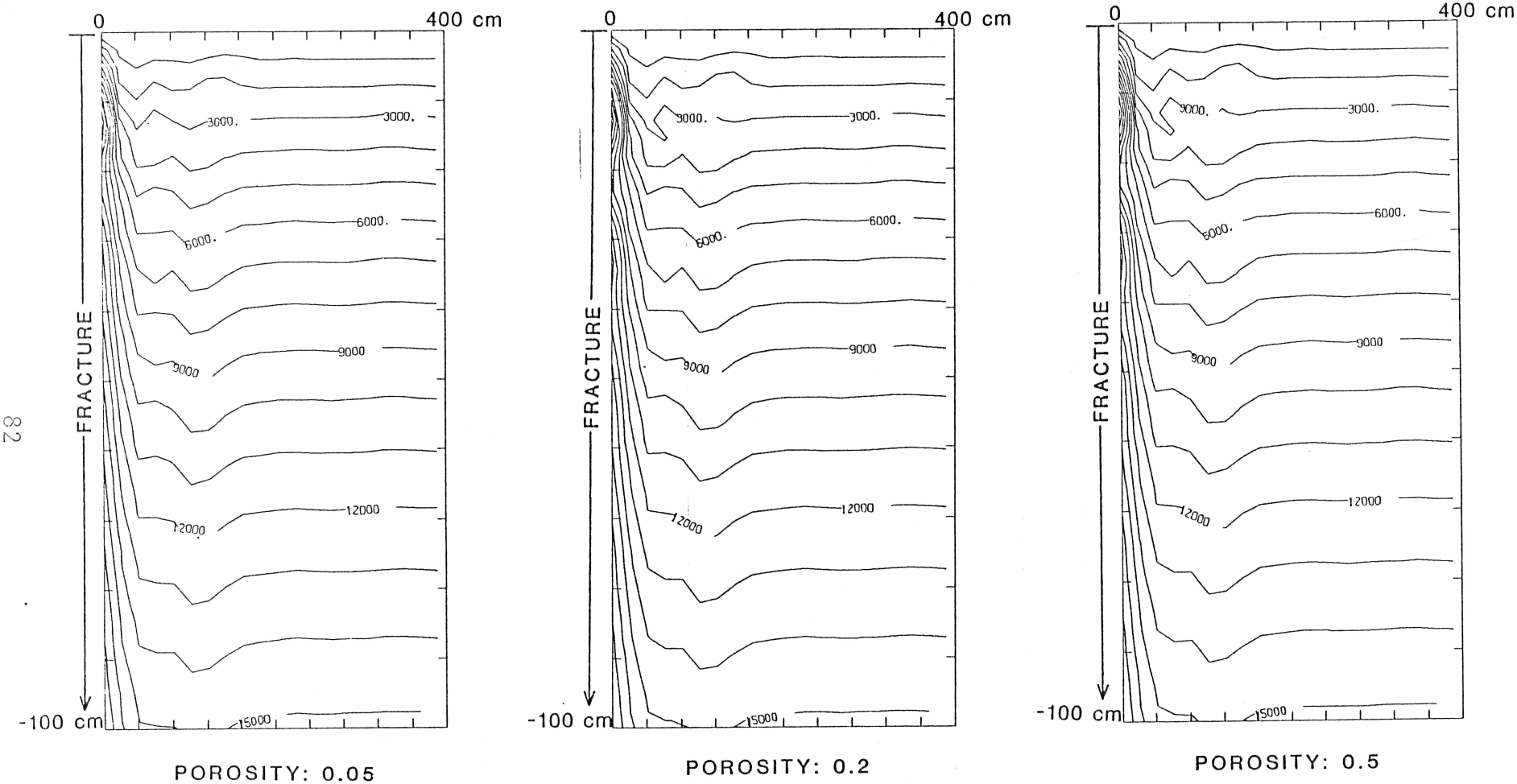

Figure 4-10b: Effect of soil porosity on radon concentrations ($atoms/cm^3$) in soil with cracks 400 cm deep, 0.06 cm wide and spaced 800 cm apart after 6 hours of decreasing atmospheric pressure.

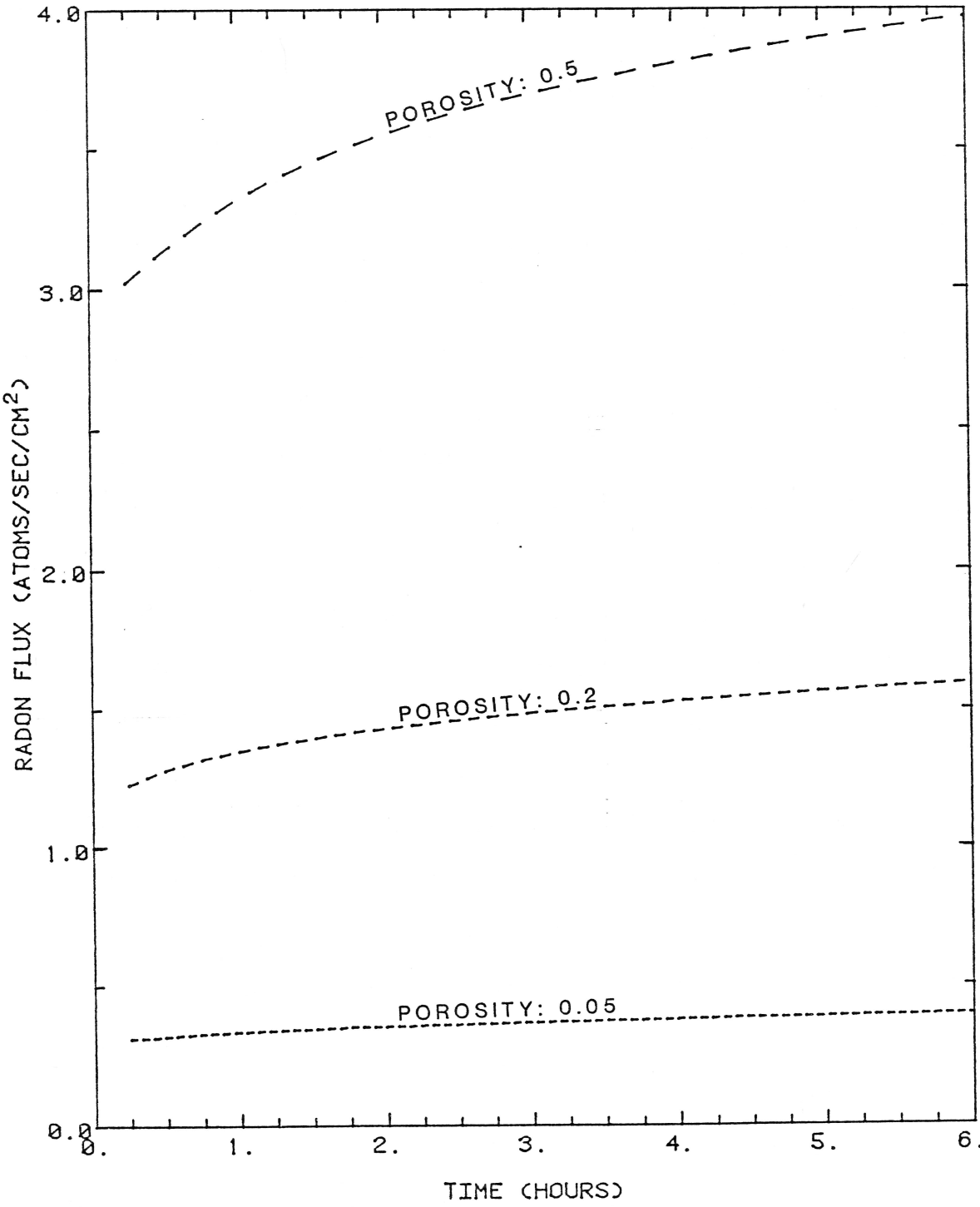

Figure 4-10c: Effect of soil porosity on radon flux density from soil with cracks 400 cm deep, 0.06 cm wide and spaced 800 cm apart during 6 hours of decreasing atmospheric pressure.

4.2.2 Permeability

The permeability of the soil was varied while the porosity was held at 0.35 and the radon diffusion coefficient in soil (D_d^*) at 2.6 x 10^{-2} cm^2/s. The permeabilities are were taken from Schery and Siegel (in prep.). The different permeabilities are for the same soil, but determined by different experimental methods.

In figure 4-11a, decreasing soil permeability prevents pressure decreases from propagating into the soil, increasing the pressure gradients in the soil and crack. Soil velocities are not changed much by a change in permeability, because velocities are proportional to the pressure gradient and the permeability, and as one increases the other decreases. Therefore, the concentrations in the soil show little change with a change in permeability (figure 4-11b). However, pressure gradients increase in the crack as the soil permeability decreases. The crack permeability remains the same, so the crack velocities increase with a decrease in soil permeability. As a result, the concentrations close to the crack increase significantly with a decrease in soil permeability. This causes a nonlinear increase in flux density (figure 4-11c) because the increase is due almost entirely to an increase in flux density from the crack while the flux density from the soil remains the same.

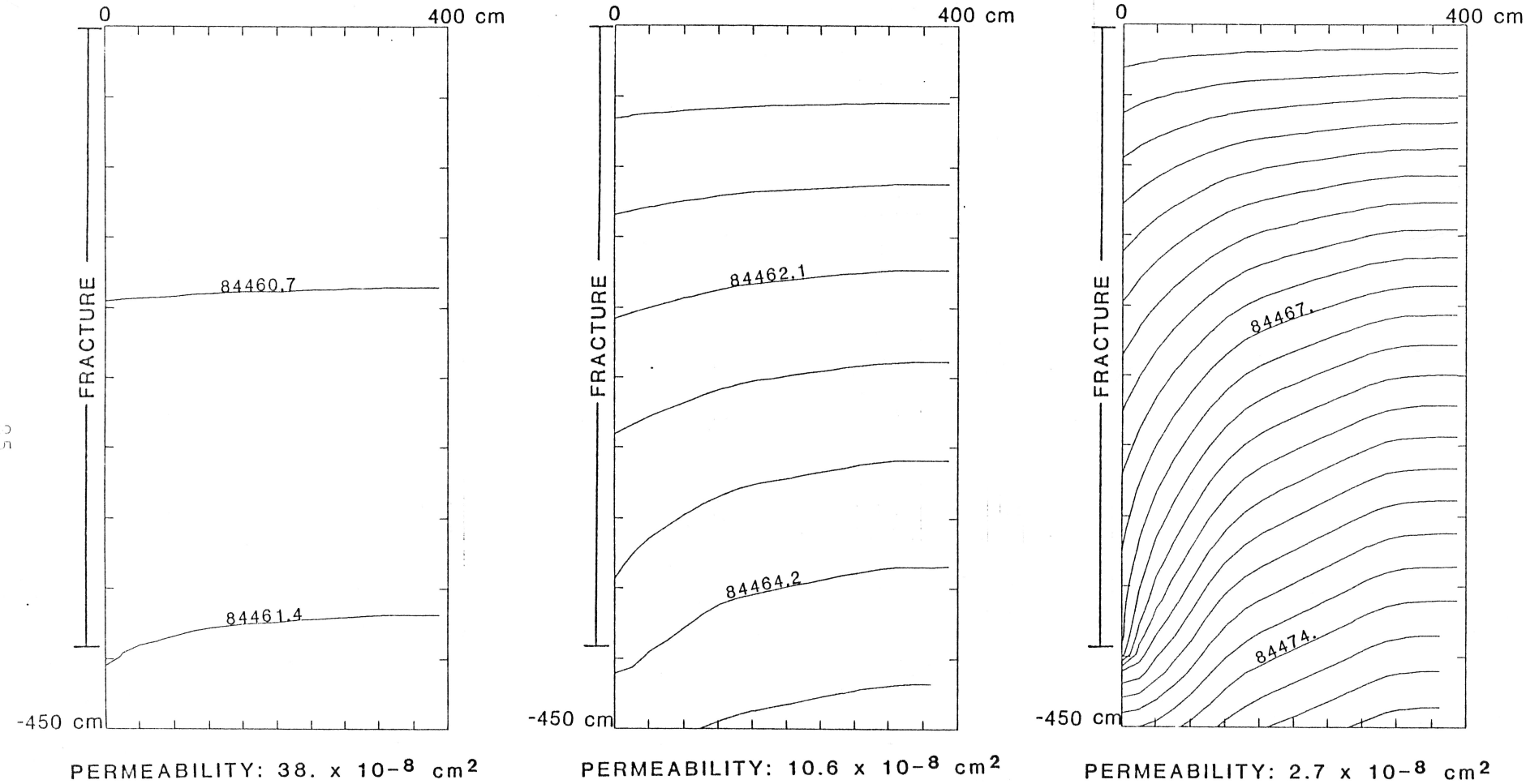

Figure 4-11a: Effect of soil permeability on gas pressures (Pascals) in soil with cracks 400 cm deep, 0.06 cm wide and spaced 800 cm apart after 6 hours of decreasing atmospheric pressure.

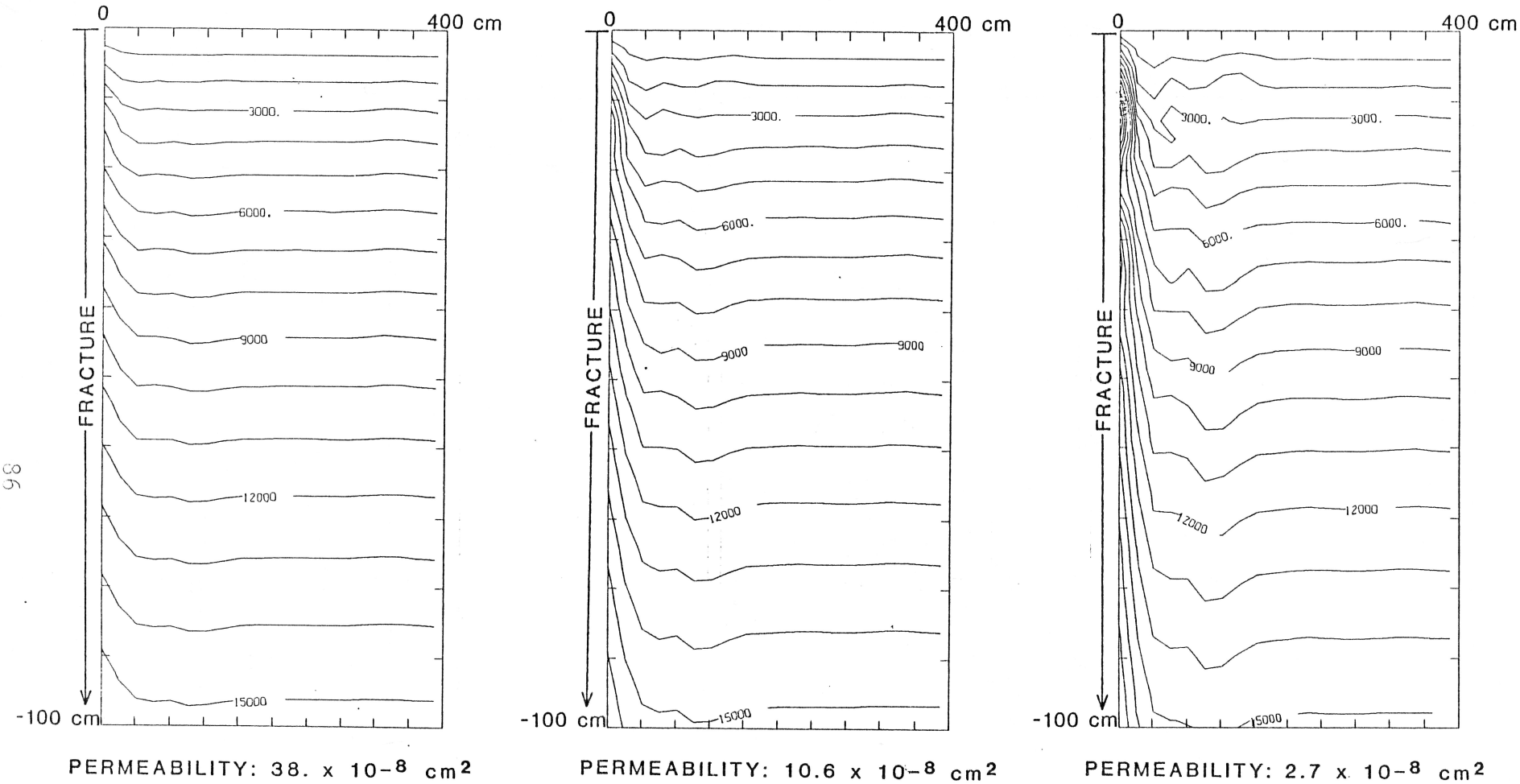

Figure 4-11b: Effect of soil permeability on radon concentrations (atoms/cm^3) in soil with cracks 400 cm deep, 0.06 cm wide and spaced 800 cm apart after 6 hours of decreasing atmospheric pressure.

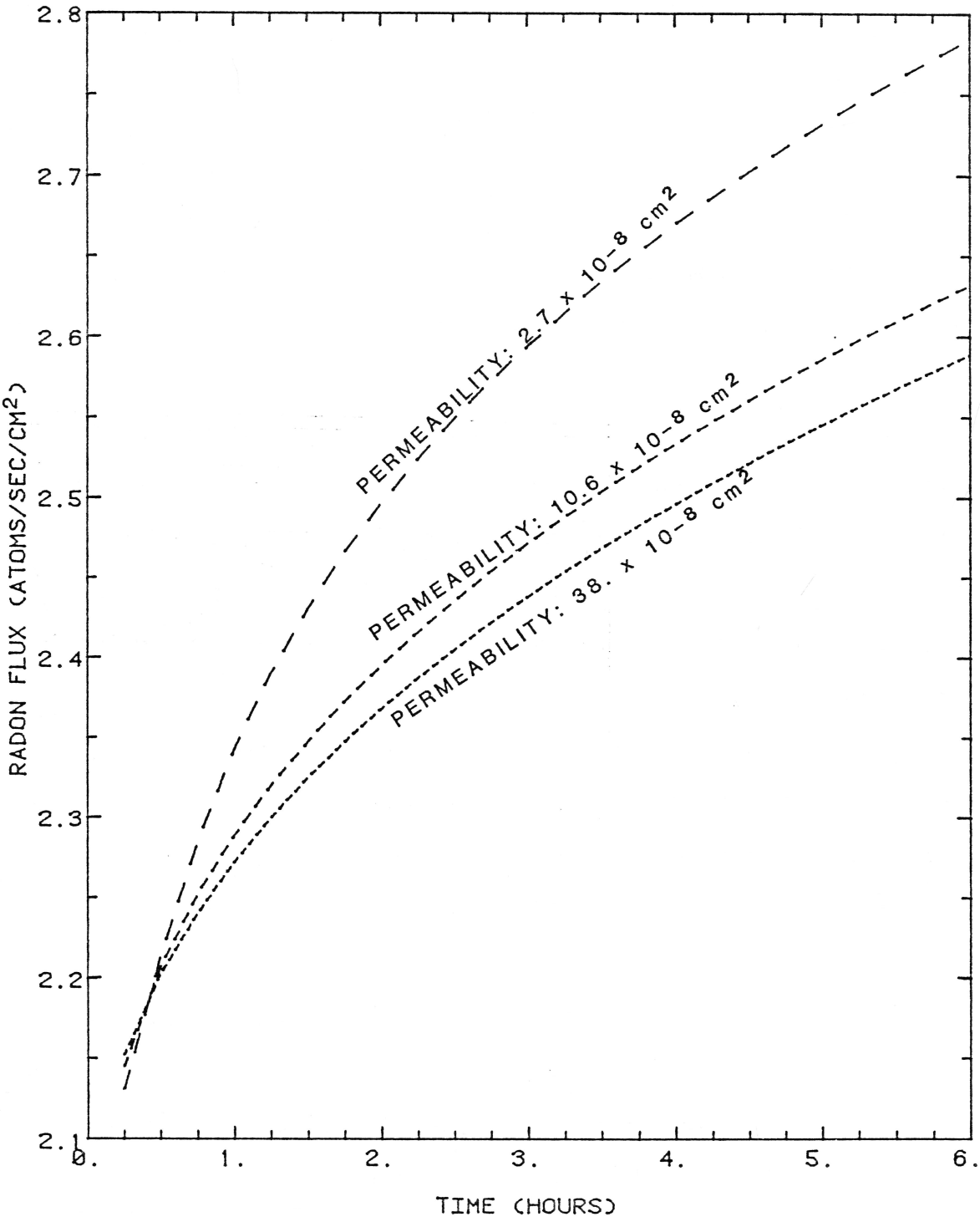

Figure 4-11c: Effect of soil permeability on radon flux density from soil with cracks 400 cm deep, 0.06 cm wide and spaced 800 cm apart during 6 hours of decreasing atmospheric pressure.

4.2.3 Diffusion Coefficient

The diffusion coefficient for radon in soil (D_d^*) was varied while the porosity (n) was held at 0.35 and the permeability (k) at 2.7×10^{-8} cm^2. The two diffusion coefficients chosen were simply five times greater and five times less than the one used in previous simulations.

As shown in figure 4-12a, decreasing the diffusion coefficient causes an increase in concentrations in the crack and soil. With a smaller diffusion coefficient in the soil, the radon cannot escape at the surface and concentrations increase in the soil. Also, the crack brings radon up which cannot diffuse as fast into the soil, and concentrations build up in the crack. Since a larger diffusion coefficient allows more radon to escape across the soil/air interface, the flux density increases as the diffusion coefficient in the soil increases (figure 4-12b). The radon flux curves for different diffusion coefficients have the same slope at late times, but at early times the slope is higher for the flux curve representing a small soil diffusion coefficient. The early-time nonlinear increase in flux from a soil with a small diffusion coefficient is due to a rapid buildup of radon concentrations in the crack. At later times, the concentrations in the crack have reached equilibrium and the increase in flux is steady.

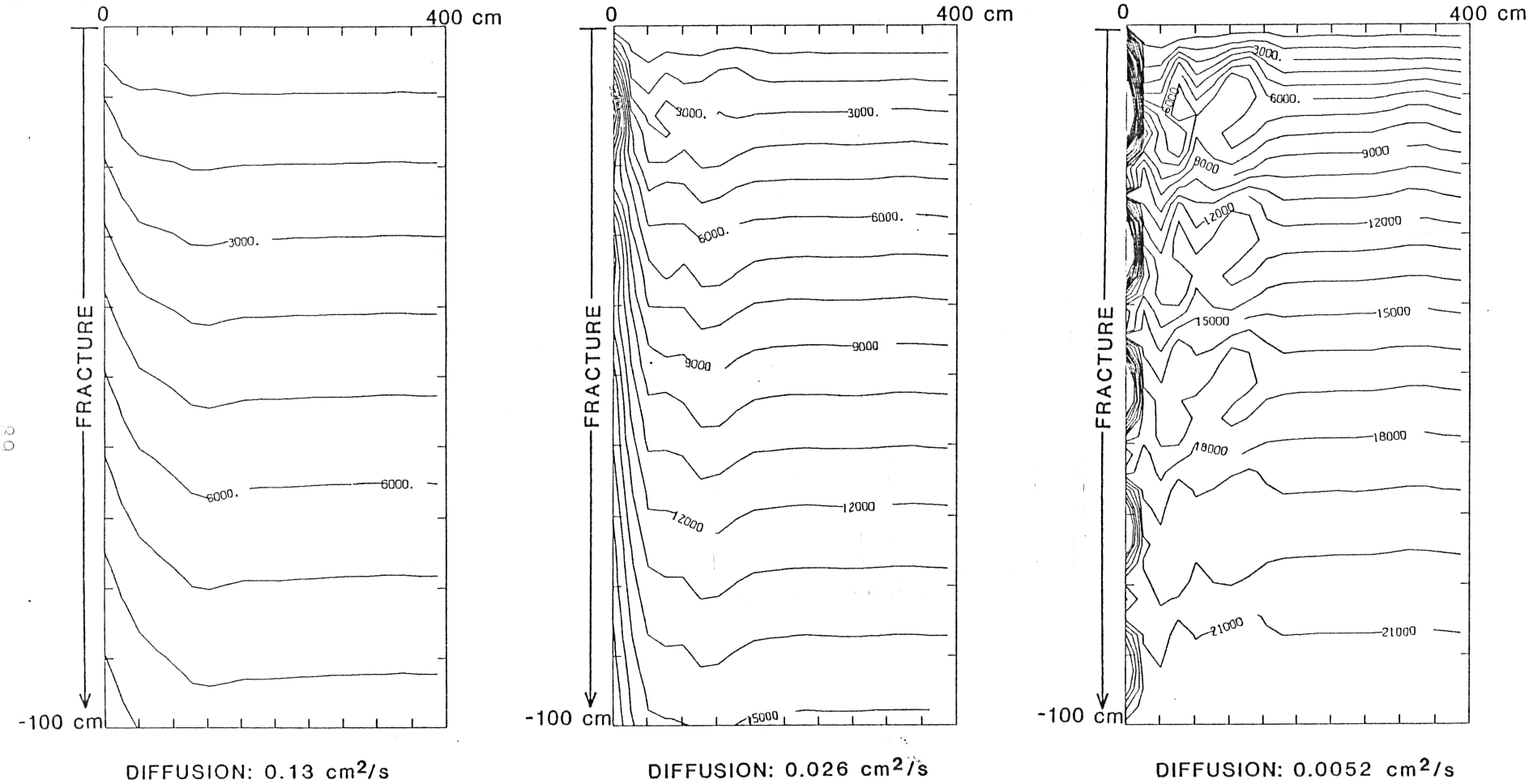

Figure 4-12a: Effect of soil diffusion coefficient on radon concentrations (atoms/cm^3) in soil with cracks 400 cm deep, 0.06 cm wide and spaced 800 cm apart after 6 hours of decreasing atmospheric pressure. (The plotting program, NCAR, had trouble with the last frame due to strong concentration gradients and too coarse a grid near the fracture)

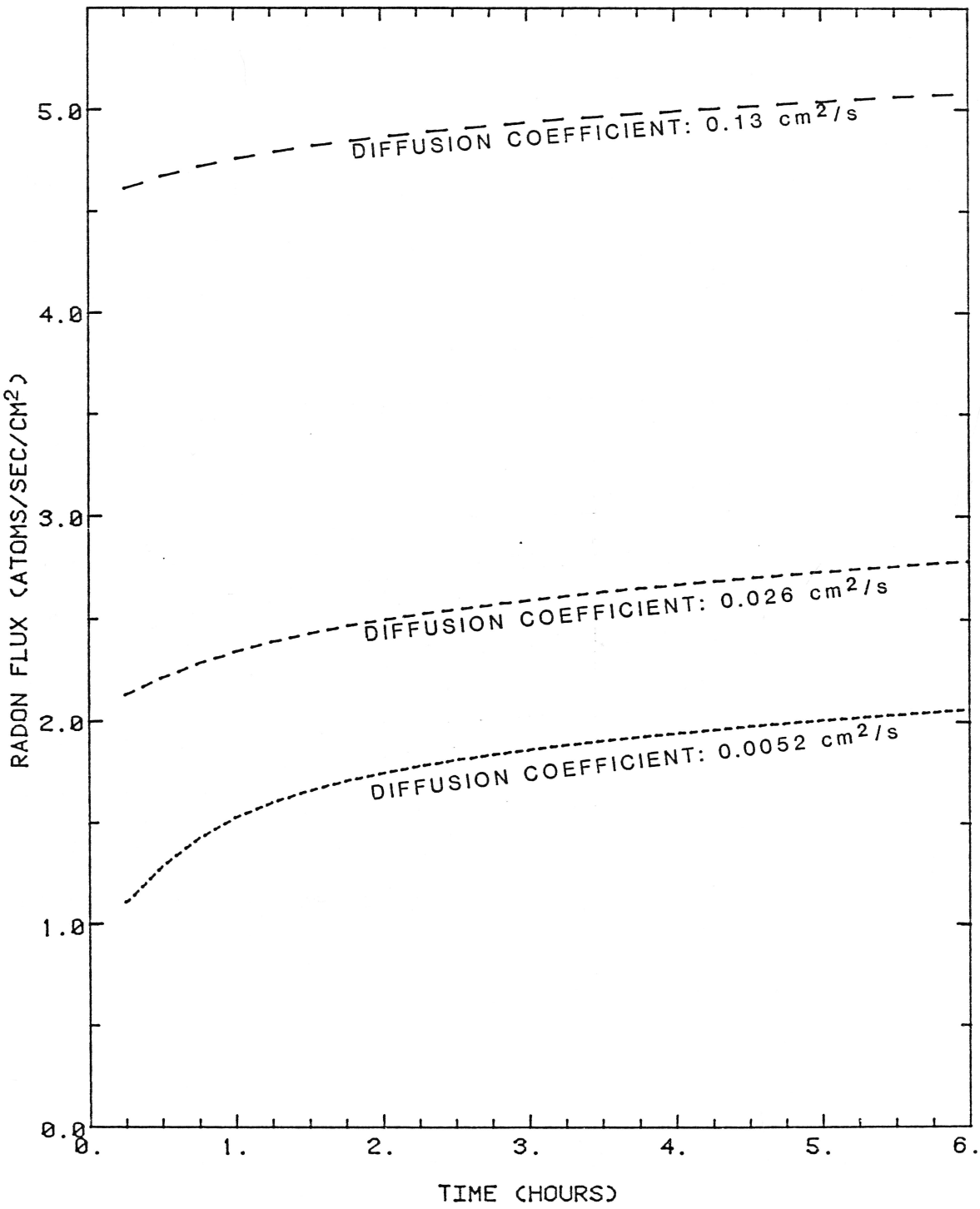

Figure 4-12b: Effect of soil diffusion coefficient on radon flux density from soil with cracks 400 cm deep, 0.06 cm wide and spaced 800 cm apart after 6 hours of decreasing atmospheric pressure.

4.3 PRESSURE VARIATIONS

This section examines the effect of increasing and decreasing atmospheric pressure, consistent with rates measured in the field by Schery et. al. (1984). Also, the effects of short term sinusoidal fluctuations in surface pressure are examined. Certain parameters were kept constant in this section and are listed in the table 4-4.

Table 4-4: Constant parameters for section 4-3

Crack spacing	800 cm
Crack width	0.6 cm
Crack depth	400 cm
Soil porosity (n)	0.35
Soil intrinsic permeability (k)	2.7×10^{-8} cm^2
Radon diffusion coefficient in soil (Dd*)	2.6×10^{-2} cm^2/s

4.3.1 Constant changes

The effect of decreasing atmospheric pressure at the top of the soil at different rates is shown in figure 4-13a. As the rate of pressure decrease increases, the subsurface pressure gradients in the soil and crack increase by the same proportion. The velocities in the

soil and crack increase, bringing up radon from zones of greater concentration at depth, causing an increase in concentrations (figure 4-13b). The faster the radon moves, the less is lost to radioactive decay before it reaches the surface.

A similar effect on pressures is seen when the surface pressure is increased at a constant rate (figure 4-14a). The increase in subsurface gradient is proportional to the increase in rate of pressure change. Increasing surface pressures cause the direction of gas flow to reverse; air now flows from the surface down into the crack and into the soil. This causes concentrations to decrease in the soil and crack (figure 4-14b).

Interestingly, figure 4-15 shows that the decrease in flux density for a certain rate of increasing pressure is not as great as the increase in flux density for a decrease in pressure of the same magnitude. Although the pressure gradients are downward for the case of increasing atmospheric pressure, the concentration gradients in the soil and crack are still upward. The diffusive transport of radon is still towards the surface, because the concentration of radon in the atmosphere is zero.

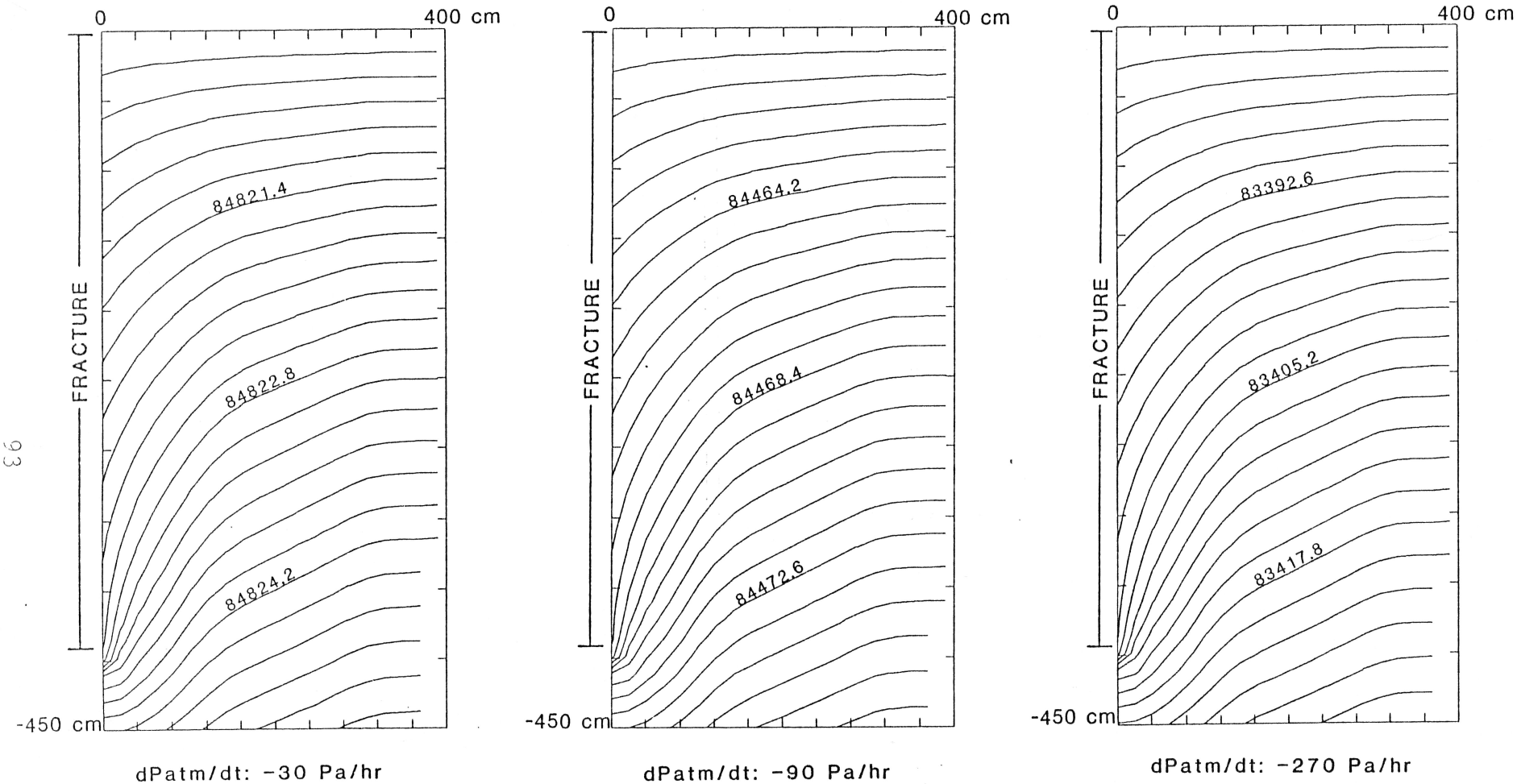

Figure 4-13a: Effect of constantly decreasing atmospheric pressure on gas pressures (Pascals) in soil with cracks 400 cm deep, 0.06 cm wide and spaced 800 cm apart after 6 hours.

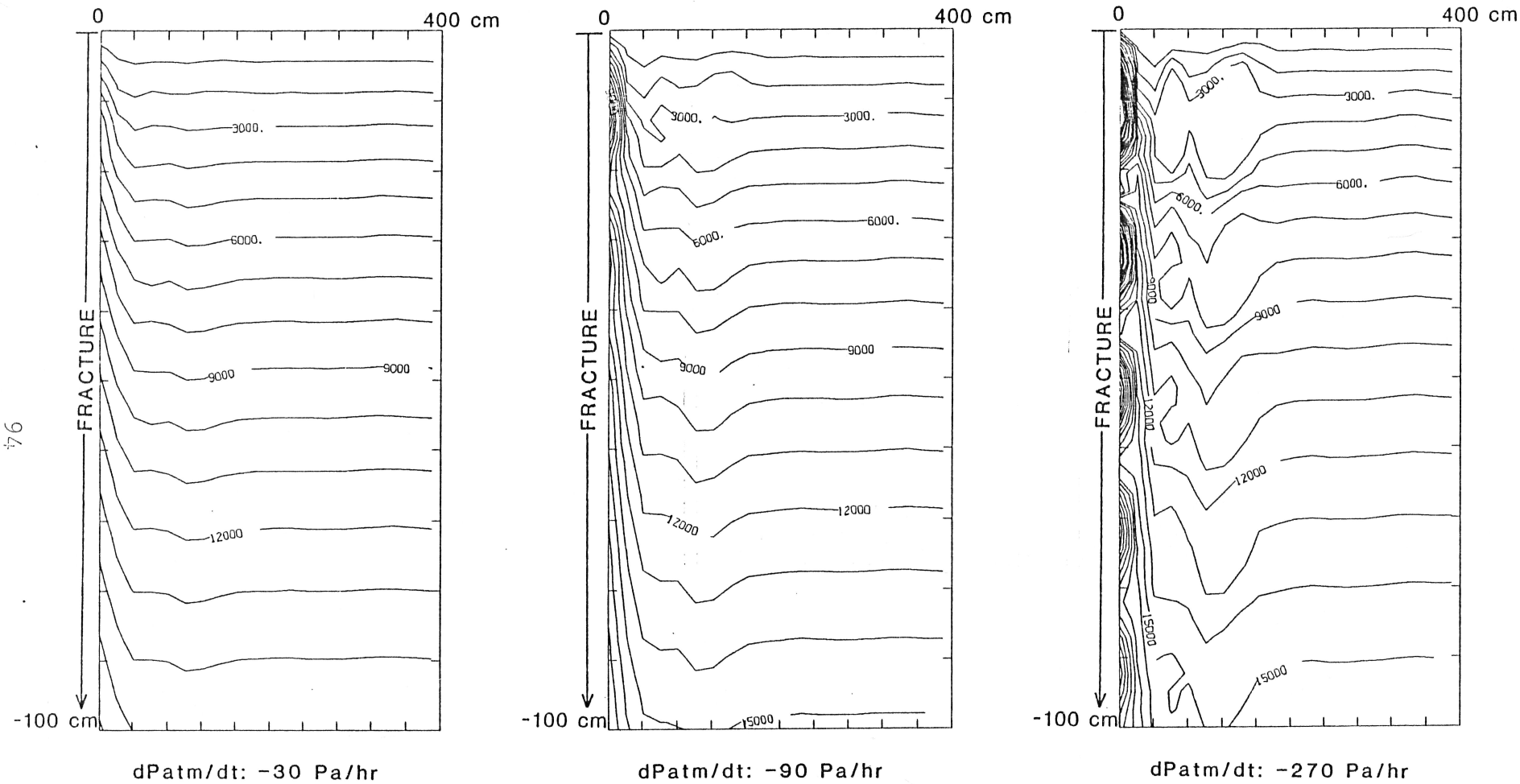

Figure 4-13b: Effect of constantly decreasing atmospheric pressure on radon concentrations (atoms/cm^3) in soil with cracks 400 cm deep, 0.06 cm wide and spaced 800 cm apart after 6 hours. (The plotting program, NCAR, had trouble with the last frame due to strong concentration gradients and too coarse a grid near the fracture)

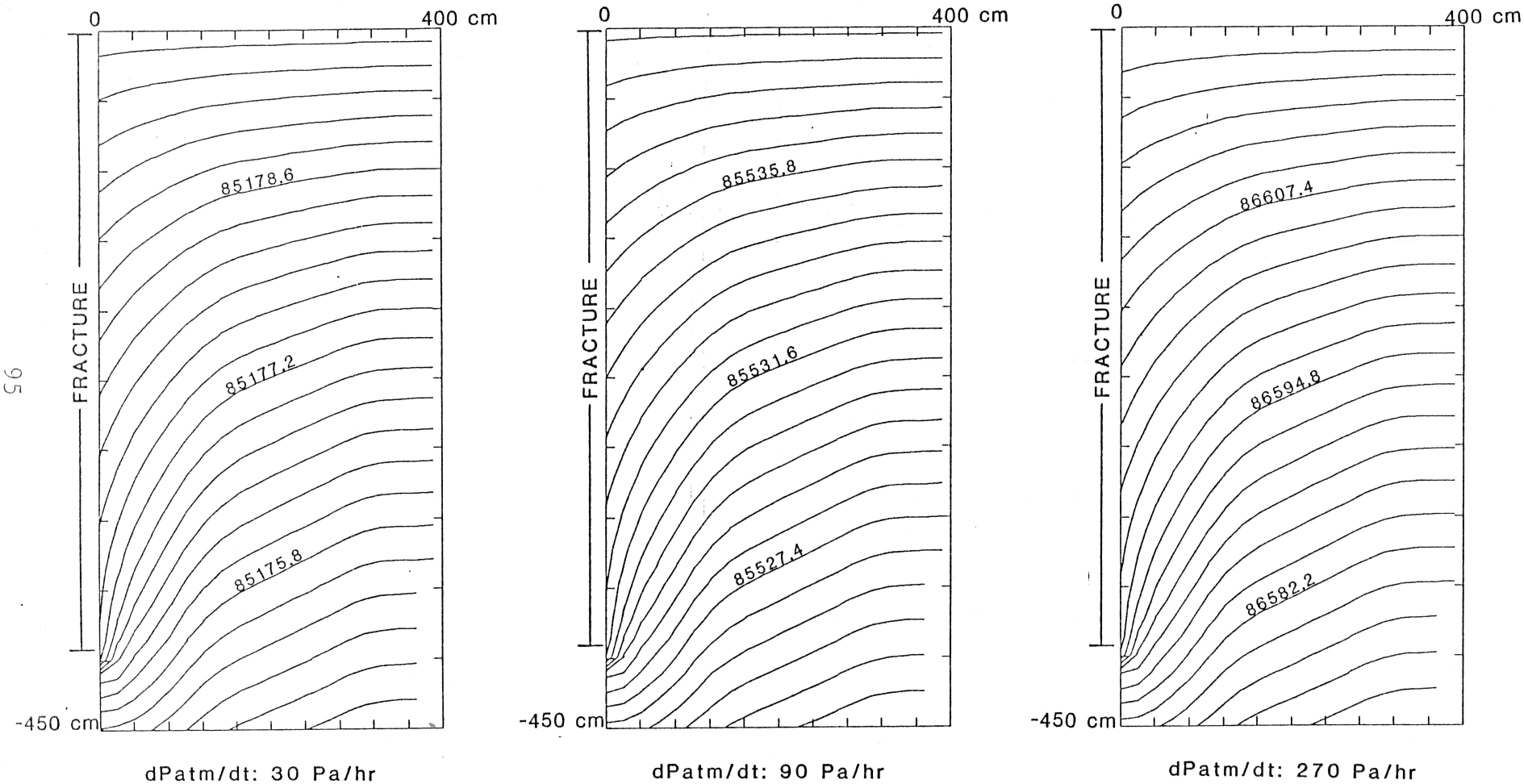

Figure 4-14a: Effect of constantly rising atmospheric pressure on gas pressures (Pascals) in soil with cracks 400 cm deep, 0.06 cm wide and spaced 800 cm apart after 6 hours.

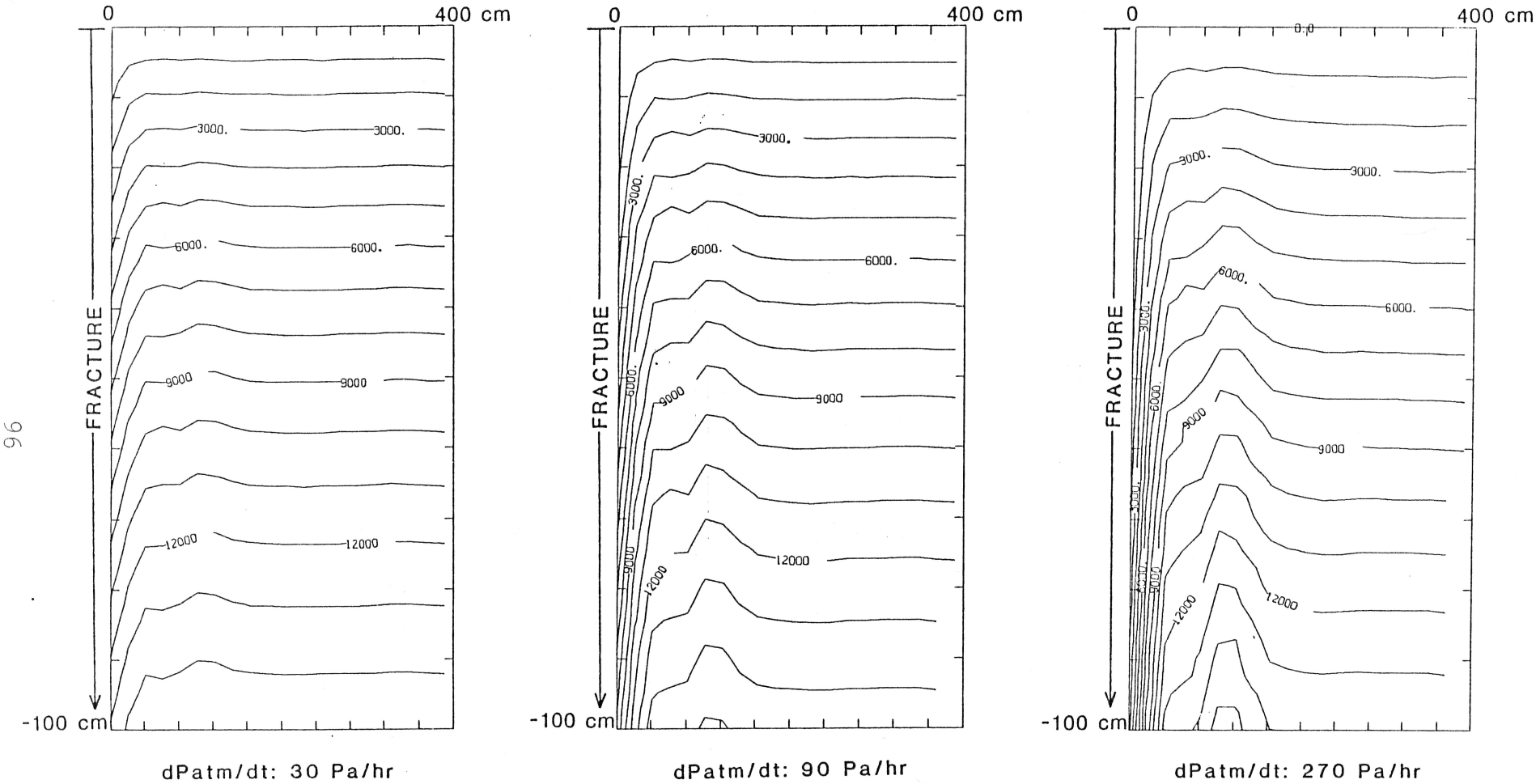

Figure 4-14b: Effect of constantly rising atmospheric pressure on radon concentrations (atoms/cm^3) in soil with cracks 400 cm deep, 0.06 cm wide and spaced 800 cm apart after 6 hours.

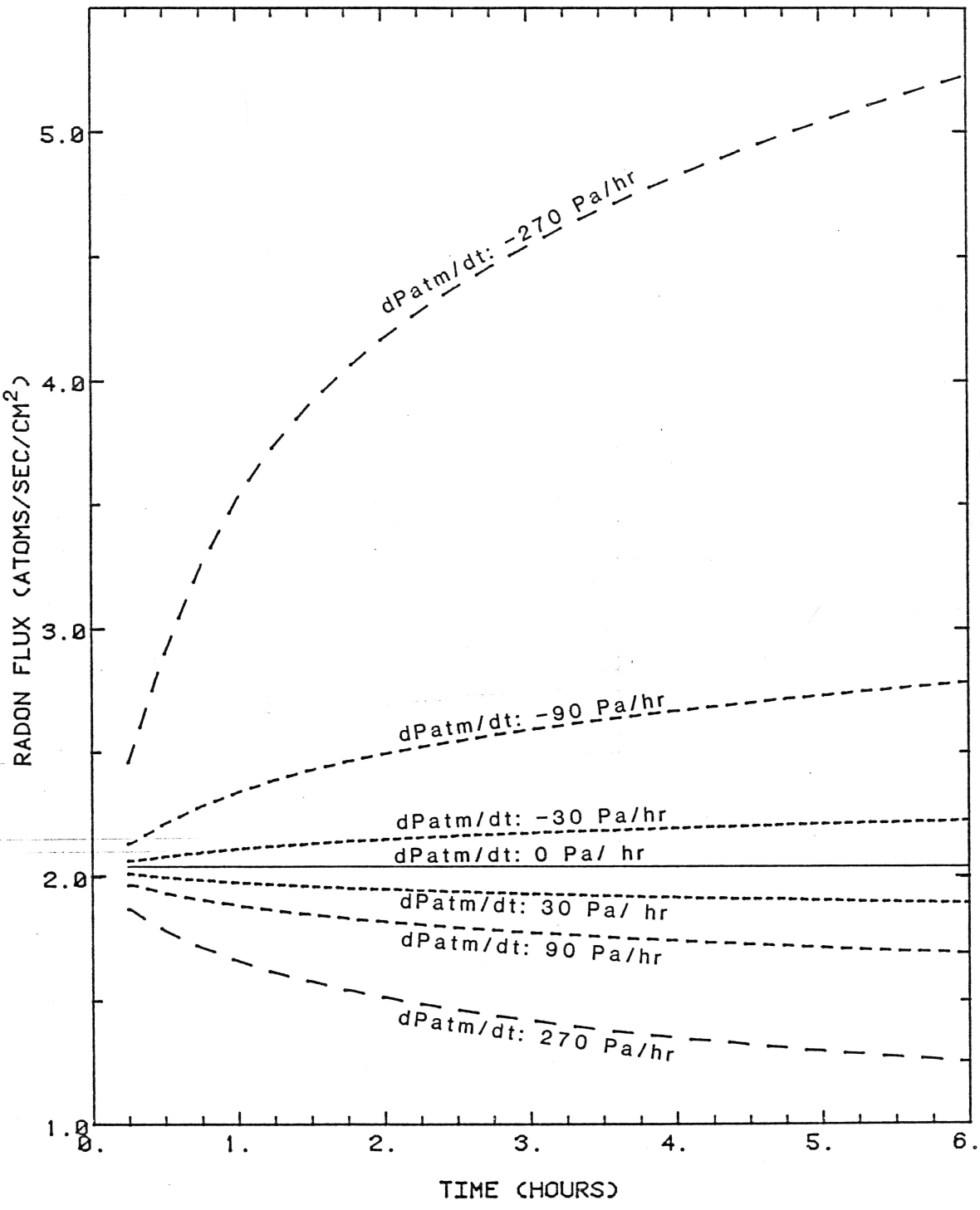

Figure 4-15: Effect of constantly changing atmospheric pressure on radon flux density from soil with cracks 400 cm deep, 0.06 cm wide and spaced 800 cm apart during 6 hours.

4.3.2 Sinusoidal variations

In this section, sinusoidal variations in atmospheric pressure about a mean value of 85000 Pascals were applied at the upper boundary of the model. The period and amplitude of the sine function were varied.

Figure 4-16a shows the effect of a sinusoidal atmospheric pressure variation over time on gas pressures in the soil. The first frame was taken when the surface pressure was at the bottom of a pressure decrease. The gradient is very strong towards the surface and crack. The second frame was taken when the pressure is increasing and is at the mean value of the sinusoidal variation. Pressures have begun to rise near the surface and near the crack, but gradients are still upward in most of the soil. The third frame was taken at the peak of a rise in pressure, and the gradient is predominantly downward.

Figure 4-16b shows the effect of a sinusoidal pressure variation over time on radon concentrations. These results were recorded after two complete periods of sinusiodal atmospheric pressure variation. Since the first frame was taken at the end of a pressure decrease, concentrations are very high in the crack. The second frame was taken when pressures have been increasing; concentrations have begun to decrease near the crack. The third frame is at the end of a rise in pressure; concentrations are mostly decreasing, but still rise near the surface. This is the origin of the wiggles in

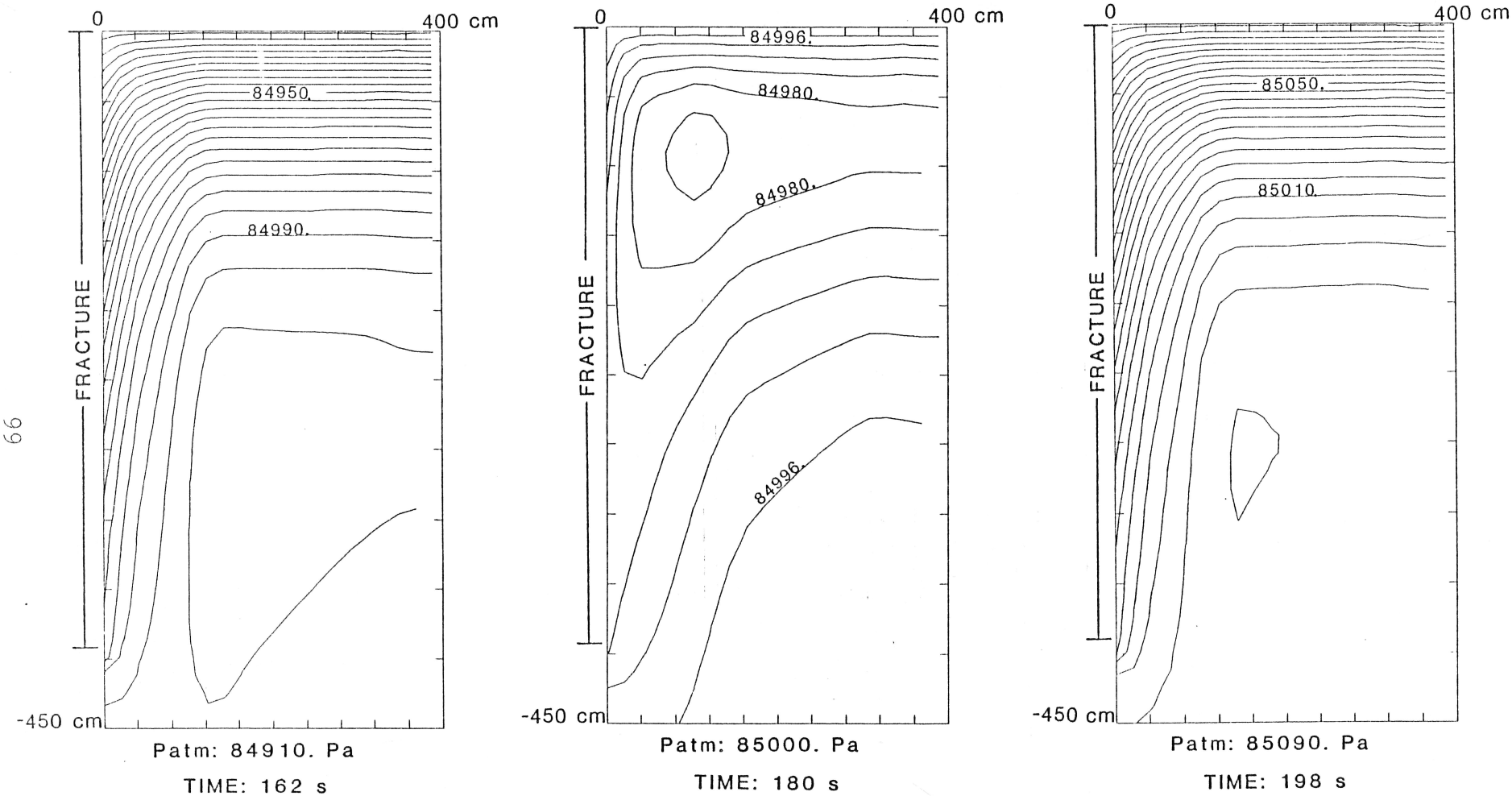

Figure 4-16a: Effect of sinusoidal atmospheric pressure variation with time of period = 72 s, amplitude = 90 Pa on on gas pressures (Pascals) in soil with cracks 400 cm deep, 0.06 cm wide and spaced 800 cm apart.

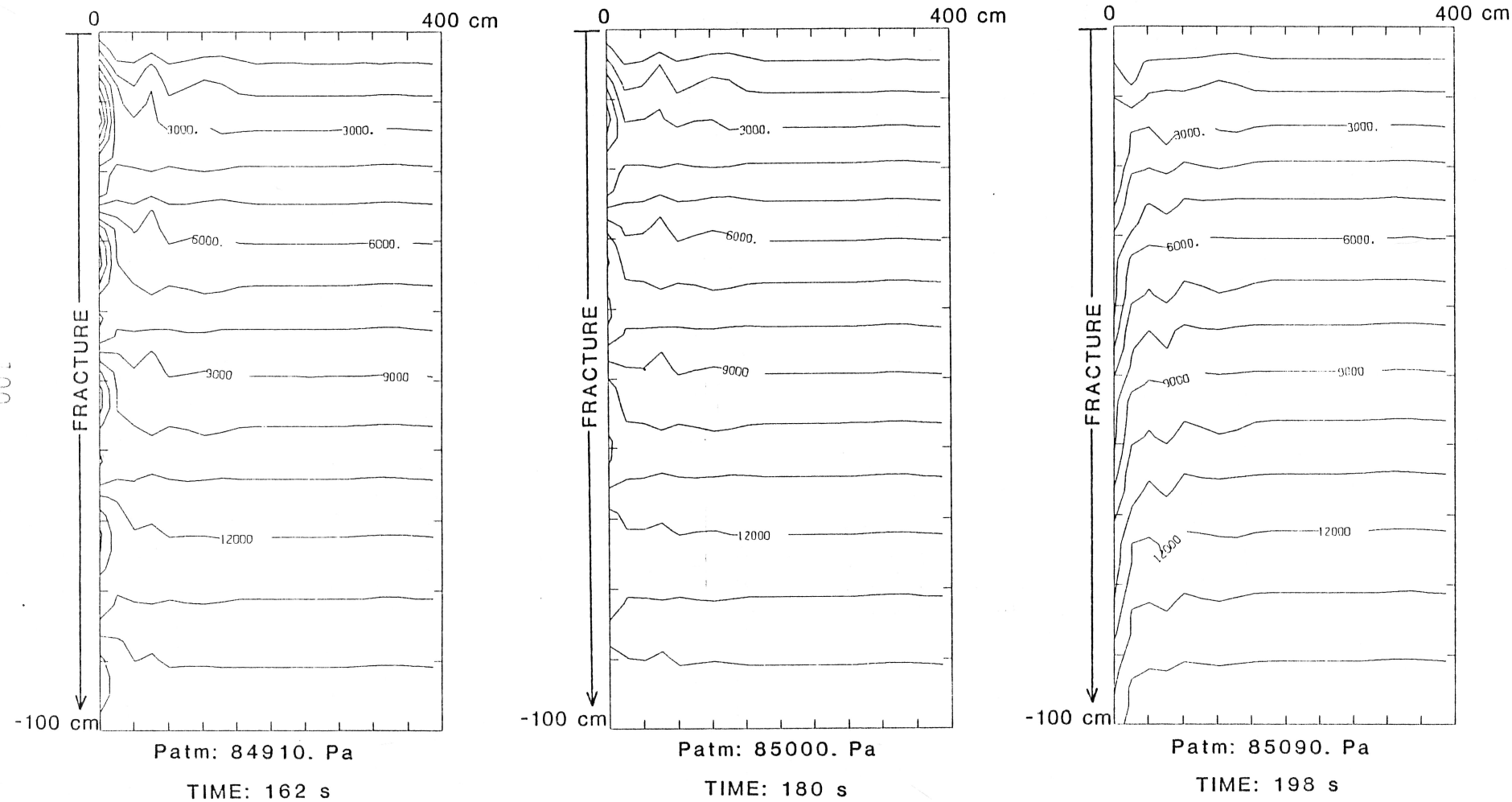

Figure 4-16b: Effect of sinusoidal atmospheric pressure variation with time of period = 72 s, amplitude = 90 Pa on on radon concentrations (atoms/cm^3) in soil with cracks 400 cm deep, 0.06 cm wide and spaced 800 cm apart.

concentration contours near the crack. The contour wiggles are manifestations of the increases and decreases which have occured in the crack and have moved out into the soil, becoming damped out as they go.

Figure 4-17 shows the effect that a sinusoidal pressure variation with a long period (2 hours) has on radon flux density. Soil with cracks shows a greater variation in flux than a soil without cracks, and the mean flux increases slightly. Decreasing the period of the pressure change by 10 times, and then 100 times but keeping the amplitude the same (figures 4-18 and 4-19) causes a small increase in the mean flux but a large change in the deviation about the mean (figure 4-20). Standard deviation is used as a comparative measure rather than amplitude, since the flux curves are sinusoidally assymetric. The standard deviation is, in most cases, about 75 percent of the amplitude of the radon flux density with time.

The increase in the mean flux can be explained by the results of the previous section, where a decrease in pressure cause a greater change in flux than a rise in pressure of the same magnitude. The increase in flux deviation with a decrease in period results from the amplitude being kept constant, so that the variation in atmospheric pressure per unit time is larger.

Notably, there appears to be very little phase lag between a change in surface pressure and the response of

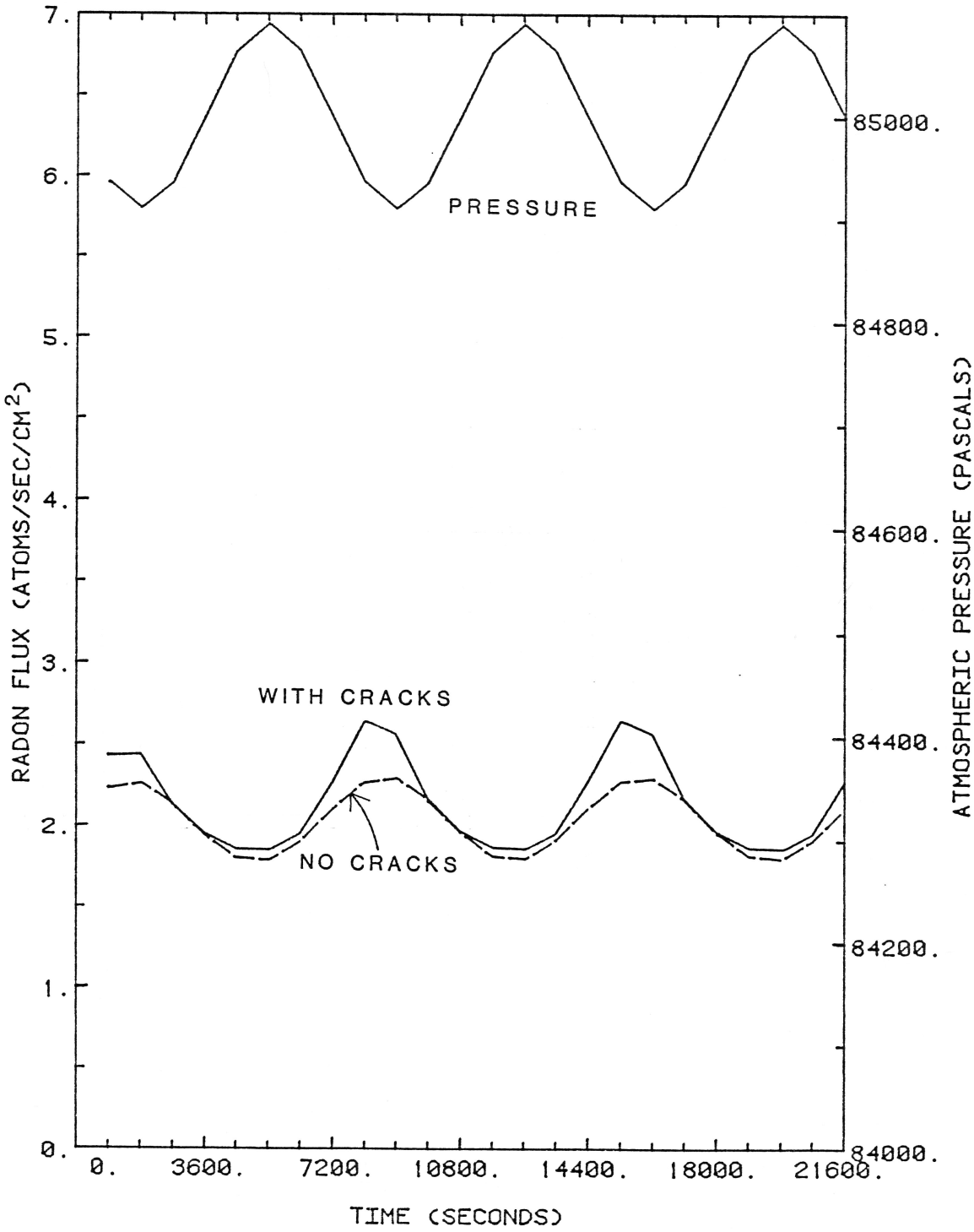

Figure 4-17: Effect of sinusoidal atmospheric pressure variation of period = 7200 s and amplitude = 90 Pa on radon flux density from soil with cracks (400 cm deep, 0.06 cm wide and spaced 800 cm apart) and soil without cracks.

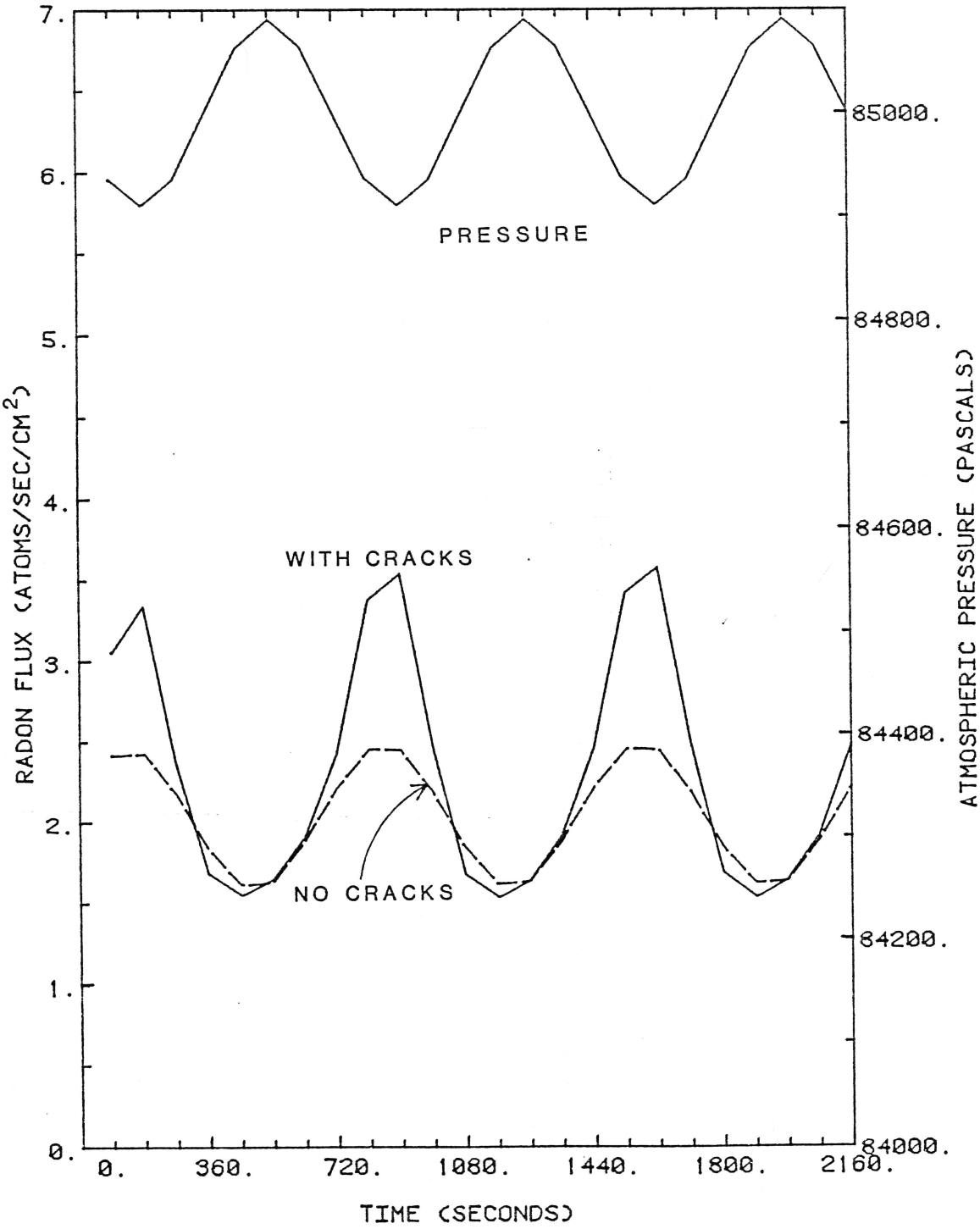

Figure 4-18: Effect of sinusoidal atmospheric pressure variation of period = 720 s and amplitude = 90 Pa on radon flux density from soil with cracks (400 cm deep, 0.06 cm wide and spaced 800 cm apart) and soil without cracks.

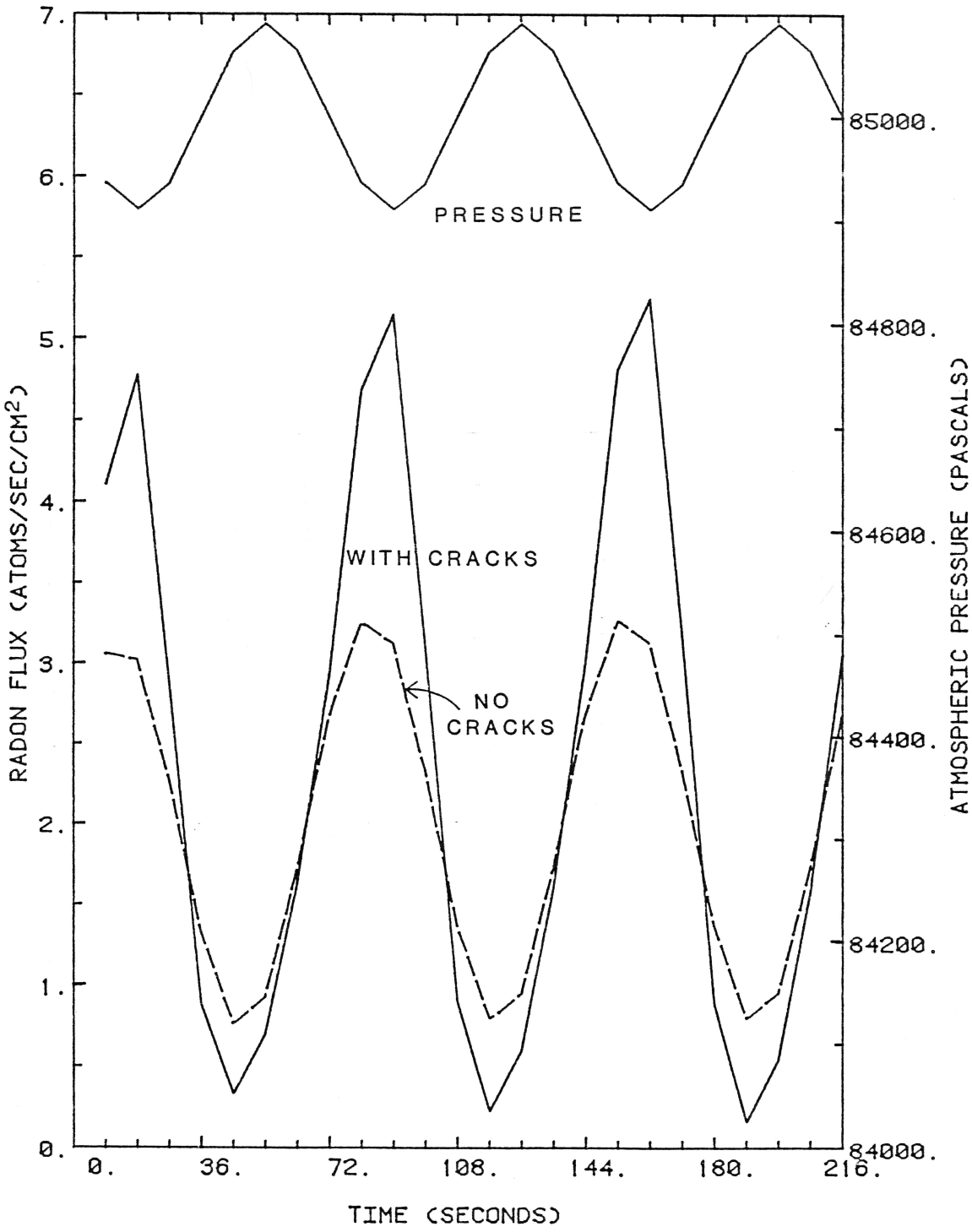

Figure 4-19: Effect of sinusoidal atmospheric pressure variation of period = 72 s and amplitude = 90 Pa on radon flux density from soil with cracks (400 cm deep, 0.06 cm wide and spaced 800 cm apart) and soil without cracks.

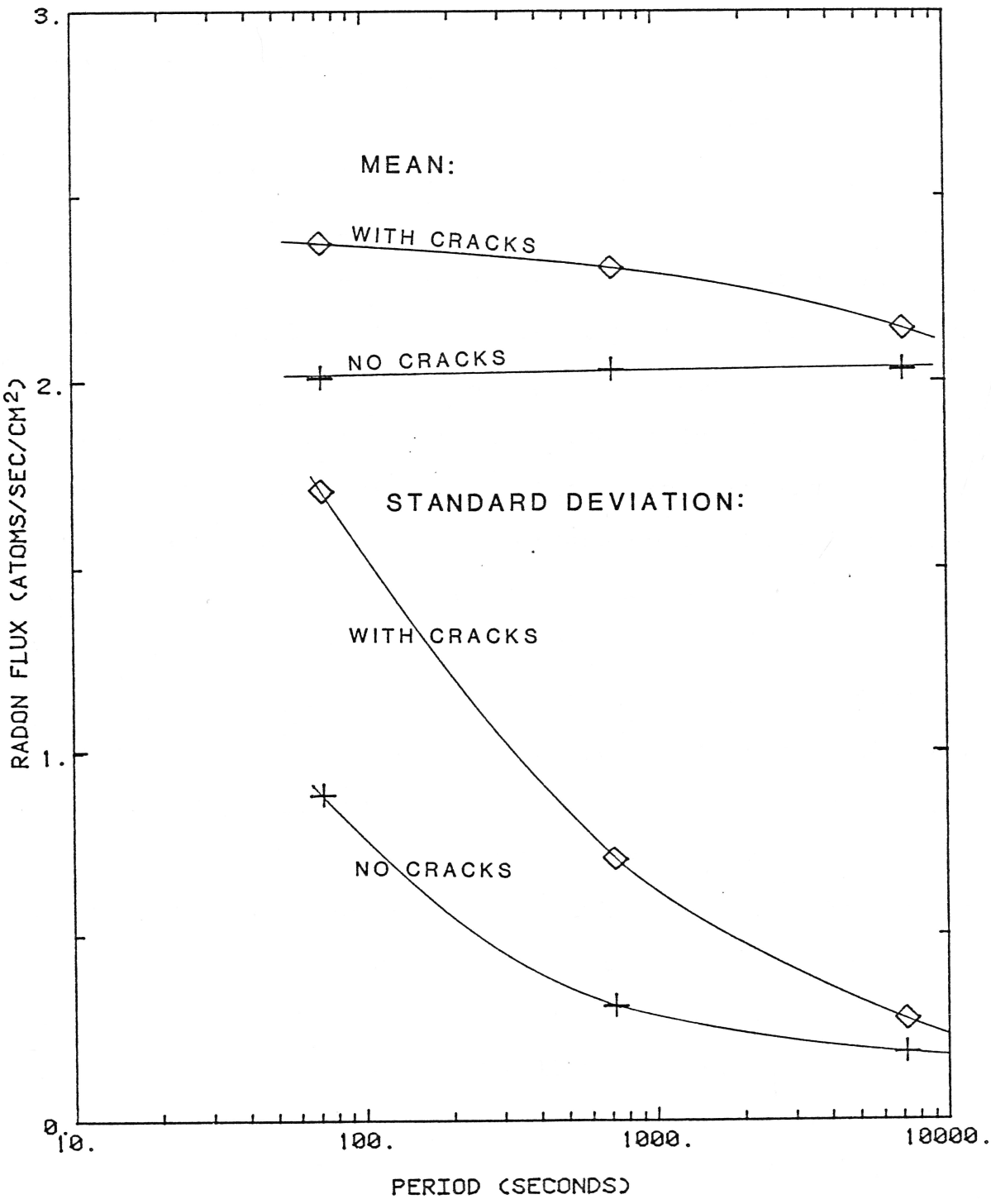

Figure 4-20: Effect of period of sinusoidal atmospheric pressure variation on mean and standard deviation of radon flux density from soil with cracks (400 cm deep, 0.06 cm wide and spaced 800 cm apart) and soil without cracks.

the radon flux density in figures 4-17 through 4-19. This is because the flux is calculated from the concentrations of nodes near the surface; the lag time between changes in surface pressure and changes in concentrations near the surface is very short.

It may also be observed that the response of surface flux to changes in pressure equillibrates rapidly. In other words, the standard deviation of the fluxes in figures 4-17 through 4-19 increase only slightly with time. This is not surprising, since pressures and concentratons were observed to reach equillibrium quickly for constant changes in pressures (see discussion related to figures 4-2a through 4-2c).

Decreasing the period of the sinusoidal fluctuation allows less time for subsurface pressures in the soil and crack to equillibrate (figure 4-21a). With a period of 7200 seconds, when the pressure has been decreasing at the surface, the gradient curves smoothly towards the crack and surface. Decreasing the period to 720 seconds does not allow the pressure decrease to move completely into the soil, the gradient is still upward in the portion of the soil furthest from the surface and crack. Decreasing the period to 72 seconds keeps the pressure decrease from moving into the soil except close to the surface and crack. Upward gradients near the surface and crack are very strong, while the gradient is downward everywhere else in the soil.

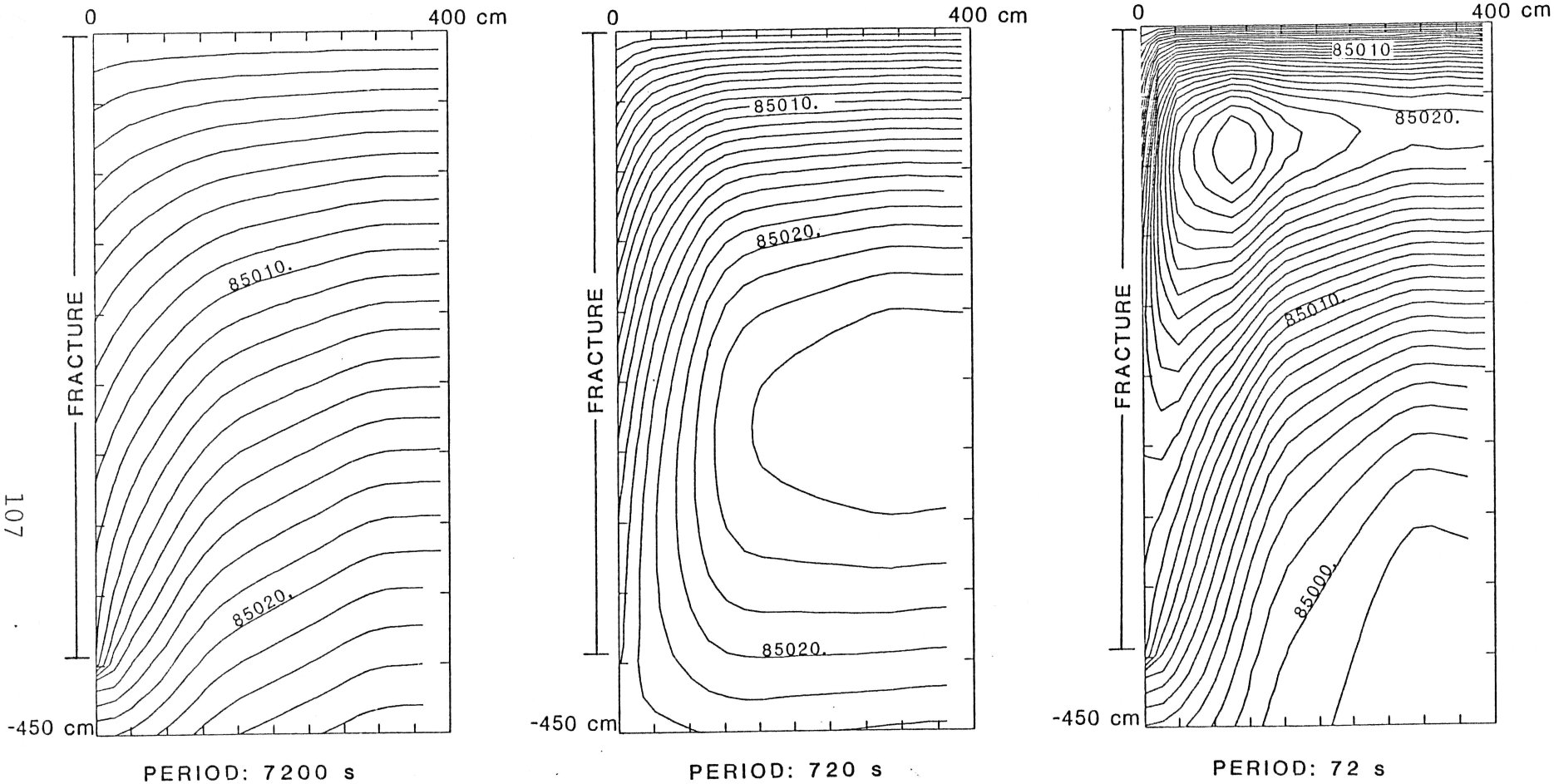

Figure 4-21a: Effect of period of sinusoidal atmospheric pressure variation on gas pressures (Pascals) in soil with cracks 400 cm deep, 0.06 cm wide and spaced 800 cm apart at 21600, 2160, and 216 seconds, respectively.

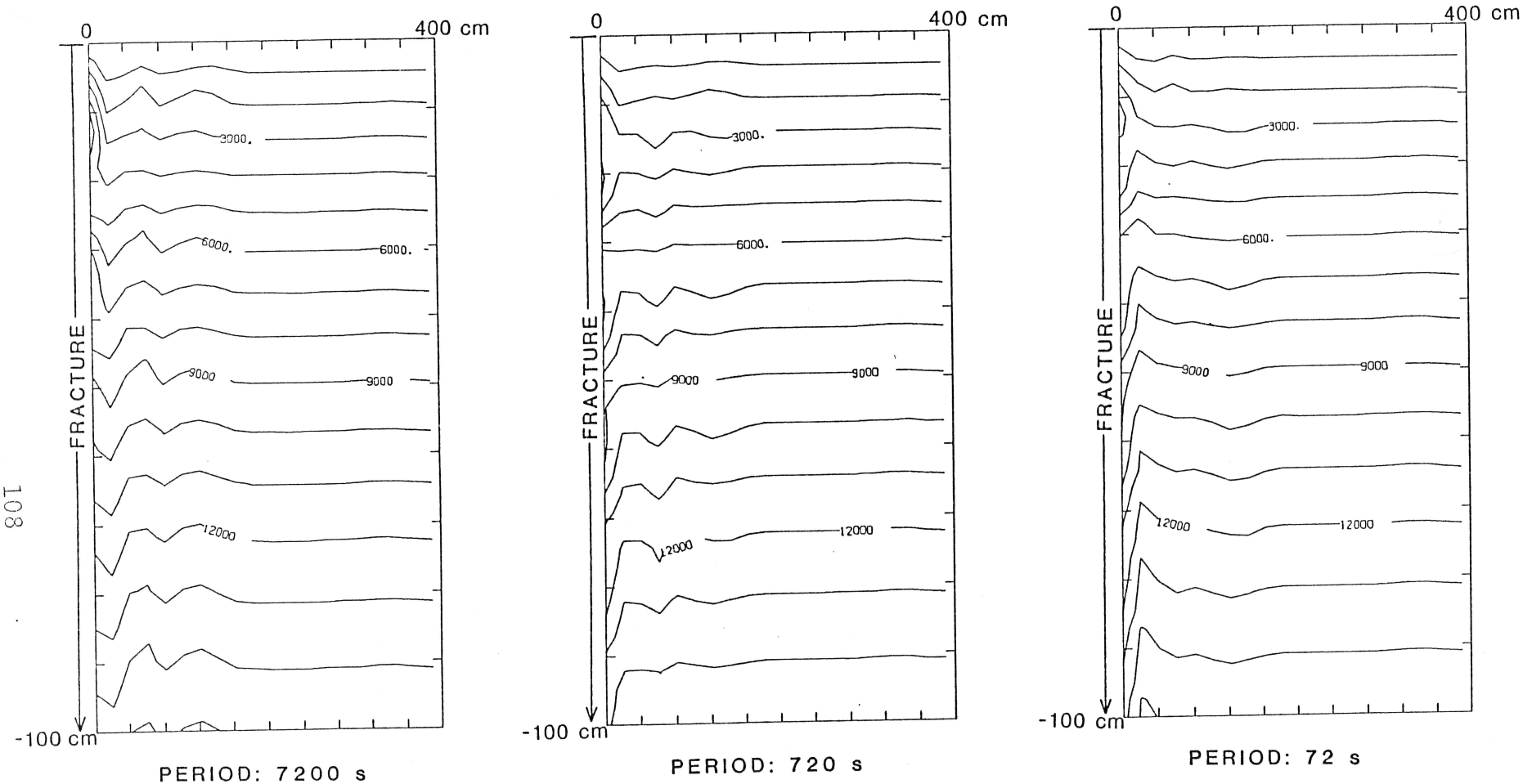

Figure 4-21b: Effect of period of sinusoidal atmospheric pressure variation on radon concentrations (atoms/cm^3) in soil with cracks 400 cm deep, 0.06 cm wide and spaced 800 cm apart at 21600, 2160, and 216 seconds, respectively.

Decreasing the period of the sinusoidal variation also allows less time for changes in concentration to occur in the crack and move into the soil (figure 4-21b). Concentration contours wiggle up and down near the crack, remnants of previous fluctuations in the crack which have moved into the soil. These variations are most clearly seen for a period of 7200 seconds, and become less distinct for smaller periods. For a period of 7200 seconds, concentrations rise consistently near the crack because pressure has been decreasing for the last few time steps. However, for shorter periods, the concentrations still decrease near the crack because pressure gradients in the crack are either weakly upward (720 seconds) or downward (72 seconds).

Increasing the amplitude of the sinusoidal variation in surface pressure while keeping the period constant (figures 4-22 and 4-23) effectively increases the change in pressure per unit time. This causes a much greater change in flux from cracked soil than from soil with no cracks. With an increase in amplitude, the mean and deviation of radon flux density from cracked soil increase rapidly compared to soil with no cracks (figure 4-24).

The increase in mean and deviation of flux for soil with cracks is almost linear, relating to the linear increase in subsurface pressure gradient with an increase in amplitude (figure 4-25a). Of course these increases in subsurface pressure are probably linear only for fairly

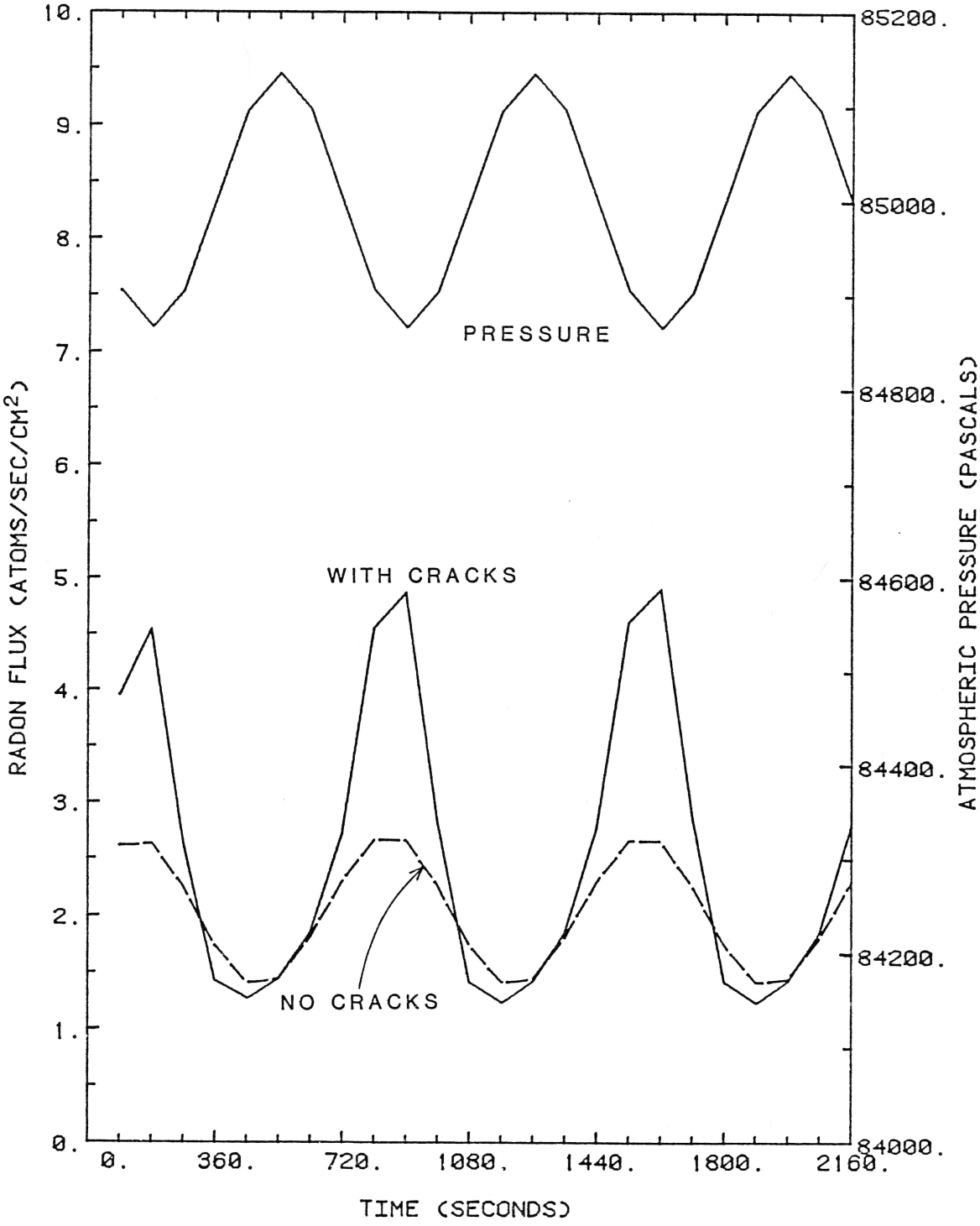

Figure 4-22: Effect of sinusoidal atmospheric pressure variation of period = 720 s and amplitude = 135 Pa on radon flux density from soil with cracks (400 cm deep, 0.06 cm wide and spaced 800 cm apart) and soil without cracks.

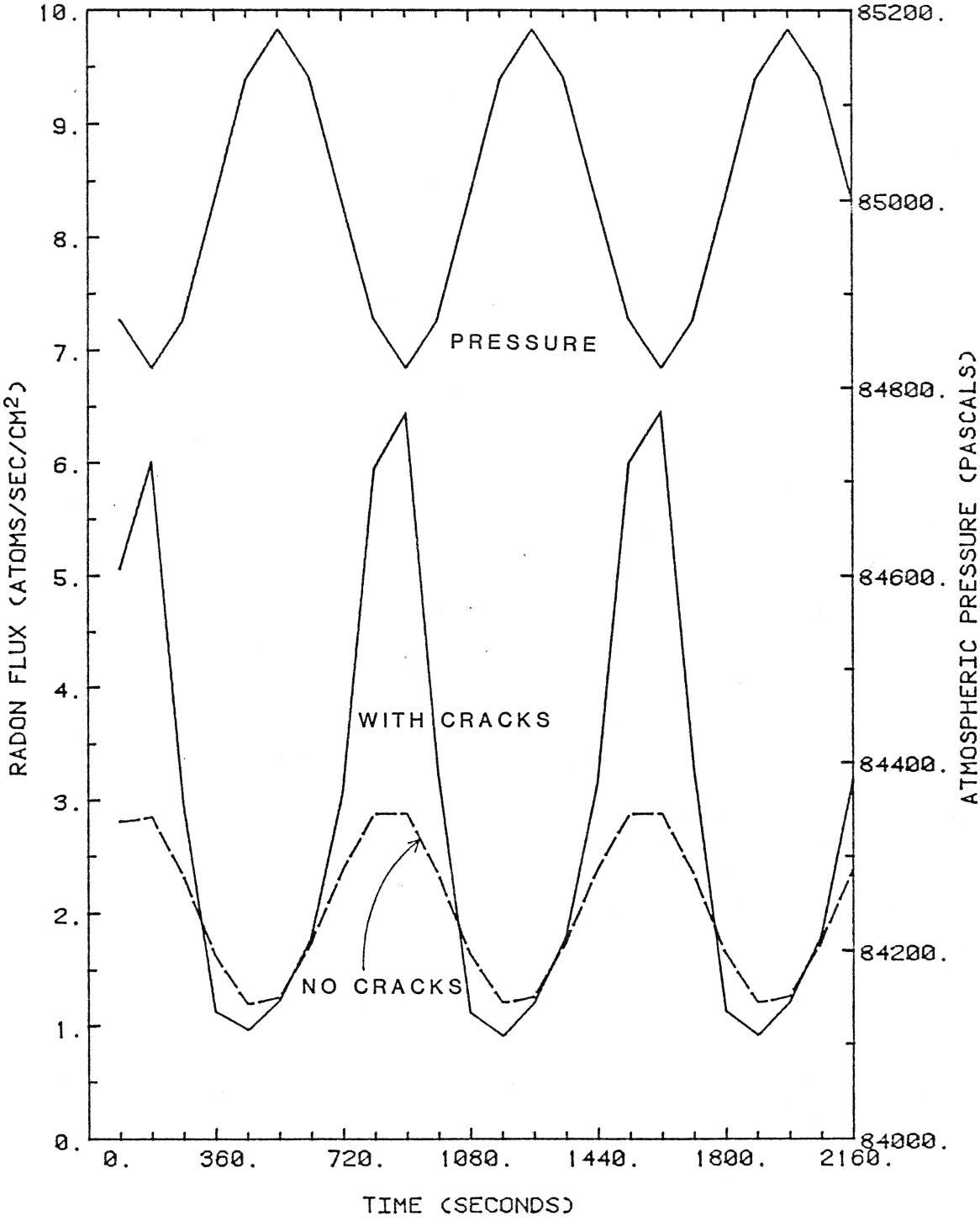

Figure 4-23: Effect of sinusoidal atmospheric pressure variation of period = 720 s and amplitude = 180 Pa on radon flux density from soil with cracks (400 cm deep, 0.06 cm wide and spaced 800 cm apart) and soil without cracks.

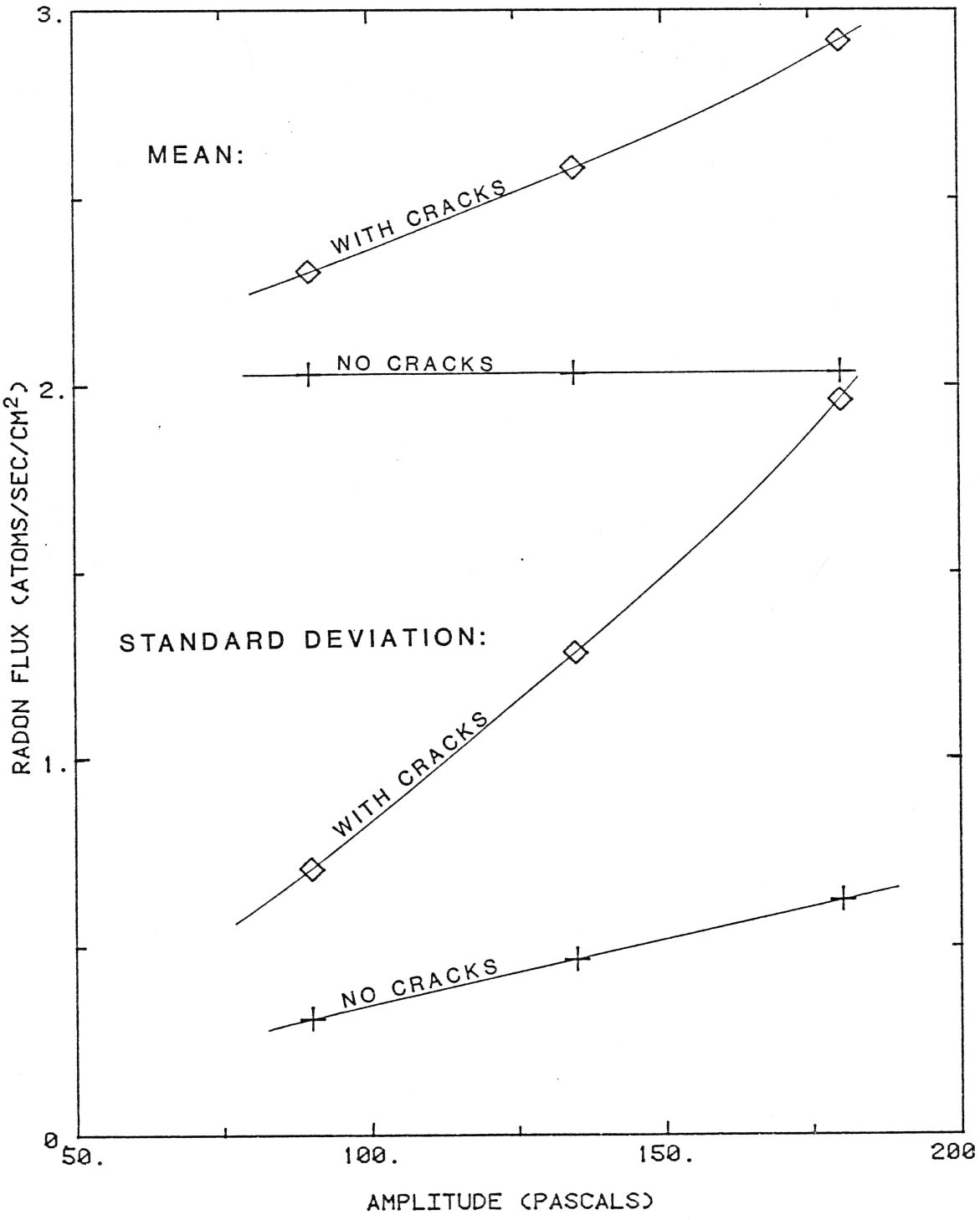

Figure 4-24: Effect of amplitude of sinusoidal atmospheric pressure variation on mean and standard deviation of radon flux density from soil with cracks (400 cm deep, 0.06 cm wide and spaced 800 cm apart) and soil without cracks.

small changes in amplitude; the ones shown here are for a 50 and 100 percent increase.

In figure 4-25b, an increase in amplitude of the sinusoidal pressure variation causes concentrations in and near the crack to increase, but has less of an effect on concentrations in the soil, illustrating why fluxes from a soil with cracks change more with a change in amplitude than soil without cracks.

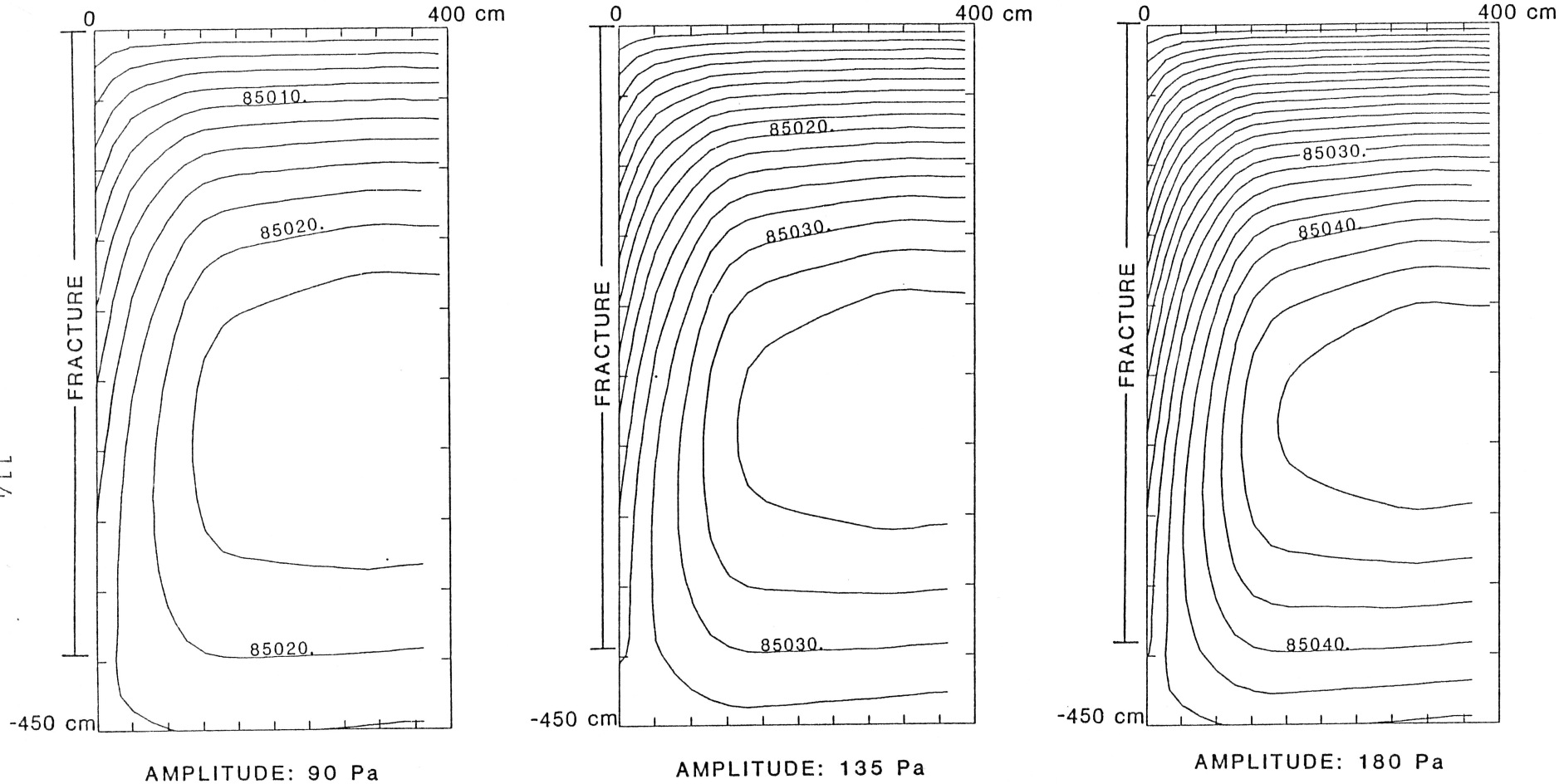

Figure 4-25a: Effect of amplitude of sinusoidal atmospheric pressure variation with a period of 720 seconds on gas pressures (Pascals) in soil with cracks 400 cm deep, 0.06 cm wide and spaced 800 cm apart at 2160 seconds.

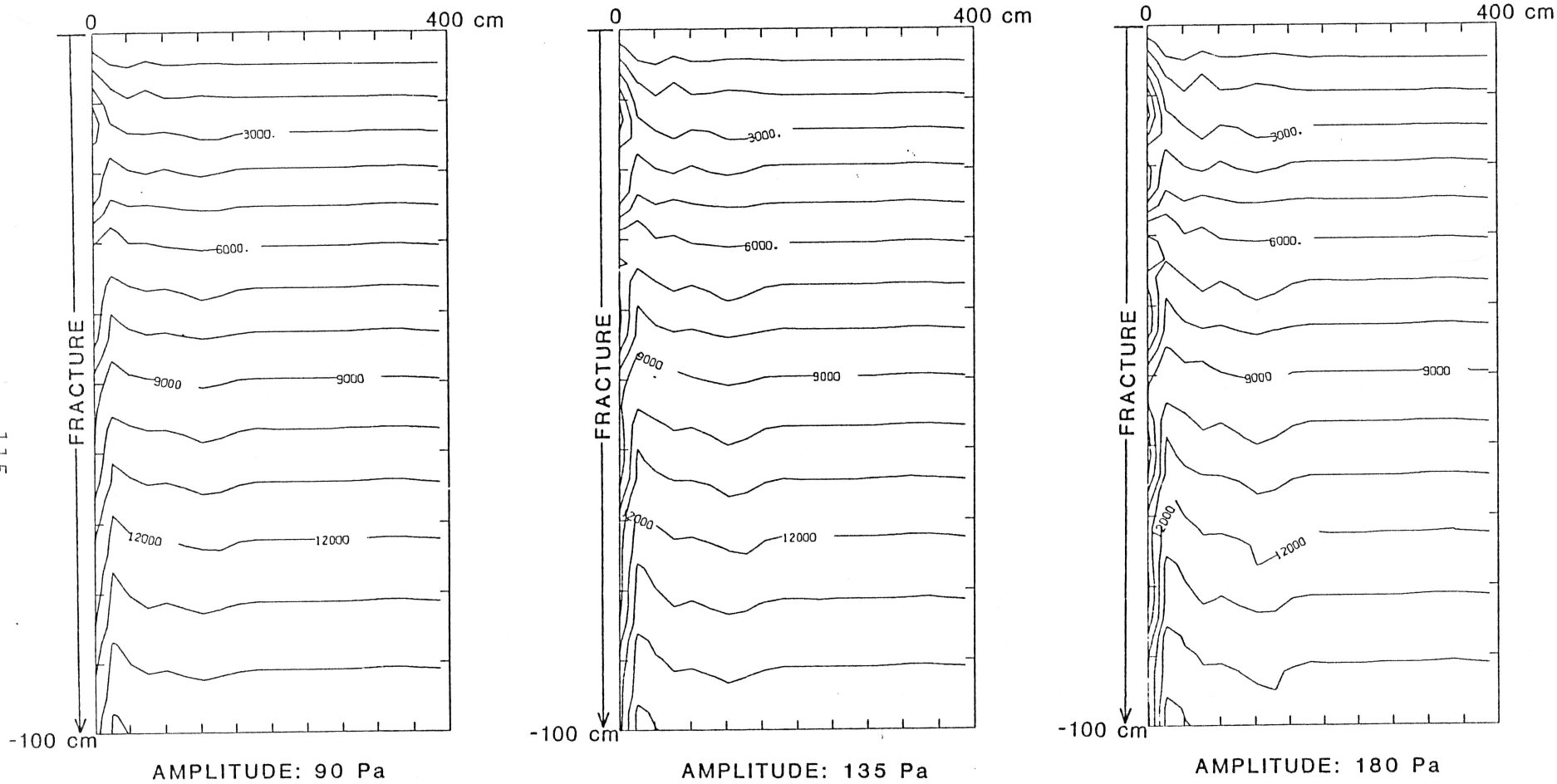

Figure 4-25b: Effect of amplitude of sinusoidal atmospheric pressure variation with a period of 720 second on radon concentrations ($atoms/cm^3$) in soil with cracks 400 cm deep, 0.06 cm wide and spaced 800 cm apart at 2160 seconds.

5. COMPARISON OF SENSITIVITY ANALYSIS TO FIELD DATA

The purpose of this chapter is to compare the results of the sensitivity analysis to data collected in the field by Schery et. al. (1984). The effects of long-term atmospheric pressure changes and of shorter-term wind speed fluctuations on radon fluxes from soil will be considered.

Figure 5-1 shows atmospheric pressure and radon flux density measured at two-hour intervals. A typical pressure drop is between 30 Pa/hr and 90 Pa/hr with a few changes of up to 240 Pa/hr. The atmospheric pressures in figure 4-1 were used as the top boundary condition for a transient, one-dimensional run. The one-dimensional model uses the same governing equations and boundary conditions developed in chapter 2, except that no cracks are included in the soil. The soil parameters in tables 4-1 and 4-2 were used. Figure 5-1 also shows the results of this simulation. The model results show considerably less deviation about a mean flux of about 2.0 atoms/s/cm^2 than do the field flux measurements. This is not surprising, since the field fluxes show more variation than the atmospheric pressures measured.

The large pressure drop in figure 5-1, lasting between 84 and 108 hours, is approximately 90 Pa/hr. The difference between flux densities predicted by the model and flux densities observed in the field is sometimes as

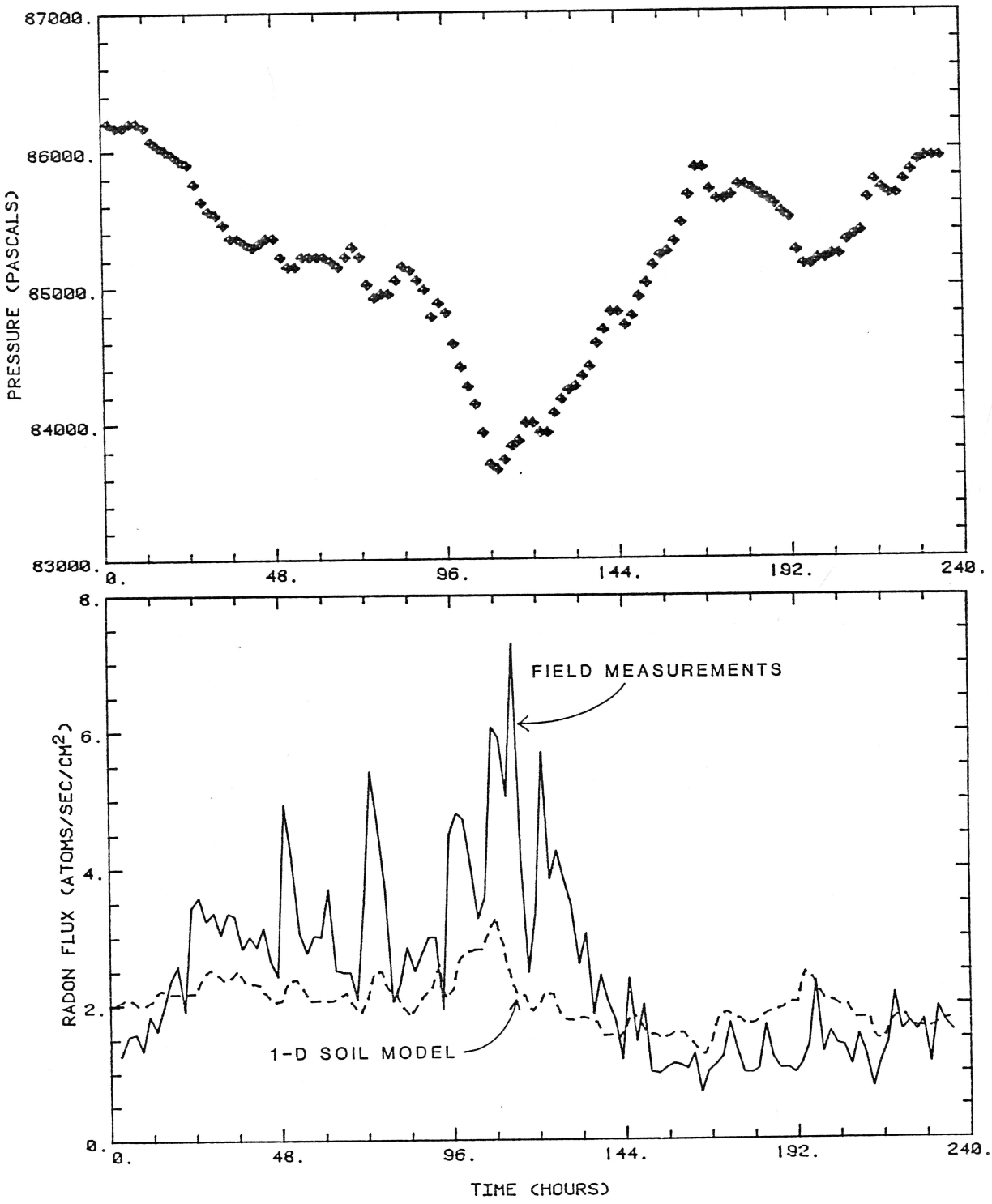

Figure 5-1: Atmospheric pressure and radon flux density measurements at field site of Scherey et. al. (1984). One-dimensional soil model used pressures and soil parameters from same article.

great as 100 percent. For soil with relatively shallow cracks, 30 cm, the model predicted an enhancement of flux of 1.5 percent (figure 4-3a) for a decrease in pressure of 90 Pa/hr. For a deeper crack, 400 cm, the predicted increase in flux is up to 20 percent (figure 4-3b). Even a soil model with very deep cracks can not replicate the fluxes observed in the field for a similar decrease in atmospheric pressure.

As mentioned before, there are variations in the observed fluxes shown in figure 5-1 which do not correlate to the changes in atmospheric pressure. Something other than long-term atmospheric pressure fluctuations must be affecting radon flux density from the soil. Changes in wind velocity are a likely candidate. Figure 5-2 shows measurements of subsurface pressure gradients taken between 5 cm and 56 cm below the surface, atmospheric pressure, and wind speed recorded at Schery's field site. The subsurface pressure gradients clearly show more correlation to wind speed than atmospheric pressure. Pressure gradients of 0.1 Pa/cm are typical, while a few are as high as 0.5 Pa/cm.

In section 4.3, sinusoidal variatons in surface pressure were applied with periods of 2 hours to about one minute. The predicted pressure gradients in the top 50 cm of soil (figures 4-16a, 4-21a, and 4-25a) are in the range of 0.1 Pa/cm to 0.5 Pa/cm. As mentioned above, similar pressure gradients were measured in the field and may be

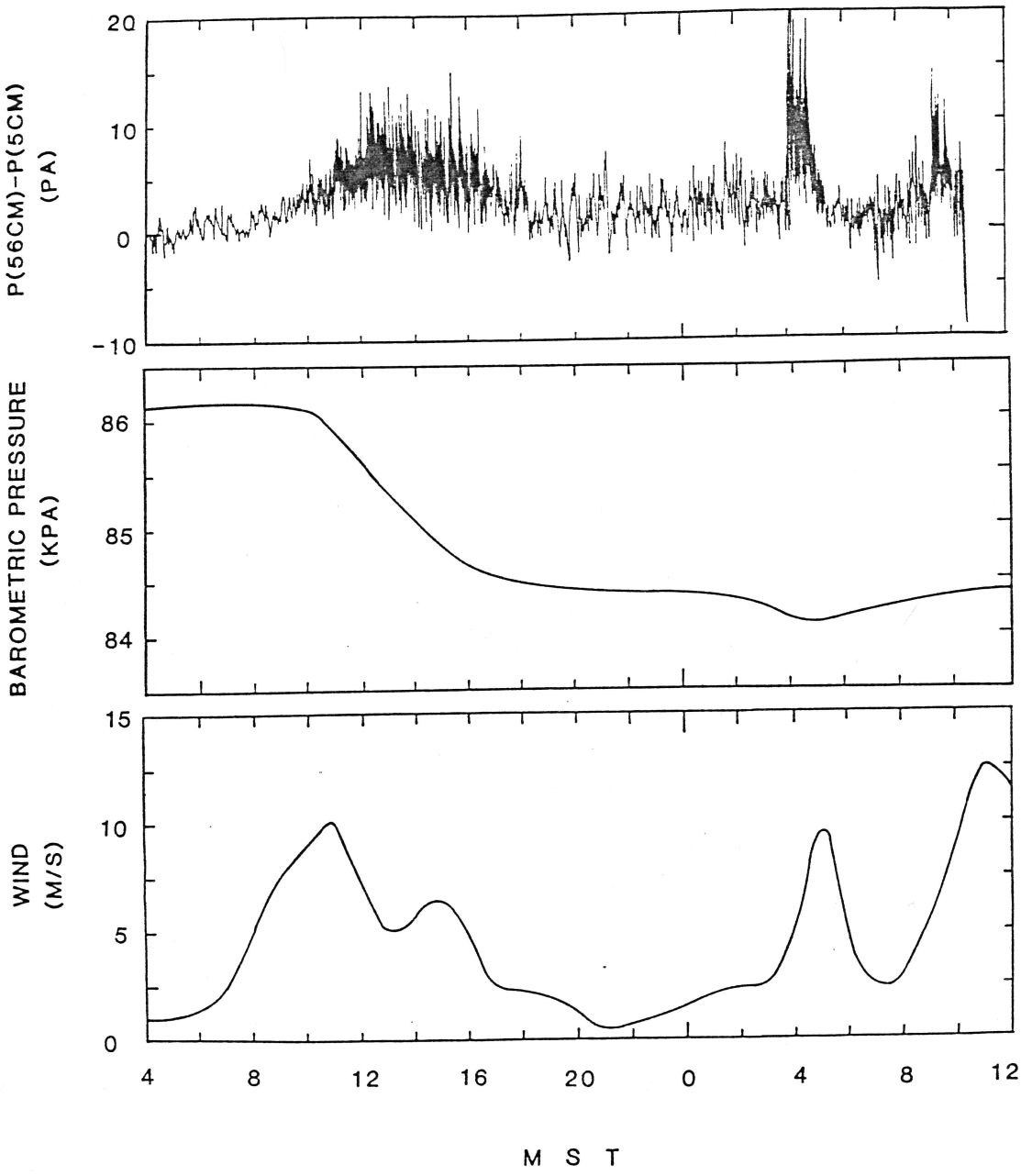

Figure 5-2: Measurements of subsurface pressure gradients, barometric pressure, and wind speed taken at field site of Schery and Siegel (in prep.) over a 32-hour period.

attributed to changes in wind speed at the surface. Sinusoidal variations in surface pressure with periods between 2 hours and 72 seconds an amplitude of 90 Pa show deviations in flux of up to 70 percent greater than a 1-D model, and mean fluxes up to 25 percent greater than a 1-D model (figure 4-20). Sinusoidal variations in atmospheric pressure with amplitudes between 90 and 180 Pa and a period of 720 seconds (12 minutes) show deviations in flux of up to 100 percent greater than a 1-D model, and mean fluxes up to 50 percent greater than a 1-D model (figure 4-24). Even the deviaton of flux densities predicted by the one-dimensional model is as great as 45 percent, but there is effectively no change in mean flux (figure 4-19). Pressure changes of short period, attributable to wind, at the surface of cracked soil can cause an increase in mean flux of radon from the soil, and also large deviations in flux.

The enhancement of radon flux densities caused by soil cracks and short-term variations in pressure attributed to wind are sufficient to explain the difference in mean flux between a one-dimensional soil model and observed radon fluxes. The variation in observed fluxes seen in figure 5-1 which do not correlate to atmospheric pressure changes are best explained by changes in wind speed.

The fact that rather large, widely spaced cracks are needed in the model to show a significant enhancement of

flux suggests that the shallow cracks observed on the soil surface at the site may be of negligible importance in enhancing the radon flux densities. Holes left by decayed plant roots, which are observed to be deep and widely spaced in an arid environment, may be a more significant factor than soil cracks in affecting radon fluxes.

6. SUMMARY

A brief summary of the major results and conclusions regarding radon flux densities in chapters 4 and 5 follow.

Crack Geometry:

Decreasing crack spacing causes an increase in radon flux density for decreasing pressure, if spacing is greater than depth. If spacing is less than depth, flux drops sharply with closer crack spacing. With close crack spacing, pressure decreases in adjacent cracks interfere, resulting in reduced pressure gradients in the soil towards the surface and crack.

Increasing the width of a crack causes an increase in radon flux density for decreasing atmospheric pressure, up to some limit governed by the spacing and depth.

Increasing the depth of a crack causes an increase in radon flux density for decreasing atmospheric pressure, up to an asymptotic value governed by the velocity near the bottom of the crack.

Soil type:

Pressure gradients are directly proportional to porosity because increasing soil porosity increases the gas storage capacity of the soil for changes in pressure, and pressure decreases do not move as far down into the soil. Radon concentrations do not change with a change in porosity because the only term in the transport equation

divided by the porosity is the specific discharge velocity, which is directly proportional to porosity. Although concentration gradients remain the same, diffusive flux from the soil increases because it is proportional to soil porosity. The pressure gradient in the crack increases proportionally to the porosity of the soil, resulting in more advective flux out of the crack.

Decreasing the permeability of the soil causes an increase in radon flux density. Stronger pressure gradients occur in the soil because decreased permeability does not allow pressure drops at the surface and crack to move into the soil. Stronger pressure gradients in the crack increase concentrations and surface flux.

Increasing the diffusion coefficient of the soil causes an increase in radon flux density because radon can diffuse towards the surface faster, and the diffusive flux across the top boundary is proportional to the diffusion coefficient.

Constant Pressure Variations:

The decrease in flux density caused by rising pressure is not as great as the increase in flux density caused by dropping pressure of the same magnitude. Therefore, periods of alternately dropping and rising pressure (such as a sinusoidal variation) show a net enhancement of flux.

Sinusoidal Pressure Fluctuations:

Decreasing the period of a sinusoidal variation in

atmospheric pressure but keeping the amplitude the same causes a small increase in mean radon flux densities but a large change in the deviation about the mean. The changes are up to 70 percent larger for a soil with cracks than a soil without cracks.

Increasing the amplitude of a sinusoidal variation in atmospheric pressure but keeping the period the same causes an increase in mean radon flux densities and also in the deviation about the mean. The changes in mean flux and standard deviation are up to 100 percent larger for a soil with cracks than for a soil without cracks.

Comparison of Sensitivity Analysis to Field Data

Radon flux densities observed in the field show more variation than do measurements of atmospheric pressure. Even a model with very deep cracks can not predict the large changes in flux observed in the field.

Pressure changes of short period, attributable to wind, at the surface of cracked soil can cause an increase in mean flux of radon from the soil, and also large deviations in flux. Shallow cracks in the soil probably have little effect on radon flux density. Changes in atmospheric pressure, coupled with changes in wind speed acting on soil with deep cracks or plant roots is the most likely explanation for the changes in radon flux densities observed in the field.

7. FUTURE WORK

Further investigations into the effects of changes in wind speed on radon fluxes would be enhanced by collection of field data by continuous recording instruments. The simultaneous collection of radon flux densities, subsurface pressures, wind speed measurements, and atmospheric pressures would be necessary to conclusively prove the theory that changes in wind speed influence radon flux densities more than atmospheric pressure changes.

Radon flux densities can be measured over smaller areas to determined whether plant roots significantly enhance radon fluxes. This can be accomplished by setting up two radon flux accumulators, one over an area with many plants, the other over an area with no plants.

Future models can be constructed to examine the effect of root holes. Solution of the pressure equation can be greatly simplified by the use of analytical solutions. Analytical solutions that might suffice are available for linear flow to partially penetrating wells (Lohman, 1979).

In any case, future modeling efforts could be greatly simplified by linearizing the pressure equation. During the present modeling, it was observed that by selecting small enough time steps for the nonlinear pressure equations in the finite element model CRACK, only two

iterations were required for convergence. This indicates that for small enough pressure changes, the equation is nearly linear. If the equation were assumed to be linear, the amount of computation time could be reduced by 30 percent with no significant loss of accuracy. Also, the greatest computing expense comes from having to double precision arrays in CRACK because such small pressure changes were being applied to very large absolute pressures. Using double precision arrays slows the program down considerably, and could be avoided by linearizing the pressure equation, which would then deal with pressure changes and not absolute pressures.

Appendix A: Conversion Factors

Pressure:

$1\ Pa = 10\ g/cm/s^2 = 9.869 \times 10^{-6}\ atm$

Concentrations:

$1\ atom/cm^3 = 5.68 \times 10^{-5}\ pCi/cm^3$

Flux density:

$1\ atom/cm^2/s = 1 \times 10^4\ atoms/m^2/2$

$= 5.68 \times 10^{-5}\ pCi/m^2/2$

Appendix B: Listing of Finite Element Program CRACK

```
C=====================================================================
C FORTRAN PROGRAM CRACK (final version)
C   SOLVES 2-D FLOW OF A COMPRESSIBLE, IDEAL GAS IN A POROUS MEDIA WITH
C   A SINGLE FRACTURE BY THE GALERKIN FINITE ELEMENT METHOD, ITERATES TO
C   REACH NONLINEAR SOLUTION; THEN CALCULATES THE VELOCITIES AT EACH
C   ELEMENT FROM THE PRESSURE HEAD DISTRIBUTION; THEN SOLVES 2-D
C   ADVECTIVE-DISPERSION EQUATION WITH UNIFORM FLOW, SOURCE TERM,
C   RADIOACTIVE DECAY, AND CONSTANT CONCENTRATION BOUNDARY CONDITIONS
C   FOR A POROUS MEDIA WITH A SINGLE FRACTURE BY
C   THE GALERKIN FINITE ELEMENT METHOD USING LINEAR RECTANGLAR ELEMENTS;
C   USES UPSTREAM WEIGHTING TO DAMP OUT NUMERICAL OSCILLATIONS
C   BY DIANA J. HOLFORD                 1/86                N.M.I.M.T.
C---------------------------------------------------------------------
C  Array parameters:
C   MN              Max. no. of nodes program arrays dimensioned to
C   MB              Max. bandwidth program arrays dimensioned to
C   ME              Max. no. of elements program arrays dimensioned to
C
C  Input Variables: (can be generated by DATGEN.FOR)
C   NN              No. of nodes
C   NNX             No. of nodes in X-direction
C   NNZ             No. of nodes in Z-direction
C   X(MN)           X-coordinate of node
C   Z(MN)           Z-coordinate of node
C   NE              no. of elements
C   NEX             no. of elements in X-direction
C   NEZ             no. of elements in Z-direction
C   IJKL(ME,4)      corner node nos. for each element
C   DELX0           Smallest X-direction grid spacing
C   DELXMX          Largest X-direction grid spacing
C   DELZ0           Smallest Z-direction grid spacing
C   DELZMX          Largest Z-direction grid spacing
C   TLX             Total model length in X-direction
C   TLZ             Total model length in Z-direction
C   WTRTBL          Depth to watertable
C   P0              Initial condition pressure
C   PATM            Pressure at top boundary of soil
C   DPDT            Change in pressure per unit time
C   PERIOD          Period of sinusoidal variation in PATM w/ time
C   AMPL            Amplitude of sinusoidal variation in PATM w/ time
C   INPATM          If .TRUE.  PATM vs. time read from CRACKD.ATM
C                   If .FALSE. PATM generated by function
C   C0              Top boundary condition concentration
C   CINFIN          Bottom boundary condition concentration
C   PORs            Effective Porosity of soil
```

```
C   KXXf            X-direction intrinsic permeability in fracture
C   KZZf            Z-direction intrinsic permeability in fracture
C   KXXs            X-direction intrinsic permeability in porous media
C   KZZs            Z-direction intrinsic permeability in porous media
C   MU              Dynamic viscosity of air
C   Dair            Diffusion coefficient in air (fracture)
C   Dsoil           Diffusion coefficient in porous media
C       SOURCE              Source constant
C       LAMBDA              Decay constant
C   FDEPTH          Fracture depth
C   HWIDTH          Fracture width divided by two
C   NNFX            No. nodes in fracture in X-direction
C   NNFZ            No. nodes in fracture in Z-direction
C   UPSLON          Upstream weighting parameter for Z-direction
C   EPS             Time weighting factor:
C                   0=Explicit,.5=Crank-Nicholson,1=Implicit
C   TOLp            Steady-State tolerance criteria for pressure
C   TOLc            Steady-State tolerance criteria for concentration
C   DELT            Time increment
C   DTMULT          Time step multiplication factor
C   NSTEPS          Number of time steps
C   TO              Initial simulation time
C   FINTIM          Final simulation time
C   ITERMX          Max. no. of iterations per time step
C   SBW             Semi-bandwidth
C   BW              Bandwidth
C   STEADY          If .TRUE.  program gives steady-state diffusive profile
C   NOFRAC          If .TRUE.  runs 1-D porous media model w/ no fracture
C                   If .FALSE. runs 2-D porous media model w/ 1 fracture
C   CONTIP          If .TRUE.  initial pressures read from CRACKD.PRS
C                   If .FALSE. initial pressures set equal to PO
C   CONTIC          If .TRUE.  initial concentrations read from CRACKD.CNC
C                   If .FALSE. initial concentrations set equal to CO
C
C  Program Variables:
C   LHS(MN,MB)      Global left-hand side matrix
C   RHS(MN)         Global right-hand side matrix
C   PRES(MN)        Pressures at each node, [LHS]{PRES}={RHS}
C   CONC(MN)        Concentrations at each node, [LHS]{CONC}={RHS}
C       POR         Porosity of an element
C   VZ(ME)          Darcy velocity in Z-direction of an element
C       VX(ME)              Darcy velocity in X-direction of an element
C   KXX             X-direction intrinsic permeability of an element
C   KZZ             Z-direction intrinsic permeability of an element
C   DXX             X-direction diffusion coefficient of an element
C   DZZ             Z-direction diffusion coefficient of an element
C   SIGMA           Same as Radon source term
C   DELTA           Same as POR/DELT
C   AA,BB           Dimensions of element
C   XSI(4),ETA(4)   Sampling points for Gaussian quadrature
C   NS(4)           Linear shape function
C   WS(4)           Upstream weighted shape function
C   NX(4),NZ(4)     Spatial derivatives of shape function
C   AE(4,4)         Rectangular element matrix (multiplied by C)
```

```
C       BE(4,4)              Rectangular element matrix (multiplied by dC/dt)
C       CE(4,4)            Rectangular element matrix (multiplied by 1)
C   TIME              Simulation time
C   NSTEP             Time step number
C   DIRAC             Dirac delta function, =-1 if true, =0 if false
C   Pp                Pressure at previous time step at a node
C-----------------------------------------------------------------------
    DOUBLE PRECISION X(1500),Z(1500),LHS(1500,49),RHS(1500),
     &       PRES(1500),CONC(1500),OLPRES(1500),Pp,
     &       XSI(4),ETA(4),NS(4),NX(4),NZ(4),WS(4),AMPL,
     &       AE(4,4),BE(4,4),CE(4,4),PO,PATM,DPDT,PERIOD,CO,CINFIN,
     &       MU,PORs,KXXs,KZZs,KXXf,KZZf,KXX,KZZ,POR,LAMBDA,
     &           VX(1500),VZ(1500),ERR,PMAX,UPSLON,HWIDTH,FDEPTH,
     &           INTERP,Pg(4),FLUX(49),COEF1(49,49),COEF2(49),AA,BB
    INTEGER IJKL(1500,4),EL,BW,SBW
    LOGICAL STEADY,CONTIP,CONTIC,CONVRG,INPATM,NOFRAC
    COMMON/LOGI/STEADY,CONTIP,CONTIC,CONVRG,INPATM,NOFRAC
    COMMON/FLUXS/FLUXF,FLUXM,FLUX,AVEFLX
    COMMON/GAUSSP/XSI,ETA,NS,NX,NZ,WS
    COMMON/ELEMS/I,J,K,L,AA,BB,Pp
    COMMON/EMATRC/AE,BE,CE
    COMMON/GMATRC/LHS,RHS
    COMMON/ANSWER/PRES,CONC
    COMMON/MATRL/MU,PORs,KXXs,KZZs,KXXf,KZZf,Dsoil,Dair,
     &                    SOURCE,LAMBDA,WTRTBL
    COMMON/VEL/VX,VZ
    COMMON/FRAC/FDEPTH,HWIDTH,NNFX,NNFZ
    COMMON/SIZES/MN,MB,ME,NN,NNX,NNZ,NE,NEX,NEZ
    COMMON/GRID1/DELXO,DELZO,DELXMX,DELZMX,TLX,TLZ,BW,SBW
    COMMON/GRID2/IJKL,X,Z
    COMMON/BC/PO,PATM,DPDT,AMPL,PERIOD,CO,CINFIN
    COMMON/TIMES/EPS,TOLp,TOLc,DELT,DTMULT,NSTEPS,TO,FINTIM,ITERMX
    COMMON/LOOP/EL,IQ,M,N
    COMMON/UPSTRM/UPSLON
    DATA MN,MB,ME/1500,49,1500/
    DATA XSI/-.57735,.57735,.57735,-.57735/
    DATA ETA/-.57735,-.57735,.57735,.57735/
    DATA PI/3.14159265/
C-----------------------------------------------------------------------
C  create input and output files
C-----------------------------------------------------------------------
    OPEN(31,FILE='CRACKD.DAT') ! input
    OPEN(30,FILE='CRACKD.ALL') ! output
    OPEN(35,FILE='CRACKD.VEL') ! velocities
    OPEN(43,FILE='CRACKD.FLX') ! model flux predictions
    OPEN(44,FILE='CRACKD.FXA') ! average fluxes
    OPEN(45,FILE='CRACKD.FXF') ! fracture fluxes
    OPEN(46,FILE='CRACKD.FXM') ! soil fluxes
    OPEN(48,FILE='CRACKD.CNC') ! concentrations for contour plots
    OPEN(49,FILE='CRACKD.PRS') ! pressures for contour plots
    OPEN(42,FILE='CRACKD.PRE') ! PATM vs. time output
```

```
      OPEN(50,FILE='CRACKD.ATM') ! PATM vs. time input
C-----------------------------------------------------------------------
      CALL HEADER
      CALL INDATA
      CALL INITAL(TIME)
      IF (CONTIP) PATM=SQRT(PRES(1))
C-----------------------------------------------------------------------
C  begin time loop
C-----------------------------------------------------------------------
      IF (STEADY) GO TO 200
  100       DO 500 NSTEP=1,NSTEPS
      DELT=DELT*DTMULT
      TIME=TIME+DELT
      WRITE(5,*)' TIME(',NSTEP,')=',TIME
C-----------------------------------------------------------------------
C********************* SOLVE FLOW EQUATIONS ****************************
C-----------------------------------------------------------------------
C  update top pressure boundary condition
C-----------------------------------------------------------------------
      IF (INPATM) THEN
        READ(50,*) NDUM,TDUM,PATM
      ELSE
        PMEAN=PMEAN+DPDT*DELT
        PATM=PO+AMPL*SIN(TIME/PERIOD*2.*PI)+PMEAN
      ENDIF
      WRITE(5,*)' PATM=',PATM
      WRITE(42,*) NSTEP,TIME,PATM
C-----------------------------------------------------------------------
C  save pressures from last time step
C-----------------------------------------------------------------------
      DO 101 N=1,NN
  101         OLPRES(N)=PRES(N)
C-----------------------------------------------------------------------
C  begin iteration loop
C-----------------------------------------------------------------------
      DO 190 ITER=1,ITERMX
      WRITE(5,*)' ITER=',ITER
C-----------------------------------------------------------------------
C  form matrix equations
C-----------------------------------------------------------------------
      DO 110 EL=1,NE                                    ! element loop
```

```
      CALL ELPROP(KXX,KZZ,POR,DXX,DZZ,SIGMA,DELTA)
      DO 110 IQ=1,4                                  ! Gauss point loop
        CALL GAUSSQ(0.0)
        Pp=SQRT(INTERP(PRES))        ! pressure at previous time step
        DO 110 M=1,4                                  ! summation loops
        DO 110 N=1,4
 110              CALL MATRX(OLPRES,0.,0.,KXX/MU,KZZ/MU,0.,DELTA/Pp,0.)
C-------------------------------------------------------------------------
    CALL BOUND1(PATM**2,1,NNX,0.,0,0)
    CALL SLBNS(LHS,RHS,NN,BW,MN,MB)
C-------------------------------------------------------------------------
C  check to see if flow field has converged
C-------------------------------------------------------------------------
    CONVRG=.TRUE.
    ERR=0.
    PMAX=0.
    DO 120 N=1,NN
    PMAX=DMAX1(ABS(PRES(N)),PMAX)
 120        ERR=DMAX1(ABS(PRES(N)-RHS(N)),ERR)
    ERR=ERR/PMAX
    IF(ERR.GT.TOLp) CONVRG=.FALSE.
    WRITE(5,*)'              ERR=',ERR
C-------------------------------------------------------------------------
C  reset matrices
C-------------------------------------------------------------------------
 130        DO 140 I=1,NN
      PRES(I)=RHS(I)      ! subroutine returns answers in RHS matrix
      RHS(I)=0.0
    DO 140 J=1,BW
 140          LHS(I,J)=0.0
C-------------------------------------------------------------------------
C  end iteration loop
C-------------------------------------------------------------------------
    IF (CONVRG) GO TO 199
 190        CONTINUE
    WRITE(5,*)' PRESSURE SOLUTION FAILED TO CONVERGE WITHIN ',
     &      ITERMX,' ITERATIONS AT TIME=',TIME
C-------------------------------------------------------------------------
C******************** SOLVE VELOCITY EQUATIONS **************************
C-------------------------------------------------------------------------
 199        CALL VELOCI
C-------------------------------------------------------------------------
C******************** SOLVE TRANSPORT EQUATIONS *************************
```

```
C-----------------------------------------------------------------------
 200        DO 210 EL=1,NE                                    ! element loop
      CALL ELPROP(KXX,KZZ,POR,DXX,DZZ,SIGMA,DELTA)
      DO 210 IQ=1,4                                  ! Gauss point loop
        CALL GAUSSQ(UPSLON)
        DO 210 M=1,4                                  ! summation loops
        DO 210 N=1,4
 210              CALL MATRX(CONC,VX(EL),VZ(EL),DXX*POR,DZZ*POR,
     $                                  LAMBDA*POR,DELTA,SIGMA*POR)
C-----------------------------------------------------------------------
C  save matrix coefficients for flux calculations
C-----------------------------------------------------------------------
    DO 215 NR=NNFX,NNX
    COEF2(NR)=RHS(NR)
    DO 215 NC=1,BW
 215        COEF1(NR,NC)=LHS(NR,NC)
C-----------------------------------------------------------------------
    CALL BOUND1(CO,NNFX,NNX,0.,0,0)
    CALL SLBNS(LHS,RHS,NN,BW,MN,MB)
C-----------------------------------------------------------------------
C  check to see if transient concentraton field has reached steady-state
C-----------------------------------------------------------------------
    DO 220 N=1,NN
 220        IF(ABS(CONC(N)-RHS(N)).GT.TOLc) GO TO 230
    WRITE(30,*)'*** CONCENTRATION FIELD REACHED STEADY-STATE AT TIME
     &= ',TIME,' ***'
C-----------------------------------------------------------------------
C  reset matrices
C-----------------------------------------------------------------------
 230        DO 240 I=1,NN
      CONC(I)=RHS(I)      ! subroutine returns answers in RHS matrix
      RHS(I)=0.0
    DO 240 J=1,BW
 240          LHS(I,J)=0.0
C-----------------------------------------------------------------------
C***************** SOLVE BOUNDARY FLUX EQUATIONS ************************
C-----------------------------------------------------------------------
C  calculate flux across top boundary: FLUX OUT (+), FLUX IN (-)
C-----------------------------------------------------------------------
 300        FLASTF=FLUXF
   FLASTM=FLUXM
```

```
    FLASTA=AVEFLX
    FLUXF=0.
    FLUXM=0.
    AVEFLX=0.
C-------------------------------------------------------------------------
C  Back substitute to get flux integrated over boundary at soil nodes
C-------------------------------------------------------------------------
    DO 310 NR=NNFX,NNX
      FLUX(NR)=COEF2(NR)
      DO 310 NC=1,BW
        JC=-SBW+NC+NR
        IF(JC.LE.0) GO TO 310
        FLUX(NR)=FLUX(NR)-COEF1(NR,NC)*CONC(JC)
 310        CONTINUE
    DO 320 NR=NNFX+1,NNX
 320      FLUXM=FLUXM+FLUX(NR)/TLX
    IF (NOFRAC) THEN
      FLUXM=FLUXM+FLUX(NNFX)/TLX
    ELSE
      FLUXF=FLUX(NNFX)/TLX       ! Diffusive flux out of fracture
    ENDIF
C-------------------------------------------------------------------------
C  Divide fluxes by length of boundary around node to get flux/unit area
C-------------------------------------------------------------------------
    DO 330 NR=NNFX,NNX-1
 330          FLUX(NR)=FLUX(NR)/(X(NR+1)-X(NR-1))*2
    FLUX(NNX)=FLUX(NNX)/(X(NNX)-X(NNX-1))*2
C-------------------------------------------------------------------------
C  Solve for advective fluxes out of fracture
C-------------------------------------------------------------------------
    IF (NOFRAC) GO TO 335
    DO 333 NR=1,NNFX-1
    FLUX(NR)=VZ(NR)*CONC(NR)
 333        FLUXF=FLUXF+FLUX(NR)/(NNFX-1)*HWIDTH/2/TLX
 335        AVEFLX=FLUXM+FLUXF
    DFLUXM=FLASTM-FLUXM
    DFLUXF=FLASTF-FLUXF
    DAVFLX=FLASTA-AVEFLX
C-------------------------------------------------------------------------
C  print out fluxes
C-------------------------------------------------------------------------
    WRITE(43,*)' TIME= ',TIME,' dPdt=',DPDT,' PATM=',PATM
    WRITE(43,*)' FLUXF=',FLUXF,' FLUXM=',FLUXM,' AVEFLX=',AVEFLX
    WRITE(5,*)' FLUXF=',FLUXF,' FLUXM=',FLUXM
       WRITE(43,*)' dFLUXF=',dFLUXF,' dFLUXM=',dFLUXM,' dAVEFLX=',DAVFLX
```

```
      WRITE(5,*)' dFLUXF=',dFLUXF,' dFLUXM=',dFLUXM
  DO 340 N=1,NNX
340       WRITE(43,*)N,FLUX(N)
  WRITE(43,*)'~~~~~~~~~~~~~~~~~~~~~~~~~~~~~~~~~~~~~~~~~~~~~~~~~~~'
  WRITE(44,*) NSTEP,TIME,AVEFLX
  WRITE(45,*) NSTEP,TIME,FLUXF
  WRITE(46,*) NSTEP,TIME,FLUXM
C-----------------------------------------------------------------------
C  end time loop
C-----------------------------------------------------------------------
  IF (STEADY) GO TO 600
500       CONTINUE
C-----------------------------------------------------------------------
C  print out final results
C-----------------------------------------------------------------------
600       CALL OUTDAT (TIME,NSTEP)
C-----------------------------------------------------------------------
C  close files
C-----------------------------------------------------------------------
  CLOSE(30)
  CLOSE(31)
  CLOSE(35)
  CLOSE(43)
  CLOSE(44)
  CLOSE(45)
  CLOSE(46)
  CLOSE(48)
  CLOSE(49)
  CLOSE(42)
  CLOSE(50)
C-----------------------------------------------------------------------
C  end of main program
C-----------------------------------------------------------------------
  END



C=======================================================================
```

```
      SUBROUTINE HEADER
C-----------------------------------------------------------------------
C - Prints time and date, my name, problem title, problem no.,
C   program name, and comments
C-----------------------------------------------------------------------
      DOUBLE PRECISION TITLE(20)
      INTEGER PROB
      LOGICAL STEADY,CONTIP,CONTIC,CONVRG,INPATM,NOFRAC
      external *TIME,*date
      COMMON/LOGI/STEADY,CONTIP,CONTIC,CONVRG,INPATM,NOFRAC
      call date(ndate,mdate)
      CALL TIME(ETUNIM,TZERO)
      WRITE(30,1000)NDATE,MDATE,ETUNIM
      WRITE(30,*)'CRACKD.FOR (final version)'! WRITE PROGRAM NAME
      WRITE(30,*)'DIANA J. HOLFORD'      ! WRITE NAME
      WRITE(30,*)'*****************************************************
     &*******************'
      IF (NOFRAC) THEN
        WRITE(30,*)' *** 1-D POROUS MEDIA W/ NO FRACTURE ***'
      ELSE
        WRITE(30,*)' *** 2-D POROUS MEDIA W/ ONE FRACTURE ***'
      ENDIF
      WRITE(30,*)'*****************************************************
     &*******************'
      READ(31,1001)(TITLE(I),I=1,20)
      WRITE(30,1001)(TITLE(I),I=1,20)    ! WRITE PROBLEM TITLE
      read(31,1002) NRUN
      write(30,1003) NRUN
c     10      READ (31,1001) (TITLE(I),I=1,20)
c     IF (TITLE(1).EQ.'*') THEN          ! COMMENTS MUST START WITH A *
c       WRITE(30,1001) (TITLE(I),I=1,20) ! WRITE COMMENTS
c       GO TO 10
c     ENDIF
      WRITE(30,*)'*****************************************************
     &*******************'
 1000       format(1X,5A5)
 1001       FORMAT(20A4)
 1002       FORMAT(I6)
 1003       FORMAT(' RUN NUMBER ',I6)
      end

C=======================================================================
```

```
      SUBROUTINE INDATA
C-----------------------------------------------------------------------
C     Reads in all input data (which can be generated by DATGEN.FOR)
C-----------------------------------------------------------------------
      DOUBLE PRECISION X(1500),Z(1500),UPSLON,
     &       MU,PORs,KXXs,KZZs,KXXf,KZZf,KXX,KZZ,POR,LAMBDA
     &       ,PO,PATM,DPDT,PERIOD,AMPL,CO,CINFIN,FDEPTH,HWIDTH
      INTEGER IJKL(1500,4),EL,BW,SBW
      LOGICAL STEADY,CONTIP,CONTIC,CONVRG,INPATM,NOFRAC
      COMMON/LOGI/STEADY,CONTIP,CONTIC,CONVRG,INPATM,NOFRAC
      COMMON/MATRL/MU,PORs,KXXs,KZZs,KXXf,KZZf,Dsoil,Dair,
     &             SOURCE,LAMBDA,WTRTBL
      COMMON/FRAC/FDEPTH,HWIDTH,NNFX,NNFZ
      COMMON/SIZES/MN,MB,ME,NN,NNX,NNZ,NE,NEX,NEZ
      COMMON/GRID1/DELXO,DELZO,DELXMX,DELZMX,TLX,TLZ,BW,SBW
      COMMON/GRID2/IJKL,X,Z
      COMMON/BC/PO,PATM,DPDT,AMPL,PERIOD,CO,CINFIN
      COMMON/TIMES/EPS,TOLp,TOLc,DELT,DTMULT,NSTEPS,TO,FINTIM,ITERMX
      COMMON/UPSTRM/UPSLON
C-----------------------------------------------------------------------
C  read in x,z coordinates for each node
C-----------------------------------------------------------------------
      READ(31,*)NN,NNX,NNZ
      DO 10 N=1,NN
   10         READ(31,*) NODE,X(NODE),Z(NODE)
C-----------------------------------------------------------------------
C  read in i,j,k,l nodes for each element
C-----------------------------------------------------------------------
      READ(31,*)NE,NEX,NEZ
      DO 20 N=1,NE
   20         READ(31,*) EL,IJKL(EL,1),IJKL(EL,2),IJKL(EL,3),IJKL(EL,4)
C-----------------------------------------------------------------------
C  read in other data
C-----------------------------------------------------------------------
      READ(31,*)STEADY,CONTIP,CONTIC,NOFRAC
      READ(31,*)PO,PATM,dPdt,AMPL,PERIOD,INPATM
      READ(31,*)CO,CINFIN
      READ(31,*)KXXs,KZZs,KXXf,KZZf
      READ(31,*)Dsoil,Dair
      READ(31,*)PORs,MU,WTRTBL
      READ(31,*)SOURCE,LAMBDA
      READ(31,*)FDEPTH,HWIDTH,NNFX,NNFZ
      READ(31,*)EPS,TOLp,TOLc,DELT,DTMULT,NSTEPS,TO,FINTIM,ITERMX
      READ(31,*)UPSLON
      READ(31,*)DELXO,DELZO,DELXMX,DELZMX,TLX,TLZ
      READ(31,*)SBW,BW
```

```
      IF((NN.GT.MN).OR.(NE.GT.ME).OR.(BW.GT.MB)) THEN
        WRITE(5,*)' *** MATRIX TOO LARGE *** PROGRAM STOPPED ***'
        IF(NN.GT.MN) WRITE(5,*) ' NN=',NN,' > MN=',MN
        IF(NE.GT.ME) WRITE(5,*) ' NE=',NE,' > ME=',ME
        IF(BW.GT.MB) WRITE(5,*) ' BW=',BW,' > MB=',MB
        STOP
      ENDIF
      RETURN
      END

C=======================================================================
```

```
      SUBROUTINE INITAL (TIME)
C-----------------------------------------------------------------------
C   Initializes time counter and arrays
C-----------------------------------------------------------------------
      DOUBLE PRECISION PRES(1500),CONC(1500),UPSLON
     &          ,PO,PATM,DPDT,PERIOD,AMPL,CO,CINFIN
      LOGICAL STEADY,CONTIP,CONTIC,CONVRG,INPATM,NOFRAC
      COMMON/LOGI/STEADY,CONTIP,CONTIC,CONVRG,INPATM,NOFRAC
      COMMON/ANSWER/PRES,CONC
      COMMON/SIZES/MN,MB,ME,NN,NNX,NNZ,NE,NEX,NEZ
      COMMON/BC/PO,PATM,DPDT,AMPL,PERIOD,CO,CINFIN
      COMMON/TIMES/EPS,TOLp,TOLc,DELT,DTMULT,NSTEPS,TO,FINTIM,ITERMX
C-----------------------------------------------------------------------
C  set initial conditions
C-----------------------------------------------------------------------
      TIME=TO
      IF (STEADY) THEN
        WRITE(5,*) '<<< STEADY-STATE RUN >>>'
        WRITE(30,*) '<<< STEADY-STATE RUN >>>'
        GO TO 45
      ENDIF
C-----------------------------------------------------------------------
      IF (CONTIP) THEN
        WRITE(5,*) '<<< CONTINUATION RUN FOR PRESSURES>>>'
        WRITE(30,*) '<<< CONTINUATION RUN FOR PRESSURES>>>'
        DO 10 N=1,NN
 10   READ(49,*) NDUM,XDUM,ZDUM,PRES(N)
      ELSE
        WRITE(5,*) '<<< TRANSIENT RUN FOR PRESSURES >>>'
        WRITE(30,*) '<<< TRANSIENT RUN FOR PRESSURES >>>'
        DO 20 N=1,NN
 20       PRES(N)=PO
      ENDIF
C-----------------------------------------------------------------------
      IF (CONTIC) THEN
        WRITE(5,*) '<<< CONTINUATION RUN FOR CONCENTRATIONS >>>'
        WRITE(30,*) '<<< CONTINUATION RUN FOR CONCENTRATIONS >>>'
        DO 30 N=1,NN
 30   READ(48,*) NDUM,XDUM,ZDUM,CONC(N)
      ELSE
        WRITE(5,*) '<<< TRANSIENT RUN FOR CONCENTRATIONS >>>'
        WRITE(30,*) '<<< TRANSIENT RUN FOR CONCENTRATIONS >>>'
        DO 40 N=1,NN
 40       CONC(N)=CO
      ENDIF
C-----------------------------------------------------------------------
 45   DO 50 N=1,NN
```

```
 50 PRES(N)=PRES(N)**2     ! solving equations with pressure squared
C-------------------------------------------------------------------------
    REWIND(48)
    REWIND(49)
C
    RETURN
    END

C=========================================================================
```

```
      SUBROUTINE ELPROP (KXX,KZZ,POR,DXX,DZZ,SIGMA,DELTA)
C-----------------------------------------------------------------------
C     Determines corner node numbers, dimensions, and
C     properties of each element
C-----------------------------------------------------------------------
      DOUBLE PRECISION X(1500),Z(1500),
     &  PRES(1500),CONC(1500),FDEPTH,HWIDTH,
     &  MU,PORs,KXXs,KZZs,KXXf,KZZf,KXX,KZZ,POR,AA,BB
      INTEGER IJKL(1500,4),EL,BW,SBW
      LOGICAL STEADY,CONTIP,CONTIC,CONVRG,INPATM,NOFRAC
      COMMON/LOGI/STEADY,CONTIP,CONTIC,CONVRG,INPATM,NOFRAC
      COMMON/TIMES/EPS,TOLp,TOLc,DELT,DTMULT,NSTEPS,TO,FINTIM,ITERMX
      COMMON/ANSWER/PRES,CONC
      COMMON/MATRL/MU,PORs,KXXs,KZZs,KXXf,KZZf,Dsoil,Dair,
     &                        SOURCE,LAMBDA,WTRTBL
      COMMON/FRAC/FDEPTH,HWIDTH,NNFX,NNFZ
      COMMON/SIZES/MN,MB,ME,NN,NNX,NNZ,NE,NEX,NEZ
      COMMON/GRID1/DELXO,DELZO,DELXMX,DELZMX,TLX,TLZ,BW,SBW
      COMMON/GRID2/IJKL,X,Z
      COMMON/ELEMS/I,J,K,L,AA,BB,Pp
      COMMON/LOOP/EL,IQ,M,N
C-----------------------------------------------------------------------
C  corner node numbers for each element
C-----------------------------------------------------------------------
      I=IJKL(EL,1)
      J=IJKL(EL,2)
      K=IJKL(EL,3)
      L=IJKL(EL,4)
C-----------------------------------------------------------------------
C  dimensions of element
C-----------------------------------------------------------------------
      AA=ABS(ABS(X(J))-ABS(X(I)))/2
      BB=ABS(ABS(Z(L))-ABS(Z(I)))/2
C-----------------------------------------------------------------------
C  assign material properties
C-----------------------------------------------------------------------
      IF((X(I).LT.HWIDTH).AND.(ABS(Z(I)).LE.FDEPTH)) THEN ! fracture
        KXX=KXXf
        KZZ=KZZf
        POR=1.0
        DXX=Dair
        DZZ=Dair
        SIGMA=0.
        DELTA=POR/DELT
      ELSE IF ((Z(I).EQ.TLZ).AND.(ABS(TLZ).LT.WTRTBL)) THEN ! bottom
        KXX=KXXs
```

```
      DXX=Dsoil
      KZZ=KZZs/(ABS(WTRTBL)-ABS(TLZ))*DELXMX
      POR=PORS*(ABS(WTRTBL)-ABS(TLZ))*DELXMX
      DZZ=Dsoil/(ABS(WTRTBL)-ABS(TLZ))*DELXMX
      SIGMA=SOURCE
      DELTA=POR/DELT
    ELSE                              ! soil
      KXX=KXXs
      KZZ=KZZs
      POR=PORs
      DXX=Dsoil
      DZZ=Dsoil
      SIGMA=SOURCE
      DELTA=POR/DELT
    ENDIF
    IF (STEADY) DELTA=0.0
    RETURN
    END

C=======================================================================
```

```
   SUBROUTINE GAUSSQ (UPSLON)
C-----------------------------------------------------------------------
C      Solves shape function integrals at a node by Gaussian quadrature
C-----------------------------------------------------------------------
   DOUBLE PRECISION X(1500),Z(1500),UPSLON,
    &           VX(1500),VZ(1500),AA,BB,FDEPTH,HWIDTH,
    &       XSI(4),ETA(4),NS(4),NX(4),NZ(4),WS(4)
   INTEGER IJKL(1500,4),EL,BW,SBW
   COMMON/GAUSSP/XSI,ETA,NS,NX,NZ,WS
   COMMON/ELEMS/I,J,K,L,AA,BB,Pp
   COMMON/GRID2/IJKL,X,Z
   COMMON/LOOP/EL,IQ,M,N
   COMMON/VEL/VX,VZ
   COMMON/FRAC/FDEPTH,HWIDTH,NNFX,NNFZ
C-----------------------------------------------------------------------
C  Calculate shape functions (NS) and their spatial derivatives (NX,NZ)
C  at a Gauss point IQ (IQ=1,4)
C-----------------------------------------------------------------------
      NS(1)=(1-XSI(IQ))*(1-ETA(IQ))/4.
      NS(2)=(1+XSI(IQ))*(1-ETA(IQ))/4.
      NS(3)=(1+XSI(IQ))*(1+ETA(IQ))/4.
      NS(4)=(1-XSI(IQ))*(1+ETA(IQ))/4.
      NX(1)=-(1-ETA(IQ))/4./AA
      NX(2)= (1-ETA(IQ))/4./AA
      NX(3)= (1+ETA(IQ))/4./AA
      NX(4)=-(1+ETA(IQ))/4./AA
      NZ(1)=-(1-XSI(IQ))/4./BB
      NZ(2)=-(1+XSI(IQ))/4./BB
      NZ(3)= (1+XSI(IQ))/4./BB
      NZ(4)= (1-XSI(IQ))/4./BB
C-----------------------------------------------------------------------
C  UPSLON is (+) if Vz is (+), and UPSLON is (-) if Vz is (-)
C-----------------------------------------------------------------------
   IF(UPSLON.NE.0.) UPSLON=DSIGN(ABS(UPSLON),VZ(IQ))
C-----------------------------------------------------------------------
C  add upstream weighting to damp out numerical oscillations
C  due to high fracture velocities in the Z-direction
C-----------------------------------------------------------------------
      IF((X(I).LT.HWIDTH).AND.(ABS(Z(I)).LE.FDEPTH)) THEN
        WS(1)=NS(1)*((-3.*UPSLON*ETA(IQ)-3.*UPSLON-2.)+4.)/2. ! fracture
        WS(2)=NS(2)*((-3.*UPSLON*ETA(IQ)-3.*UPSLON-2.)+4.)/2.
        WS(3)=NS(3)*((-3.*UPSLON*ETA(IQ)-3.*UPSLON-2.)+4.)/2.
        WS(4)=NS(4)*((-3.*UPSLON*ETA(IQ)-3.*UPSLON-2.)+4.)/2.
        NZ(1)=NZ(1)*(1.-3.*UPSLON*ETA(IQ))
            NZ(2)=NZ(2)*(1.-3.*UPSLON*ETA(IQ))
```

```
          NZ(3)=NZ(3)*(1.-3.*UPSLON*ETA(IQ))
          NZ(4)=NZ(4)*(1.-3.*UPSLON*ETA(IQ))
        ENDIF
      RETURN
      END

C=====================================================================
```

```
      SUBROUTINE MATRX (ANSW,A1,A2,A3,A4,A5,B1,C1)
C-----------------------------------------------------------------------
C     Forms matrix for each element, then forms global matrix
C-----------------------------------------------------------------------
      DOUBLE PRECISION X(1500),Z(1500),LHS(1500,49),RHS(1500),
     &       XSI(4),ETA(4),NS(4),NX(4),NZ(4),WS(4),
     &       AE(4,4),BE(4,4),CE(4,4),FDEPTH,HWIDTH,
     &       MU,PORs,KXXs,KZZs,KXXf,KZZf,KXX,KZZ,POR,LAMBDA,
     &           VX(1500),VZ(1500),P0,PATM,DPDT,PERIOD,AMPL,C0,CINFIN,
     &           INTERP,UPSLON,AA,BB,A1,A2,A3,A4,A5,
     &       ANSW(1500)            ! solution vector, either PRES or CON          C
      INTEGER IJKL(1500,4),EL,BW,SBW
      LOGICAL DIRAC
      COMMON/GAUSSP/XSI,ETA,NS,NX,NZ,WS
      COMMON/ELEMS/I,J,K,L,AA,BB,Pp
      COMMON/EMATRC/AE,BE,CE
      COMMON/GMATRC/LHS,RHS
      COMMON/MATRL/MU,PORs,KXXs,KZZs,KXXf,KZZf,Dsoil,Dair,
     &                      SOURCE,LAMBDA,WTRTBL
      COMMON/VEL/VX,VZ
      COMMON/FRAC/FDEPTH,HWIDTH,NNFX,NNFZ
      COMMON/SIZES/MN,MB,ME,NN,NNX,NNZ,NE,NEX,NEZ
      COMMON/GRID1/DELX0,DELZ0,DELXMX,DELZMX,TLX,TLZ,BW,SBW
      COMMON/GRID2/IJKL,X,Z
      COMMON/BC/P0,PATM,DPDT,AMPL,PERIOD,C0,CINFIN
      COMMON/TIMES/EPS,TOLp,TOLc,DELT,DTMULT,NSTEPS,T0,FINTIM,ITERMX
      COMMON/LOOP/EL,IQ,M,N
      COMMON/UPSTRM/UPSLON
C-----------------------------------------------------------------------
C  form element matrix
C-----------------------------------------------------------------------
      DIRAC=M.EQ.N
      AE(M,N)=A1*(NS(M)*NX(N))*AA*BB     ! Advection (x)
     &             +A2*(NS(M)*NZ(N))*AA*BB     ! Advection (z)
     &             +A3*(NX(M)*NX(N))*AA*BB     ! Conductance or Dispers. (x)
     &             +A4*(NZ(M)*NZ(N))*AA*BB     ! Conductance or Dispers. (z)
     &             +A5*(NS(M)*NS(N))*AA*BB     ! Decay
      BE(M,N)=B1*(NS(M)*NS(N))*AA*BB     ! Time
      CE(M,N)=C1*NS(M)*AA*BB*(-1*DIRAC)  ! Source
C-----------------------------------------------------------------------
C  convert from local to global coordinates
C-----------------------------------------------------------------------
      IR=IJKL(EL,M)
      JC=IJKL(EL,N)
C-----------------------------------------------------------------------
C  add element contribution to left-hand side matrix...
```

```
C-----------------------------------------------------------------------
      LHS(IR,SBW+JC-IR)=LHS(IR,SBW+JC-IR)+EPS*AE(M,N)+BE(M,N)
C-----------------------------------------------------------------------
C  ...and right-hand side matrix
C-----------------------------------------------------------------------
      RHS(IR)=RHS(IR)+ANSW(JC)*((EPS-1)*AE(M,N)+BE(M,N))+CE(M,N)
      RETURN
      END

C=======================================================================
```

```
      SUBROUTINE BOUND1 (BCTOP,NL1,NR1,BCBOT,NL2,NR2)
C-----------------------------------------------------------------------
C   Assigns prescribed value boundary conditions to boundary nodes
C-----------------------------------------------------------------------
      DOUBLE PRECISION LHS(1500,49),RHS(1500),BCTOP,BCBOT,
     &                 FDEPTH,HWIDTH
      INTEGER EL,BW,SBW
      COMMON/GMATRC/LHS,RHS
      COMMON/FRAC/FDEPTH,HWIDTH,NNFX,NNFZ
      COMMON/SIZES/MN,MB,ME,NN,NNX,NNZ,NE,NEX,NEZ
      COMMON/GRID1/DELX0,DELZ0,DELXMX,DELZMX,TLX,TLZ,BW,SBW
      COMMON/TIMES/EPS,TOLp,TOLc,DELT,DTMULT,NSTEPS,T0,FINTIM,ITERMX
C-----------------------------------------------------------------------
C  The top b.c. = BCTOP, and extends from node NL1 to node NR1
C  The bottom b.c. = BCBOT, and extends from node NL2 to node NR2
C-----------------------------------------------------------------------
      IF (NL1.EQ.0) GO TO 151
      DO 150 N=NL1,NR1
        LHS(N,SBW)=LHS(N,SBW)*1.0E+15
  150   RHS(N)=LHS(N,SBW)*BCTOP              ! top B.C.
      IF (NL2.EQ.0) GO TO 159
  151 DO 155 N=NL2,NR2
        LHS(N,SBW)=LHS(N,SBW)*1.0E+15
  155   RHS(N)=LHS(N,SBW)*BCBOT              ! bottom B.C.
  159 RETURN
      END

C=======================================================================
```

```
      SUBROUTINE VELOCI
C-----------------------------------------------------------------------
C     Calculates x and z components of velocity vector
C-----------------------------------------------------------------------
      DOUBLE PRECISION X(1500),Z(1500),
     &       VX(1500),VZ(1500),AA,BB,FDEPTH,HWIDTH,
     &   PRES(1500),CONC(1500),
     &   MU,PORs,KXXs,KZZs,KXXf,KZZf,KXX,KZZ,POR,
     &       PI,PJ,PK,PL,G1,G2,G3,G4
      INTEGER IJKL(1500,4),EL,BW,SBW
      COMMON/ANSWER/PRES,CONC
      COMMON/MATRL/MU,PORs,KXXs,KZZs,KXXf,KZZf,Dsoil,Dair,
     &                       SOURCE,LAMBDA,WTRTBL
      COMMON/FRAC/FDEPTH,HWIDTH,NNFX,NNFZ
      COMMON/SIZES/MN,MB,ME,NN,NNX,NNZ,NE,NEX,NEZ
      COMMON/GRID1/DELX0,DELZ0,DELXMX,DELZMX,TLX,TLZ,BW,SBW
      COMMON/GRID2/IJKL,X,Z
      COMMON/ELEMS/I,J,K,L,AA,BB,Pp
      COMMON/LOOP/EL,IQ,M,N
      COMMON/VEL/VX,VZ
C-----------------------------------------------------------------------
C  Darcy velocity = permeability / viscocity * average pressure gradient
C                                              in that direction
C-----------------------------------------------------------------------
      DO 100 EL=1,NE
        CALL ELPROP (KXX,KZZ,POR,DXX,DZZ,SIGMA,DELTA)
        G1=(SQRT(PRES(L))-SQRT(PRES(K)))/(X(K)-X(L))  ! gradient along...
        G2=(SQRT(PRES(I))-SQRT(PRES(J)))/(X(J)-X(I))  ! ...an element side
        G3=(SQRT(PRES(I))-SQRT(PRES(L)))/(Z(L)-Z(I))
        G4=(SQRT(PRES(J))-SQRT(PRES(K)))/(Z(K)-Z(J))
        VX(EL)=KXX/MU*(G1+G2)/2.
        VZ(EL)=KZZ/MU*(G3+G4)/2.
  100   CONTINUE
      RETURN
      END

C=======================================================================
```

```
      SUBROUTINE OUTDAT (TIME,NSTEP)
C-----------------------------------------------------------------------
C     Print out final results
C-----------------------------------------------------------------------
      DOUBLE PRECISION X(1500),Z(1500),UPSLON,
     &           VX(1500),VZ(1500),FDEPTH,HWIDTH,AMPL,
     &        PRES(1500),CONC(1500),PO,PATM,DPDT,PERIOD,CO,CINFIN,
     &        MU,PORs,KXXs,KZZs,KXXf,KZZf,KXX,KZZ,POR,LAMBDA,FLUX(49)
      INTEGER IJKL(1500,4),EL,BW,SBW
      COMMON/ANSWER/PRES,CONC
      COMMON/MATRL/MU,PORs,KXXs,KZZs,KXXf,KZZf,Dsoil,Dair,
     &                       SOURCE,LAMBDA,WTRTBL
      COMMON/VEL/VX,VZ
      COMMON/FRAC/FDEPTH,HWIDTH,NNFX,NNFZ
      COMMON/SIZES/MN,MB,ME,NN,NNX,NNZ,NE,NEX,NEZ
      COMMON/GRID1/DELXO,DELZO,DELXMX,DELZMX,TLX,TLZ,BW,SBW
      COMMON/GRID2/IJKL,X,Z
      COMMON/BC/PO,PATM,DPDT,AMPL,PERIOD,CO,CINFIN
      COMMON/TIMES/EPS,TOLp,TOLc,DELT,DTMULT,NSTEPS,TO,FINTIM,ITERMX
      COMMON/UPSTRM/UPSLON
      COMMON/FLUXS/FLUXF,FLUXM,FLUX,AVEFLX
C-----------------------------------------------------------------------
      WRITE(30,*)'*****************************************************
     &*******************'
      WRITE(30,*)' NN=',NN,' NNX=',NNX,' NNZ=',NNZ
      WRITE(30,*)' NE=',NE,' NEX=',NEX,' NEZ=',NEZ
      WRITE(30,*)' DELXO=',DELXO,' DELZO=',DELZO
      WRITE(30,*)' DELXMX=',DELXMX,' DELZMX=',DELZMX
      WRITE(30,*)' TLX=',TLX,' TLZ=',TLZ
      WRITE(30,*)' WTRTBL=',WTRTBL
      WRITE(30,*)' KXXs=',KXXs,' KZZs=',KZZs
      WRITE(30,*)' KXXf=',KXXf,' KZZf=',KZZf
      WRITE(30,*)' FDEPTH=',FDEPTH,' FWIDTH=',HWIDTH*2
      WRITE(30,*)' NNFX=',NNFX,' NNFZ=',NNFZ
      WRITE(30,*)' MU=',MU,' PORs=',PORs
      WRITE(30,*)' Po=',PO,' Patm=',PATM,' dPdt=',DPDT
      WRITE(30,*)' PERIOD=',PERIOD,' AMPL=',AMPL
      WRITE(30,*)' Dair=',Dair,' Dsoil=',Dsoil
      WRITE(30,*)' Co=',CO,' Cinfin=',CINFIN
      WRITE(30,*)' SOURCE=',SOURCE,' LAMBDA=',LAMBDA
      WRITE(30,*)' UPSLON=',UPSLON
      WRITE(30,*)' TOLp=',TOLp,' TOLc=',TOLc,' ITERMX=',ITERMX
      WRITE(30,*)' DELT=',DELT,' NSTEPS=',NSTEPS,' DTMULT=',DTMULT
          WRITE(30,*)' To=',TO,' FINTIM=',FINTIM,' EPS=',EPS
      WRITE(30,*)' SBW=',SBW,' BW=',BW
      WRITE(30,*)'*****************************************************
     &*******************'
            DO 220 N=1,NN
        WRITE(48,*) N,X(N),Z(N),CONC(N)
        WRITE(49,*) N,X(N),Z(N),sqrt(PRES(N))
  220       CONTINUE
```

```
      DO 230 EL=1,NE
        I=IJKL(EL,1)
        J=IJKL(EL,2)
        K=IJKL(EL,3)
        L=IJKL(EL,4)
 230          WRITE(35,*) EL,VX(EL),VZ(EL)
      RETURN
      END

C=======================================================================
      DOUBLE PRECISION FUNCTION INTERP (ANSW)
C-----------------------------------------------------------------------
C     Interpolation to find value of PRES or CONC for element center
C-----------------------------------------------------------------------
      DOUBLE PRECISION ANSW(1500),XSI(4),ETA(4),NS(4),NX(4),NZ(4),
     &          AA,BB
      COMMON/GAUSSP/XSI,ETA,NS,NX,NZ,WS
      COMMON/ELEMS/I,J,K,L,AA,BB,Pp
C-----------------------------------------------------------------------
      INTERP=NS(1)*ANSW(I)+NS(2)*ANSW(J)+NS(3)*ANSW(K)+NS(4)*ANSW(L)
      RETURN
      END

C=======================================================================
```

```
      SUBROUTINE SLBNS(A,B,NZ,M,NX,MX)
C-----------------------------------------------------------------------
C     SOLUTION OF LINEAR SYSTEMS OF EQUATIONS BY THE GAUSS ELIMINATION
C     METHOD, FOR NONSYMMETRIC BANDED SYSTEMS.
C
C     A :  CONTAINS THE SYSTEM MATRIX, STORED ACCORDING TO THE
C          NONSYMMETRIC BANDED SCHEME
C
C     B :  CONTAINS THE INDEPENDENT COEFFICIENTS.  AFTER SOLUTION IT
C          CONTAINS THE UNKNOWN VALUES.
C
C     NZ = NUMBER OF UNKNOWNS
C     M  = BANDWIDTH
C     NX = ROW DIMENSION OF ARRAY A AND B
C     MX = COLUMN DIMENSION OF ARRAY A
C-----------------------------------------------------------------------
      DOUBLE PRECISION A(NX,MX),B(NX),C
      N1=NZ-1
      MS=(M+1)/2
      DO 100 K=1,N1
      C=A(K,MS)
      K1=K+1
      IF(ABS(C)-0.000001)1,1,3
1     WRITE(5,2)K
2     FORMAT(' SINGULARITY IN ROW',I5)
      GO TO 30
C-----------------------------------------------------------------------
C     DIVIDE ROW BY DIAGONAL COEFFICIENT
C-----------------------------------------------------------------------
3     NI=K1+MS-2
      LZ=MINO(NI,NZ)
      DO 4 J=K1,LZ
      K2=MS+J-K
4     A(K,K2)=A(K,K2)/C
      B(K)=B(K)/C
C-----------------------------------------------------------------------
C     ELIMINATE UNKNOWN X(K) FROM ROW I
C-----------------------------------------------------------------------
      DO 10 I=K1,LZ
      K2=MS+K-I
400   FORMAT(6I10)
      C=A(I,K2)
      DO 5 J=K1,LZ
      K2=MS+J-I
      K3=MS+J-K
5     A(I,K2)=A(I,K2)-C*A(K,K3)
10    B(I)=B(I)-C*B(K)
100   CONTINUE
```

```
C-------------------------------------------------------------------------
C   COMPUTE LAST UNKNOWN
C-------------------------------------------------------------------------
    IF(ABS(A(NZ,MS))-0.000001)1,1,101
101 B(NZ)=B(NZ)/A(NZ,MS)
C-------------------------------------------------------------------------
C   APPLY BACK SUBSTITUTION PROCESS TO COMPUTE REMAINING UNKNOWNS
C-------------------------------------------------------------------------
    DO 200 I=1,N1
    K=NZ-I
    K1=K+1
    NI=K1+MS-2
    LZ=MINO(NI,NZ)
    DO 200 J=K1,LZ
    K2=MS+J-K
200 B(K)=B(K)-A(K,K2)*B(J)
30  RETURN
    END
C=========================================================================
```

Appendix C: Subroutines of FORTRAN Program CRACK

HEADER

Prints time and date, my name, problem title, problem number, program name and any additional comments to CRACK.ALL. Problem number and title defined in DATGEN.FOR (see Appendix D).

INDATA

Reads in all material properties and grid data from data file CRACK.DAT. This data file can be created easily using DATGEN.FOR (see Appendix D).

INITAL

Reads in initial conditions from CRACK.PRS (pressures) and CRACK.CNC (concentrations), or sets them to uniform values depending on information supplied by DATGEN.FOR in data file CRACK.DAT (see Appendix D).

ELPROP

For a particular element, returns the four corner node numbers, X- and Z-dimensions, and material properties such as intrinsic permeabilities, diffusion coefficients, porosity, source and storage terms.

GAUSSQ

Solves shape function integrals at a node by Gaussian quadrature. An excellent discussion of Gaussian quadrature as used in this subroutine can be found in Wang and Anderson (1982) pages 158-159.

MATRX

Forms matrices for individual elements, then adds element contribution to coefficient matrix and load vector for entire domain. A discussion of the element matrix and the assembly of the global conductance matrix can be found on pages 123-126 of Wang and Anderson (1982). Assembles matrix according to nonsymmetric banded storage scheme used by subroutine SLBNS.

BOUND1

Alters matrix equations for first type, or prescribed value boundary conditions at a node. If we already know the value of pressure or concentration at a node, it is not necessary to solve the equation for that node. Since a direct solver (SLBNS) is used, a numerical trick can handle specified values without eliminating equations. The main diagonal component $[LHS]_{L,L}$ of the coefficient matrix is multiplied by 10^{15}, and the load vector $\{RHS\}_L$ is set equal to 10^{15} $[LHS]_{L,L}$ times the prescribed value. When the complete system of equations is solved for the column vector, then $\{PRES\}_L$ or $\{CONC\}_L$ is forced to the

specified value because all the other terms the the Lth equation are insignificant relative to the diagonal term (Wang and Anderson, 1972).

VELOCI

Uses Darcy's Law, equation (2.2.3.2), to calculate average velocity of an element based on the pressures at its four corner nodes.

OUTDAT

Prints out data to these files:

CRACK.ALL	Values of all input parameters, grid data
CRACK.CNC	Concentration distribution at last time step
CRACK.PRS	Pressure distribution at last time step
CRACK.VEL	Velocity distribution at last time step
CRACK.FLX	Fluxes for each time step
CRACK.FXA	Average fluxes vs. time
CRACK.FXM	Soil fluxes vs. time
CRACK.FXF	Crack fluxes vs. time
CRACK.PRE	PATM (top pressure B.C.) vs. time

CRACK.CNC, CRACK.PRS, and CRACK.VEL can be used to produce NCAR contour plots. CRACK.FXA, CRACK.FXM, CRACK.FXF, AND CRACK.PRE can be used to do TEKTRONIX plots.

SLBNS (from Brebbia and Ferrante, 1978)

The matrix equations obtained using the finite element method are usually nonsymmetric but banded. This means that a great deal of the matrix consists of zeros, except for a certain number of diagonal bands around the main, or center diagonal. The bandwidth (M) is this

number of bands. The semibandwidth (MS) equals 2 * M - 1. To save memory, we can store the non-zero coefficients of the matrix in a rectangular array, where the diagonals become columns. A coefficient originally located in position (I,J) will occupy position (I,MS+J-1) in the new organization. The reorganization is done in subroutine MATRX. SLBNS performs gaussian elimination on the reorganized matrix.

Appendix D: Listing of Data file-generating program DATGEN

```
C=====================================================================
C FORTRAN PROGRAM DATGEN (final version)
C CREATES THE INPUT DATA FILE "CRACKD.DAT" FOR THE PROGRAM "CRACKD.FOR":
C GENERATES 2-DIMENSIONAL FINITE ELEMENT GRID WITH GRID SPACING WHICH
C INCREASES BY A CONSTANT RATIO AND RECTANGULAR ELEMENTS.
C  BY DIANA J. HOLFORD                1/86                    N.M.I.M.T.
C---------------------------------------------------------------------
      REAL LAMBDA,MU,KZZs,KXXs,X(6000),Z(6000),KXXf,KZZf
      INTEGER SBW,BW
      CHARACTER*80 PRNAME
      LOGICAL STEADY,CONTIP,CONTIC,INPATM,NOFRAC
      OPEN(30,FILE='CRACKD.DAT')
C---------------------------------------------------------------------
C INPUT DATA (ARE ON LINES 1-40)
C---------------------------------------------------------------------
C    UNITS:  GRAMS,CENTIMETERS,SECONDS
C    CONCENTRATIONS: ATOMS/CM**3
C    PRESSURES: GRAMS/CM/SEC**2 = 0.1 Pa = 9.869E-7 atm = 2.953E-5 IN. Hg
C    DIMENSIONS: L=length,A=area,V=volume,T=time,M=mass,DIM=dimensionless
C---------------------------------------------------------------------
C Write problem name and number (first character of title should be ' ')
C---------------------------------------------------------------------
    1         PRNAME=' FIELD CALIBRATION'
      WRITE(30,1000) PRNAME
    2         NRUN=8052
      WRITE(30,*) NRUN
1000          FORMAT(A80)
C---------------------------------------------------------------------
C Problem types
C---------------------------------------------------------------------
C    STEADY = .TRUE.  gives steady state diffusion profile
C    NOFRAC = .TRUE.  runs 1-D porous media model w/ no fracture
C             .FALSE. runs 2-D porous media model w/ one fracture
C    CONTIP = .TRUE.  read initial pressures from CRACKD.PRS
C           = .FALSE. sets initial pressures to P0
C    CONTIC = .TRUE.  read initial concentrations from CRACKD.CNC
C           = .FALSE. sets initial concentrations to C0
```

```
C-------------------------------------------------------------------------
   3        STEADY=.FALSE.
   4        CONTIP=.FALSE.
   5        CONTIC=.TRUE.
   6        NOFRAC=.FALSE.
C-------------------------------------------------------------------------
C Boundary & initial conditions
C-------------------------------------------------------------------------
   7        C0=0.0                    ! TOP BOUNDARY CONDITION CONCENTRATION (M/V)
   8        CINFIN=25000.0            ! BOTTOM BOUNDARY CONDITION CONCENTRATION (M/V)
   9        P0=8.50E+05               ! INITIAL CONDITION PRESSURE (M/L/T**2)
                                 ! (note: P0 should never = 0, things go BOOM!!)
  10        PATM=8.50E+05             ! TOP BOUNDRY INITIAL COND. PRESSURE (M/L/T**2)
  11        dPdt=-900./3600.          ! CHANGE IN MEAN PATM PER UNIT TIME (M/L/T**3)
    AMPL=0.                      ! AMPLITUDE OF SINE FUNCT. VAR. IN PATM
  12        PERIOD=1.E+38             ! PERIOD OF SINE FUNCT. VARIATION IN PATM
                                 ! (SET=1.E+38 IF CONSTANT RISE/DROP WANTED)
  13        INPATM=.FALSE.            ! IF .TRUE. PATM READ FROM CRACKD.ATM
                                 ! IF .FALSE. PATM CALCULATED BY A FUNCTION
C-------------------------------------------------------------------------
C Soil and gas properties
C-------------------------------------------------------------------------
  14        PORs=0.35                 ! POROSITY OF SOIL (DIM)
  15        KZZs=2.7E-8               ! INTRINSIC PERMEABILITY IN Z-DIRECTION (A/T)
  16        KXXs=2.7e-8               ! INTRINSIC PERMEABILITY IN X-DIRECTION (A/T)
  17        MU=1.8E-4                 ! DYNAMIC VISCOSITY OF AIR (M/L/T)
  18        FDEPTH=400.0              ! DEPTH OF TABULAR FRACTURE
    IF (NOFRAC) FDEPTH=-10.
  19        FWIDTH=.066666666         ! WIDTH OF TABULAR FRACTURE
    HWIDTH=FWIDTH/2              ! HALF-WIDTH OF TABULAR FRACTURE
    KZZf=(FWIDTH**2)/12          ! FRACTURE PERMEABILITY IN Z-DIRECTION (A/T)
  20        KXXf=KXXs                 ! FRACTURE PERMEABILITY IN X-DIRECTION (A/T)
  21        Dair=0.1                  ! DIFFUSION COEFFICIENT FOR RADON IN AIR (A/T)
  24        Dsoil=0.009/0.35          ! APPARANT DIFFUSION COEFFICIENT IN SOIL (A/T)
  25        LAMBDA=2.100E-06          ! DECAY CONSTANT = ln(2)/half-life (1/T)
    SOURCE=CINFIN*LAMBDA         ! SOURCE TERM (M/V/T)
  26        WTRTBL=-3000.             ! DEPTH TO WATER TABLE
C-------------------------------------------------------------------------
C Grid parameters
C-------------------------------------------------------------------------
  27        TLX=408.15468788          ! TOTAL LENGTH OF MODEL IN X-DIRECTION (L)
  28        TLZ=-1000.0               ! TOTAL LENGTH OF MODEL IN Z-DIRECTION (L)
  29        NEFX=3                    ! ELEMENTS IN FRACTURE IN X-DIRECTION
    IF (NOFRAC) NEFX=0
    NNFX=NEFX+1                  ! NO. NODES IN FRACTURE IN X-DIRECTION
    DELX0=HWIDTH/NEFX            ! SMALLEST X-GRID SPACING (L)
```

```
    IF (NOFRAC) DELX0=TLX
 30         DELXMX=100.0              ! LARGEST X-GRID SPACING (L)
    IF (NOFRAC) DELXMX=TLX
 31         DELZ0=-10.0               ! SMALLEST Z-GRID SPACING (L)
 32         DELZMX=-10.0              ! LARGEST Z-GRID SPACING (L)
C-----------------------------------------------------------------------
C Time parameters
C-----------------------------------------------------------------------
 33         EPS=1.0                   ! TIME WEIGHTING FACTOR (DIM)
    DEL=AMIN1(DELX0,DELZ0)
    DELTm=SQRT((PORs*DEL**2)
     &       /(KZZs/MU*ABS(dPdt)))   ! STABLE TIME INCREMENT FOR SOIL (T)
    DELT=900.
 34         DTMULT=1.0                ! TIME STEP MULTIPLICATION FACTOR
 35         NSTEPS=24                 ! NO. OF TIME STEPS (DIM)
 36         T0=0.0                    ! INITIAL TIME (T)
    FINTIM=T0+DELT*NSTEPS    ! FINISH TIME
 37         ITERMX=5                  ! MAX. NO. OF ITERATIONS PER TIME STEP
 38         TOLp=1.0E-05              ! STEADY-STATE TOLERANCE CRITERIA
 39         TOLc=1.0E-07              ! STEADY-STATE TOLERANCE CRITERIA
C-----------------------------------------------------------------------
C Upstream weighting parameter
C-----------------------------------------------------------------------
 40         UPSLON=0.0                ! Upstream weighting parameter Z-direction
C-----------------------------------------------------------------------
C Generate X-direction grid spacings and assign X-coordinates to top row
C-----------------------------------------------------------------------
    DELX=DELX0
    NNX=NEFX*2+1              ! NO. NODES IN X-DIRECTION
    DO 50 N=1,NNX
 50          X(N)=(N-1)*DELX
 60         DELX=DELX*2.5
    IF (DELX.GE.DELXMX) DELX=DELXMX
    IF((X(NNX)+DELX).GE.TLX) THEN
      NNX=NNX+1
      X(NNX)=TLX
      GO TO 70
    ENDIF
    NNX=NNX+1
    X(NNX)=X(NNX-1)+DELX
    GO TO 60
C-----------------------------------------------------------------------
C Generate Z-direction grid spacings, assign coordinates to left column
C-----------------------------------------------------------------------
 70         NNZ=1
```

```
  Z(1)=0.0
  IF(ABS(Z(1)).LE.FDEPTH) NNFZ=1
  DELZ=DELZ0
80        NNZ=NNZ+1
  N=(NNZ-1)*NNX+1
  Z(N)=Z(N-NNX)+DELZ
  DELZ=DELZ*1.5
  IF(ABS(Z(N)).LE.FDEPTH) NNFZ=NNFZ+1
  IF (ABS(DELZ).GT.ABS(DELZMX)) DELZ=DELZMX
  IF(ABS(Z(N)+DELZ).LT.ABS(TLZ)) GO TO 80
-------------------------------------------------------------------------
Assign coordinates to all other nodes
-------------------------------------------------------------------------
  DO 90 I=2,NNZ
  DO 90 J=2,NNX
   N=(I-1)*NNX+J
   X(N)=X(N-NNX)
90         Z(N)=Z(N-1)
-------------------------------------------------------------------------
Calculate grid parameters
-------------------------------------------------------------------------
  NN=NNX*NNZ               ! NO. NODES TOTAL
  NEX=NNX-1                ! NO. ELEMENTS IN X-DIRECTION
  NEZ=NNZ-1                ! NO. ELEMENTS IN Z-DIRECTION
  NE=NEX*NEZ               ! NO. ELEMENTS TOTAL
  TLX=X(NN)                ! ACTUAL TOTAL LENGTH IN X-DIRECTION
  TLZ=Z(NN)                ! ACTUAL TOTAL LENGTH IN Z-DIRECTION
  SBW=NNX+2                ! SEMI-BANDWIDTH
  BW=SBW*2-1               ! BANDWIDTH
-------------------------------------------------------------------------
 Print x,z coordinates for each node
-------------------------------------------------------------------------
  WRITE(30,*)NN,NNX,NNZ
  DO 100 N=1,NN
00        WRITE(30,*) N,X(N),Z(N)
-------------------------------------------------------------------------
 Generate and print i,j,k node numbers for each rectangular element
-------------------------------------------------------------------------
  WRITE(30,*)NE,NEX,NEZ
  DO 110 NEL=1,NE
      END=0.
    IF(MOD(NEL,NEX).EQ.0) END=1.
    IR=NEL/NEX-END
    I=NEL+IR+NNX
    J=I+1
    K=NEL+IR+1
```

```
      L=K-1
 110        WRITE(30,*)NEL,I,J,K,L
C-------------------------------------------------------------------------
C  PRINT OTHER DATA
C-------------------------------------------------------------------------
    WRITE(30,*)STEADY,CONTIP,CONTIC,NOFRAC
    WRITE(30,*)PO,PATM,dPdt,AMPL,PERIOD,INPATM
    WRITE(30,*)CO,CINFIN
    WRITE(30,*)KXXs,KZZs,KXXf,KZZf
    WRITE(30,*)Dsoil,Dair
    WRITE(30,*)PORs,MU,WTRTBL
    WRITE(30,*)SOURCE,LAMBDA
    WRITE(30,*)FDEPTH,HWIDTH,NNFX,NNFZ
    WRITE(30,*)EPS,TOLp,TOLc,DELT,DTMULT,NSTEPS,TO,FINTIM,ITERMX
    WRITE(30,*)UPSLON
    WRITE(30,*)DELXO,DELZO,DELXMX,DELZMX,TLX,TLZ
    WRITE(30,*)SBW,BW
    END
```

REFERENCES

Bear, Jacob (1979). Hydraulics of Groundwater. McGraw-Hill, New York.

Brebbia, C. A. and A. J. Ferrante (1978). Computational Methods for the Solution of Engineering Problems. Crane-Russak, New York.

Carslaw H. S. and Jaeger, J. C. (1959). Conduction of Heat in Solids, 2nd edition. Oxford University Press, London.

Clements, W. E. (1974). The Effect of Atmospheric Pressure Variation on the Transport of u222 dRadon from Soil to the Atmosphere. Ph.D. Dissertation, New Mexico Institute of Mining and Technology, Socorro.

Freeze, R. A. and J. A. Cherry (1979). Groundwater. Prentice-Hall, Inc., Englewood Cliffs, New Jersey.

Grisak, G. E. and J. F. Pickens (1980a). "Solute Transport through Fractured Media: 1. The Effect of Matrix Diffusion." Water Resources Research, volume 16, number 4, pages 719-730.

Grisak, G. E. and J. F. Pickens (1980b). "Solute Transport through Fractured Media: 2. Column Study of Fractured Till." Water Resources Research, volume 16, number 4, pages 731-739.

Huyakorn, P. S., B. H. Lester, and C. R. Faust (1983a). "Finite Element Techniques for Modeling Groundwater Flow in Fractured Aquifers." Water Resources Research, volume 19, number 4, pages 1019-1035.

Huyakorn, P. S., B. H. Lester, and J. W. Mercer (1983b). "An Efficient Finite Element Technique for Modeling Transport in Fractured Porous Media: 1. Single Species Transport." Water Resources Research, volume 19, number 3, pages 841-854.

Huyakorn, P. S. and K. Nilkuha (1979). "Solution of Transient Transport Equation Using an Upstream Finite Element Scheme." Applied Mathematical Modelling, volume 3, February.

Huyakorn, P. S. and G. F. Pinder (1983). Computational Methods in Subsurface Flow. Academic Press, New York.

INTERA Environmental Consultants, Inc. (1983). "FTRANS: A Two-Dimensional Code for Simulating Fluid Flow and Transport of Radioactive Nuclides in Fractured Rock for Repository Performance Assesment," ONWI-426, prepared for Battelle Memorial Institute, Office of Nuclear Waste Isolation, Columbus, Ohio.

Lohman, S. W. (1979). Ground-Water Hydraulics. Geological Survey Professinal Paper 708, U. S. Government Printing Office, Washington, D.C.

Neretnieks, Ivars (1980). "Diffusion in the Rock Matrix: An Important Factor in Radionuclide Retardation?" J. Geophysical Research, volume 85, number B8, pages 4379-4397.

Roller, D. E. and R. Blum (1981) Physics (volume 1): Mechanics, Waves, and Thermodynamics. Holden-Day, Inc., San Francisco, California.

Schery, S. D., D. H. Gaeddert, and M. H. Wilkening (1984). "Factors Affecting Exhalation of Radon from a Gravelly Sandy Loam." J. Geophysical Research, volume 89, number D5, pages 7299-7309.

Schery, S. D. and D. Siegel (in preparation) "The Role of Channels in the Transport of Radon from the Soil."

Sudicky, E. A. and E. O. Frind (1982). "Contaminant Transport in Fractured Porous Media: Analytical Solutions for a System of Parallel Fractures." Water Resources Research, volume 18, number 6, pages 1634-1642.

Wang, H. F. and M. P. Anderson (1982). Introduction to Groundwater Modeling: Finite Difference and Finite Element Methods. W. H. Freeman and Company, San Francisco, California.

Wilson, J. L., L. R. Townley, and A. Sa da Costa (1979). Mathematical Development of a Finite Element Aquifer Flow Model, AQUIFEM-1. Ralph M. Parsons Laboratory for Water Resources and Hydrodynamics Report number 248, Massachusetts Institute of Technology, Cambridge, Massachusetts.